AD-781 403

FATIGUE OF FERRO-CEMENT

Michael G. Simpson

Naval Postgraduate School
Monterey, California

June 1974

DISCLAIMER NOTICE

THIS DOCUMENT IS BEST QUALITY PRACTICABLE. THE COPY FURNISHED TO DTIC CONTAINED A SIGNIFICANT NUMBER OF PAGES WHICH DO NOT REPRODUCE LEGIBLY.

SECURITY CLASSIFICATION OF THIS PAGE (When Data Entered)

REPORT DOCUMENTATION PAGE		READ INSTRUCTIONS BEFORE COMPLETING FORM
1. REPORT NUMBER	2. GOVT ACCESSION NO	3. RECIPIENT'S CATALOG NUMBER AD 781403
4. TITLE (and Subtitle) FATIGUE OF FERRO-CEMENT		5. TYPE OF REPORT & PERIOD COVERED Master's Thesis: June 1974 Engineer's Thesis
		6. PERFORMING ORG. REPORT NUMBER
7. AUTHOR(s) Michael G. Simpson		8. CONTRACT OR GRANT NUMBER(s)
9. PERFORMING ORGANIZATION NAME AND ADDRESS Naval Postgraduate School Monterey, California 93940		10. PROGRAM ELEMENT, PROJECT, TASK AREA & WORK UNIT NUMBERS
11. CONTROLLING OFFICE NAME AND ADDRESS Naval Postgraduate School Monterey, California 93940		12. REPORT DATE June 1974
		13. NUMBER OF PAGES 119
14. MONITORING AGENCY NAME & ADDRESS (if different from Controlling Office) Naval Postgraduate School Monterey, California 93940		15. SECURITY CLASS. (of this report) Unclassified
		15a. DECLASSIFICATION/DOWNGRADING SCHEDULE

16. DISTRIBUTION STATEMENT (of this Report)

Approved for public release; distribution unlimited.

17. DISTRIBUTION STATEMENT (of the abstract entered in Block 20, if different from Report)

18. SUPPLEMENTARY NOTES

19. KEY WORDS (Continue on reverse side if necessary and identify by block number)

fatigue
ferro-cement

20. ABSTRACT (Continue on reverse side if necessary and identify by block number) Ferro-cement is a cement mortar with a high relative volume of we dispersed steel wire reinforcement. The material properties of ferro-cement a neither those of the mortar alone nor of the reinforcement and vary as the mo tar and reinforcement configurations are changed. In this study, several variations of ferro-cement were fabricated and subjected to constant amplitude cyclic loads up to ten million cycles. Stress versus cycles-to-failure plots were developed and comparisons between the data fo various ferro-cement modifications were made. Monotonic tests were conducted by other experimenters. An investigation of the fracture surface was

DD FORM 1 JAN 73 1473 EDITION OF 1 NOV 65 IS OBSOLETE
(Page 1) S/N 0102-014-6601

SECURITY CLASSIFICATION OF THIS PAGE (When Data Entered)

Block 20. Abstract (cont.) conducted using a scanning electron microscope.

FATIGUE OF FERRO-CEMENT

by

Michael G. Simpson
Lieutenant Commander, United States Navy
B.S., University of Oklahoma, 1963

Submitted in partial fulfillment of the
requirements for the degrees of

MASTER OF SCIENCE IN MECHANICAL ENGINEERING

and

DEGREE OF MECHANICAL ENGINEER

from the

NAVAL POSTGRADUATE SCHOOL
June 1974

Author Michael G. Simpson

Approved by: Edwin A McKinnon
Thesis Advisor

John J. Brock
Second Reader

Robert K. Newman
Chairman, Department of Mechanical Engineering

Jack R. Borsting
Academic Dean

ABSTRACT

Ferro-cement is a cement mortar with a high relative volume of well dispersed steel wire reinforcement. The material properties of ferro-cement are neither those of the mortar alone nor of the reinforcement and vary as the mortar and reinforcement configurations are changed. In this study, several variations of ferro-cement were fabricated and subjected to constant amplitude cyclic loads up to ten million cycles. Stress versus cycles-to-failure plots were developed and comparisons between the data for various ferro-cement modifications were made. Monotonic tests were conducted on the ferro-cement to allow comparisons with work conducted by other experimenters. An investigation of the fracture surface was conducted using a scanning electron microscope.

TABLE OF CONTENTS

LIST OF TABLES

TABLE

LIST OF FIGURES

FIGURE

TABLE OF SYMBOLS AND ABBREVIATIONS

SYMBOLS

S	Flexural Stress, Cyclic or Monotonic
S_f	Maximum Cyclic Stress at 10^7 Cycles
S_n	Estimated Fatigue Endurance Limit
S_v	Flexural Stress at First Visible Cracking
S_p	Flexural Stress at Proportional Limit
S_y	Flexural Yield Stress
S_u	Ultimate Monotonic Flexural Stress
S_c	Ultimate Compressive Mortar Stress
E_m	Monotonic Flexural Modulus of Elasticity
E_d	Dynamic Flexural Modulus of Elasticity
E_c	Mortar Compressive Modulus of Elasticity

ABBREVIATIONS

psi	Pounds-Force per Square Inch
in	Inch

ACKNOWLEDGMENT

The research was conducted in the Department of Mechanical Engineering laboratories, U. S. Naval Postgraduate School, Monterey, California. The help and advice provided by the Mechanical Engineering Department professors and technicians had a major role in the successful completion of the study.

Special acknowledgments are deserved for:

Mr. H. R. Corbin, President, Monterey Marine, Inc. for his advice and assistance in obtaining materials;

Mrs. Vicki Culley, who provided so much help and encouragement in addition to the typing;

Professor John E. Brock, whose interest and advice throughout the study was of inestimable value.

Professor Edwin A. McKinnon, the author's advisor, gave generously of his time and attention throughout the study. His pragmatic approach to research was of major value.

This thesis is dedicated to my wife, Carol, for her patience and understanding throughout the long siege of study.

I. INTRODUCTION

Ferro-cement is a composite material consisting of a cementious mortar containing a high relative volume of steel reinforcement. The reinforcement usually consists of close-packed layers of steel wire mesh with or without steel rods included within the layers of mesh. At present the primary application of ferro-cement is in the fishing boat and yacht construction industry.

Ferro-cement appears ideally suited for innovative design applications. Almost any shape to which wire mesh may be formed can be constructed in ferro-cement. The major design constraint is insufficient ferro-cement materials data. In particular, very little information is available concerning the response of ferro-cement to cyclic loading.

The lack of cyclic data provided the motivation for this study. Data was obtained from which stress versus cycles-to-failure plots were developed for several variations of a basic ferro-cement configuration. The cyclic dependency of the flexural modulus of elasticity was considered. A series of monotonic tests were conducted to provide a data base for comparison with the results of other investigators. In an effort to gain some insight into the fatigue fracture mechanism, the fracture regions of several fatigue specimens were examined using a scanning electron microscope.

II. BACKGROUND

A. HISTORY

The first ferro-cement boat on record was built in France around the year 1848. Its design and construction was attributed to Joseph

Louis Lambot [1][1] for use at his estate in France. Impetus for the present growth of interest in ferro-cement is attributed to the work of Pier Luigi Nervi [2] who began making boats and structures of ferro-cement in Italy in 1942. Since then, construction of ferro-cement boats and structures has spread to many countries. The most ardent supporters of ferro-cement have been yachtsmen, many of whom have successfully built their own ferro-cement boats.

B. PRESENT APPLICATIONS

1. Yachts

Nervi [2] constructed in 1945 what appears to have been the first ferro-cement yacht. Twelve years later, the Russians launched a ferro-cement yacht on the Volga River [3]. Current interest in ferro-cement seems greatest in the British Commonwealth nations. Although there are numerous commercial firms which have built successful ferro-cement yachts, most of these boats have been constructed by the owners [4,5].

2. Working Craft

The primary application of ferro-cement to workboats is within the fishing industry. Fish holds and tanks may be constructed of ferro-cement with relative ease and economy. The reduction in general maintenance requirements for ferro-cement as compared to wood and steel is a significant advantage for fishermen [4-8]. Small tugboats and numerous commercial fishing craft have been constructed of ferro-cement in Canada and the United States. Barges and lifting craft have been constructed of ferro-cement in Russia [2].

---

[1]Numbers in parentheses identify references; see page 117

3. Military Craft

The hostilities in Southeast Asia have increased military interest in ferro-cement. The Vietnamese Naval Shipyard has produced various ferro-cement patrol craft up to sixty feet in length. One of the few planing hull designs for ferro-cement was developed and constructed at the U. S. Naval Ship Research and Development Center, Annapolis, Maryland [9,10]. Cost effectiveness studies for military applications of ferro-cement have been made by the U. S. Navy [11,12]. Ferro-cement appears to have good potential for military applications.

4. Land-Based Structures

A warehouse built by Nervi and Bartoli [2] in 1946 was probably the first ferro-cement land-based structure. Nervi [2] also reports a ninety-eight meter span of corrugated ferro-cement panels used in construction of the Exhibition Hall at Turin, Italy. Ferro-cement has been used as the inner lining of large precast pressure pipes for hydroelectric installations [2]. Thin-walled tanks and small prefabricated buildings of ferro-cement have been used in New Zealand [1]. The U. S. Army has studied ferro-cement for various domestic and para-military applications in Southeast Asia [13]. Ferro-cement was found suitable for many applications, including underground petroleum storage, granaries, and cisterns.

C. CONSTRUCTION TECHNOLOGY

1. Forming Methods

There are four forming methods for ferro-cement in general use. The oldest method is the pipe-frame technique in which the structure shape is formed of small-diameter iron pipe. The reinforcing

rod and mesh are then wired to the pipe framework [4]. Fabrication of the U. S. Navy "CRAB" boat involved a removable metal framework to which the reinforcing mesh was tied. After the cement mortar was applied and cured, the tie wires were cut and the framework removed. This left only a thin ferro-cement shell which required the installation of a permanent wooden framing system for hull form stiffness [9]. The wooden mold system is popular with builders. Temporary wooden frames are erected and wooden battens are attached to fair in the structure shape. Thin plastic sheeting or fine screen wire is then attached to the battens. The ferro-cement reinforcement is stapled to the battens through the plastic or screen wire. Mortar is then applied from the outside of the form. Upon completion of the curing process, the wooden frames are removed and the wooden battens may either be removed or left in place [5]. At least one commercial builder utilizes a cavity mold system in which the ferro-cement hull is constructed in a manner similar to fiberglass boat construction techniques [11].

2. Materials

There are almost as many variations of materials used in ferro-cement construction as there are builders. Most ferro-cement designers use a Portland type II or V cement, a fine sand with a well-controlled fineness modulus, and some combination of wire mesh and rod. There is no agreement in the ferro-cement industry as to an optimum configuration. It appears reasonable to assume that there is no single "best" configuration of ferro-cement for all applications. Flexibility of configuration is one of the most promising aspects of ferro-cement design.

3. New Developments

Use of lightweight aggregates, expansive cements, and various mortar additives is just starting to build up an experience data base. Very little formal testing data for these modifications are available. Polymer-impregnation of concrete has resulted in significant strength increases [14]. The ferro-cement literature does not yet report actual polymer-impregnation of ferro-cement structures. One firm has developed a system similar to ferro-cement construction utilizing a polyester resin and lightweight aggregates in lieu of Portland cement mortar [15].

D. FERRO-CEMENT DESIGN

1. Data Requirements

Engineers and architects engaged in design work utilizing any construction material require certain basic information about that material. Standards have been developed for the more common structural materials. Good knowledge of the material will allow the use of more efficient and flexible designs. Material properties such as the various moduli and strengths, resistance to impact and environment, and material response to cyclic loading are generally available for materials for which standards have been developed. There has been no agreement reached among ferro-cement designers and builders concerning a set of ferro-cement standards. Various insurance and regulatory agencies have proposed acceptability criteria, but these are admittedly based upon less data than is desirable.

2. Data Available

Some of the types of ferro-cement material data available in the literature are listed below, along with a sampling of pertinent references.

a. Compressive Strength [3,6,16,17]

b. Tensile Strength [3,6,7,16,18]

c. Flexural Strength [3,6,7,16,17,19]

d. Shear Strength [3,6,16]

e. Impact Strength [3,7,16]

f. Watertightness [3]

g. Freeze-Thaw Response [3,6,7]

h. Fatigue Loading Response [8,16,17]

A critical problem concerning usage of the data presented in the literature is the relative applicability of the data to a particular ferro-cement configuration. Similar types of data derived for different configurations may differ considerably.

3. Fatigue-Life Design

A graph showing the maximum cyclic stress versus the number of cycles to failure is a common data tool used to design for cyclically-loaded structures. These graphs, or S-N plots, are often derived for metals by applying a constant maximum cyclic strain. Conversion from strain-cycles data to stress-cycles data is acceptable only if the test material modulus of elasticity remains fairly constant throughout the fatigue life. Brauer [16] and the British Columbia Research Council [8] both report results of cyclic flexure tests of ferro-cement beams conducted on strain-control devices. Simpson and Tucker [20] conducted a series of constant maximum cyclic strain tests on ferro-cement beams. During those tests, a change in flexural modulus of elasticity was noted as the number of deflection cycles increased. This is addressed more fully in Chapter IV.

III. FATIGUE TESTS

A. SCOPE OF TEST PROGRAM

One basic ferro-cement test configuration was chosen and eleven elemental variations of that base were tested. All fatigue tests were conducted in load control rather than strain control due to the change in modulus of elasticity with cyclic loadings. A total of 132 specimens were fatigue-tested. Each test was conducted continuously at a constant 30 hertz.

B. TEST SPECIMENS

1. Specimen Description

Figures 1 and 2 show a typical specimen after failure. Specimens averaged two and three-quarter inches wide, five-eighths inch thick, and eighteen inches long. All specimens contained seven layers of one-half inch welded square mesh of either galvanized or ungalvanized steel wire. The galvanized wire was galvanized prior to welding it into the square mesh form. All specimen groups except group 3PWG were constructed with the long axis of the mesh as unrolled from the shipping roll placed parallel to the long axis of the test specimen. In group 3PWG, the second, fourth, and sixth mesh layers were placed at 45 degrees relative to the specimen axis.

2. Specimen Fabrication

a. Forms and Reinforcement

Wooden frames 25 inches by 43 inches were assembled as shown in Figure 3. Seven layers of either galvanized or ungalvanized wire mesh were then stapled to the wooden frames, as shown in Figure 4. The layers of mesh were assembled in a staggered configuration to

maximize reinforcement distribution throughout the mortar. Particular care was taken with the mesh placement to ensure that the mesh dispersion or "register" was duplicated as closely as possible in all specimens. Four mesh layers were placed with the longitudinal wires up (as seen in the finished ferro-cement specimens) and the other three layers had the longitudinal wires on the underside. This resulted in the wires nearest the specimen outer surfaces being parallel to the direction of the tensile stresses due to flexure. A plywood panel cut to fit the inside dimensions of each wooden frame was covered with a polyethylene sheet and secured in place directly against the underside of the mesh stack, as shown in Figure 4. The separate plywood backing panel allowed inspection of the mortared panels for mortar penetration in some of the early ferro-cement panels. The mesh stack was secured tightly to the backing panel with fine steel wires passed through the stack and panel and then tied.

b. Mortar

Three mortar variations were used for specimen fabrication as indicated by Table I. The 1PXX and 3PGW groups had a washed, dried, and graded beach sand, Portland type V cement, and a 0.45 water-to-cement ratio (by weight). The 2PXX groups had the same elements with a 0.40 water-to-cement ratio. The 4EXX groups had a sharp quarry sand, an expansive cement used in the Monterey/San Francisco Bay area for boatbuilding, and a 0.45 water-to-cement ratio. The beach sand particles were much smoother and more rounded than the quarry sand particles. As shown in Table II, the quarry sand included a higher percentage of "fines" than did the beach sand.

The mortar elements were proportioned carefully to within 0.05 pounds and mixed manually in 45 pound batches. Each batch completed one 18 by 36 inch panel with a little mortar left over. The mortar was applied to the forms and worked only enough to achieve full mesh penetration. Vibration of the form and mortar was held to the minimum required for complete mesh stack penetration by the mortar. The 4EXX groups were vibrated with a one inch diameter electrically-powered vibrating rod of twelve inches length (pencil vibrator); the other groups were fabricated using a vibration table to assist in achieving mortar penetration. The pencil vibrator appeared more effective than the vibration table.

c. Curing

After allowing the ferro-cement panels to achieve a final "set" over a period of about nine hours, the entire form and panel assemblies were placed in one of the curing chambers shown in Fig. 5. One chamber contained a set of water spray nozzles that provided a fine, fog-like mist. The water-cured ferro-cement panels were cured in this chamber for 28 days. The other chamber had a saturated steam inlet controlled by a manually-operated valve. Remote sensing and direct reading thermometers allowed monitoring of the chamber interior temperature. The panels for steam-curing were placed in this chamber and a period of four hours was used to bring the chamber temperature from ambient up to 160 degrees Fahrenheit. This temperature was maintained for eighteen hours. It was then gradually reduced to room temperature over another four hour interval.

d. Cutting

Upon completion of the curing process, the panels were removed from the forms and cut to specimen size on the saw shown in Fig. 6. The saw was constructed specifically for cutting ferro-cement panels and had a diamond-impregnated carbide blade. Saw feeding was accomplished by a guided table on rollers pulled by a simple weight-and-pulley arrangement. Each panel provided eleven test specimens.

e. Storage

Following the cutting process, the specimens were labeled and stored dry in the test laboratory. The laboratory atmospheric humidity was normally low and temperatures varied from 65 to 75 degrees Fahrenheit. Storage times prior to testing differed several months between some specimens and probably contributed to test data scatter.

3. Specimen Group Identification

The coding system shown in Table I was devised to facilitate understanding of references to particular specimen groups. A "P" signifies Portland type V cement and an "E" means that Kaiser CHEMCOMP, an expansive cement, was used. The "U" and "G" refer respectively to ungalvanized and galvanized reinforcing mesh. The "S" and "W" signify respectively steam or water-cured. The numerals refer to specimen group fabrication series and are explained by Table I.

4. Entrapped Gas Defects

A series of ferro-cement panels fabricated prior to those used in the test program exhibited bubble defects, as shown in Figs. 7 and 8. The mortar layer above the first mesh layer in the panel shown in Fig. 7 was much thicker than that for the panel shown in Fig. 8. The

panels were constructed concurrently, using the same batch of mortar and the same type of wire mesh reinforcement. The thicker layer of mortar required a larger volume of gas to accumulate in order to cause the mortar to separate and form the bubble. The panel reinforcement was a one-half inch welded square mesh of galvanized steel wire welded after galvanizing. The mesh had received no weathering or cleaning prior to use. A chromium trioxide solution of approximately 160 parts per million in the mortar mix water had been added to inhibit the formation of electrolytic cells at dissimilar metal surfaces within the mortar. The British Columbia Research Council [6] reported observing some similar defects, but these were in panels which were believed to be fabricated without any electrolytic cell inhibitor added. The defects occurred only in panels constructed with the welded galvanized wire mesh. An electrolytic cell appeared to form between the zinc galvanizing coating and the steel exposed by the joint welding action. The pattern of defects shown in Fig. 8 supports this hypothesis. Christensen and Williamson [21] recommended the addition of up to 300 parts per million of chromium trioxide to the mortar mix water. Increasing the amount of additive might have reduced the gas production in the panels but was not tried. The bubble defect problem was effectively eliminated by boiling all the wire mesh used in the test program for twenty minutes in a solution of five pounds of tri-sodium phosphate to twenty-five gallons of water. The original reason for the boiling process was to clean the mesh of any oils or other contaminants present on the wire when received from the manufacturer. A small amount of a white precipitate collected on the mesh welds following the boiling process. Similar weld joint

appearances were observed on identical mesh exposed to the weather for a few weeks during actual boat construction.

C. EXPERIMENTAL PROCEDURE

1. Testing System

The fatigue specimens were cycled in load control at 30 hertz using a Baldwin Locomotive Works Sonntag Model SF-1U fatigue testing machine. The specimens were loaded in pure bending using the specimen holder shown in Fig. 9. This arrangement provided a sinusoidally varying moment of equal magnitude through the center eight inches of the ferro-cement specimen. The machine was set for a zero mean load. Due to a small curvature in many of the specimens, a preload was induced when clamping the specimens in the test machine grips. This problem was noted after several specimens were tested. For subsequent specimens in groups 1PXX and 2PXX, the initial preloads due to specimen irregularities were noted. A series of tests to check the magnitude of the induced preload as a function of the number of cycles and the applied stress indicated that the induced preload lessened as the cycles increased. The rate of reduction appeared to increase with the magnitude of the applied stress. For the 4EXX specimen groups, the machine was set to compensate for specimen irregularities and all specimens of those groups were tested at a zero mean load. Examination of the data revealed no trends due to the presence of an initial induced preload; however, the preloads would be expected to cause the test results to be somewhat conservative.

An electrical cycle counting system provided the number of completed cycles to the last elapsed thousand. Power to the test machine was stopped by cut-off switches when the cyclic amplitude

exceeded one-half inch.

2. Stress Calculation

The failure stress for each specimen was calculated after failure. Mean specimen thickness and width adjacent to the failure point were measured to an accuracy of 0.01 inches. The specimen was then treated as a homogeneous beam and simple beam theory was applied to determine the failure stress. The equations used are shown in part one of Appendix A.

3. Failure Criteria

Test specimen failure was defined as the point at which the test specimen stiffness was sufficiently reduced to allow the specimen deflection to exceed one-half inch over an eight inch free beam length. This action was accompanied by pieces of mortar being thrown from the specimen, leaving no doubt as to the validity of the failure. Figure 10 shows a typical failure. The test machine stopped automatically upon failure of the specimen. Only two specimens out of 132 tested broke completely into two pieces. Some of the reinforcement normally remained intact, even though the mortar had completely failed.

4. Error Analysis

Each fatigue test was set up independently of the other tests except for the general loading level. No attempt was made to obtain a series of data points at a specific stress level. Since the specimen beams often varied in thickness over their length as much as several hundredths of an inch, it was considered more accurate to determine the failure stress based upon the actual location of the failure. Loads set into the test machine were chosen to provide a data point within a broad stress range. This method resulted in a pattern

of data points grouped primarily by the natural ferro-cement fatigue characteristics.

Data scatter for this test program was attributed to two primary causes. The major cause was variations in the test specimens. Although carefully fabricated, specimens often varied in trueness, thickness, and surface finish quality. The trueness problem resulted in some preload ef ects which have already been discussed. The surface finish differences appeared to have little, if any, effect upon the test results; however, no specimens with major surface defects such as grooves or cavities were tested. The specimen thickness differences were due to variations in the thickness of the unreinforced mortar layer on the surface of the ferro-cement, since the reinforcing mesh assembly was as identical as possible for all specimens. Bigg [22] defines a parameter called the "specific surface of reinforcement (K)" as the ratio of the total wire surface in contact with the mortar to the volume of the composite. If the composite volume is defined to include the surface mortar layer for this study, then K provides a comparative measure of the surface mortar layer thickness. Smaller values of K signify a thicker surface mortar layer. Boat builders usually try to maintain the surface mortar layer at a thickness of one to three sixteenths inches. The minimum thickness that will effectively protect the reinforcement from seawater is the optimum configuration. Surface layer thickness in the specimens used in this study varied from one to four thirty-secondths inches. Table III shows the average K for each specimen group and the standard deviation of K within each group. A comparison of the standard deviations of K with the fatigue test data indicates a correlation between cyclic failure

stress and K. No quantitative relationship was discernible due to the other previously discussed variables.

The second cause for data scatter was the error induced by experimental technique. This error was due primarily to the measurements involved in the determination of the applied cyclic stress amplitude. An error analysis on the fatigue stress calculations was performed in accordance with the method suggested by Kline and McClintock [23]. Calibration checks made on the fatigue test machine revealed no measurable errors with respect to load application or cycle frequency. The general error calculation equations are shown in part one of Appendix A. The average error due to experimental technique for each specimen group is shown in Table III.

D. RESULTS AND DATA ANALYSIS

1. S-N Plots

The graphs of failure stress versus cycles-to-failure or "S-N plots" for each of the specimen groups are shown in Figs. 11-21. Data points shown with arrows indicate "runout" or no failure at 10^7 cycles.

The solid line shown on each plot is a least square line based upon all the data points plotted except runouts. The actual mathematical calculations for determining the least square line were accomplished with a computer program. The data points were incorporated into the normal equations for a least square straight line fit and the computer program provided the coefficients. The failure stress was used as the dependent variable for these calculations. A set of solutions with failure stress as the independent variable resulted in slightly more negative slopes to the least square lines. For this study, use of the stress as the dependent variable was an arbitrary

choice.

The estimated endurance limit (S_n) is shown on the plots by broken lines. It should be emphasized that these are merely estimated values based upon the data points as shown in Figs. 11-21. No endurance limit estimate was attempted for Figs. 12, 19, and 21. This does not indicate a lack of confidence in those data sets or in those ferro-cement configurations. It was simply a result of the arbitrarily chosen data smoothing technique.

2. Discussion of S-N Plots

a. Figure 22 illustrates the influence of wire type and curing method on the fatigue life of ferro-cement made with Portland type V cement. The ungalvanized reinforcement group (1PSU and 1PWU) have a distinct fatigue strength advantage over the specimens made with galvanized reinforcement (1PSG and 1PWG.) The water-cured ungalvanized mesh reinforced specimens demonstrated the greatest fatigue strength up to about two million cycles. At that point, the steam-cured (1PSU) group appears stronger. The S-N plots in this case may be misleading. The endurance limit estimates were intentionally very conservative. Upon referring back to Fig. 14, it is apparent that with the exception of only two data points the estimated endurance limit could have been much higher for group 1PWU.

b. Figure 23 shows the influence of wire type and curing method on the fatigue life of ferro-cement made with expansive cement. The overall fatigue response of the expansive cement specimens appears to be more consistent with respect to S-N plot slope than did the Portland type V ferro-cement specimens. This may be partially due to the controlled zero preload procedure used for the fatigue tests

on the 4EXX groups.

c. Figure 24 demonstrates the relative effects of galvanized and ungalvanized reinforcement upon the fatigue life of ferro-cement made with Portland type V cement and a 0.40 water-to-cement ratio.

d. Figure 25 illustrates the influence of reinforcement orientation, water-to-cement ratio, and cement type on the fatigue life of ferro-cement. All of these specimen groups were fabricated with galvanized mesh and water cured. Groups 1PWG, 2PWG, and 4EWG had the mesh stacked parallel to the specimen axis. Group 3PWG had the second, fourth, and sixth mesh layers placed at 45° relative to the specimen axis. Group 2PWG used a 0.40 water-to-cement ratio. The other groups had a 0.45 water-to-cement ratio.

Comparing group 4EWG to group 1PWG shows the influence of cement type. The expansive cement mortar appears to be more fatigue-resistant than the Portland type V cement. The effect of water-to-cement ratio is illustrated by groups 1PWG and 2PWG. The lower ratio appears to provide a more fatigue-resistant ferro-cement. For long life, the skewed-mesh group, 3PWG, was weaker than the other groups.

e. Figure 26 compares wire and cement type effects in steam-cured specimens. The similarity of results between the expansive and Portland type V cement mortars should be noted. The specimens made with ungalvanized wire mesh had longer fatigue lives than those made with galvanized mesh. The specimens made with Portland type V cement were more sensitive to reinforcement type than those in the 4EXX groups.

f. Figure 27 illustrates the effects of mortar type on water-cured specimens fabricated with ungalvanized mesh reinforcement. A

review of the data point distributions shown in Figs. 14 and 21 indicates that the difference between the 1PWU and 4EWU groups was probably not as extreme as shown by Fig. 27. The relative position of the 2PWU plot is not considered representative and is discussed in the next section.

E. CONCLUSIONS

The fatigue life data presented appears generally consistent with the exception of the 2PWG and 2PWU groups. A water-to-cement ratio of 0.40 was expected to result in greater strength characteristics than would a 0.45 ratio. Visual inspection of the 2PWG and 2PWU specimens did not reveal an explanation for their unexpected weakness nor does a comparison of the specific reinforcement data in Table III. The only definable difference noted between the 2PWX groups and the other groups was the Portland type V cement. All Portland type V cement used in the study was purchased from a load prepared for mortaring a large ferro-cement boat. The cement used in fabricating the 2PWG and 2PWU groups was taken from a different sack than was the cement used for the other Portland cement specimens. Although no differences in the cement was noted during fabrication, the particular sack used had been stored for fifty additional days prior to use and the cement was possibly slightly hydrated.

The ungalvanized reinforcement mesh appears to impart greater fatigue resistance to ferro-cement than does the galvanized mesh for all mortar variations tested. For a 0.45 water-to-cement ratio, the steam-cured expansive mortar appears to be about equal in fatigue strength to the Portland type V mortar. The water-cured expansive

cement with ungalvanized mesh reinforcement was also comparable to the similarly fabricated Portland cement specimens. The test results for the water-cured expansive cement specimens with galvanized mesh reinforcement were significantly better than results for the similarly fabricated Portland type V specimens.

IV. DYNAMIC MODULUS OF ELASTICITY

A. BACKGROUND

A series of tests conducted by Simpson and Tucker [20] indicated a decrease in the flexural modulus of elasticity for ferro-cement beams subjected to constant amplitude cyclic deflections. The test machine used in that series was an Automation Industries model VSP-150. Figure 28 shows the test machine and a specimen mounted as a cantilever beam. Figure 29 is a typical plot of the flexural modulus of elasticity (E_f) versus cycles developed during the constant amplitude cyclic deflection tests. Although the magnitudes and durations differed, the shape of the E_f versus cycles curve was similar to those shown by Moore and Kommers [24] for unreinforced concrete in cyclic compression. The data for Fig. 29 was determined by cycling the specimen a chosen number of times, stopping the test machine, and statically measuring the specimen deflection due to a constant applied load. Data for this study shown in Fig. 30 were taken during actual bending fatigue tests in load-control. Since the load-control fatigue tests were not interrupted, a dynamic modulus of elasticity rather than a static flexural modulus was measured.

B. TEST SPECIMENS

The test specimens for the dynamic modulus of elasticity measurements were chosen at random from the fatigue test specimens. Specimen group definitions as described in Table I apply to group references in this chapter.

C. EXPERIMENTAL PROCEDURE

1. Testing System

Dynamic modulus measurements were made upon fatigue specimens during actual fatigue tests. Total specimen deflection at the specimen midpoint was measured with a wedge vibrometer installed on the test machine vertical motion platen. Due to bending fixture geometry, the vertical motion platen deflection is equal to the maximum specimen deflection until specimen failure is imminent.

2. Dynamic Modulus of Elasticity Calculations

The maximum half-cycle amplitude and the maximum bending stress were used in the equation shown in part two of Appendix A to calculate the dynamic modulus.

3. Error Analysis

Dynamic modulus of elasticity error due to experimental technique was calculated using the method suggested by Kline and McClintock [23]. The general error equation is shown in part two of Appendix A. Maximum experimental error indicated by the analysis was plus or minus eight percent.

D. RESULTS AND DATA ANALYSIS

Dynamic moduli of elasticity versus cycles for three ferro-cement variations are presented on Fig. 30. Applied cyclic loading was adjusted

to provide 1750 psi maximum cyclic stress for all three specimens. The water-cured expansive mortar specimen (4EWG) maintained a higher value of dynamic modulus than did the similarly reinforced Portland ferro-cement specimen. A comparison of the specimens from groups 1PWU and 1PWG indicates that the ungalvanized reinforcement is superior to the galvanized mesh.

E. CONCLUSIONS

The dynamic modulus of elasticity for ferro-cement is dependent upon a complex relationship of several variables. The investigation performed in this study did not provide sufficient data to allow quantification of the relationship. It did show a definite pattern of decreasing flexural stiffness with increasing cycles. For stress levels sufficiently below some undetermined percentage of the failure stress, ferro-cement appears to attain a fairly elastic configuration after an initial period of microscopic cracking.

V. MONOTONIC TESTS

A. BACKGROUND

Physical properties reported for ferro-cement are highly dependent upon the specific ferro-cement configuration tested. Proper utilization of ferro-cement test results requires a thorough knowledge of the fabrication technique and reinforcement arrangement used in the tested specimens. The compressive mortar strength and the reinforcement tensile strength should also be known. The initial flexural strength and flexural modulus of elasticity are basic considerations for any design or material comparison involving ferro-cement.

B. BEAM FLEXURE

1. Test Specimens

Test specimens for the beam flexure tests were chosen at random from the uncycled fatigue test specimens. The same test group definitions described by Table I apply to the group references in this section.

2. Experimental Procedure

a. Testing System

The specimens were loaded as shown in Fig. 31. The downward force applied at position "a" on Fig. 31 was transmitted to the specimen at positions "b" and "c". This method provided a constant moment across the specimen beam section between positions "b" and "c". Beam deflection was measured to within 0.001 inches at the midpoint of section "b-c". The applied load was recorded for every 0.050 inches deflection of the specimen midpoint. The load corresponding to the initial detection of visible cracking was recorded. All tests were conducted at a loading rate of approximately 200 pounds per minute.

b. Monotonic Flexural Strength

Monotonic flexural stress values were calculated using simple beam theory. The general equations are shown in part four of Appendix A.

Three distinct strengths were calculated. The ultimate strength was determined from the maximum supportable load. The first visible crack strength was calculated from the load required to cause visible cracks in the ferro-cement tension surface. The third measure of flexural strength was designated as the "flexural yield strength."

Various definitions related to yield strengths have been used by experimenters in ferro-cement. Haynes and Tancreto [19] defined a "first cracking strength" as the point at which the tangent modulus of the reinforced panels equaled the tangent modulus of the unreinforced mortar panels at failure. McKenny [18] used the point of departure of linear load-strain response (proportional limit) to define an "initial cracking tensile stress" for steel-fiber-reinforced concrete tensile tests. It was initially intended that the first cracking strength as defined by Haynes and Tancreto [19] would be reported for the ferro-cement configurations used in this study. However, after the desired number of fatigue specimens had been fabricated, the amount of quarry sand remaining was insufficient to allow fabrication of the unreinforced mortar beams required for determination of first cracking strengths. Rather than use a different batch of quarry sand for the plain mortar beams, a flexural yield strength was defined for this study in a manner that would be simple for other experimenters to apply to their own data for comparison. The flexural yield strength for this study was defined as the point on the flexural stress-deflection curve at which the tangent modulus was equal to the secant modulus at ultimate strength. The ratios of visible first crack strength to ultimate strength (S_v/S_u), proportional limit to ultimate strength (S_p/S_u), and flexural yield strength to ultimate strength (S_y/S_u) are shown in Table IV. The standard deviation of these ratios for the eleven ferro-cement configurations tested were calculated as shown in part 3 of Appendix A. The data presented in Table IV indicate a more consistent relationship between yield strength and ultimate strength than was observed for either the first

visible cracking or proportional limit criteria. A comparison of results with other data [19] suggested that the yield strength to ultimate strength ratio is a function of reinforcement relative volume and dispersion.

c. Monotonic flexural moduli of elasticity were calculated from stress-deflection data taken from the linear portion of the stress versus deflection curves. The pertinent equation is shown in part 5 of Appendix A.

3. Results and Data Analysis

a. Stress versus Deflection

The graphs of flexural stress versus deflection for each of the eleven ferro-cement test variations are shown in Figs. 32-35. The upper endpoint for each curve signifies the ultimate specimen flexural strength (S_u). The data points marked with a "y" or a"Y" indicate respectively the first visible cracking and the flexural yield strengths.

b. Data Comparisons

Figure 36 illustrates the effects of water-to-cement ratio and mesh type variations on water-cured Portland type V ferro-cement. The ungalvanized mesh reinforcement specimen with 0.45 water-to-cement ratio (1PWU)exhibited the greatest monotonic strength. Figure 37 indicates that the monotonic strength of the steam-cured Portland cement specimen (1PSG) with galvanized reinforcement was greater than a similarly-fabricated expansive mortar ferro-cement specimen (4ESG). The steam-cured Portland specimen with ungalvanized mesh (1PSU) had a higher monotonic flexural strength than did the expansive ferro-cement specimen (4ESU) as shown in Fig. 38. Figure 39 indicates that the

water-cured Portland ferro-cement specimen with galvanized mesh (1PWG) was not as strong in simple bending as was the water-cured expansive mortar specimen with the same type of reinforcement (4EWG). Figure 40 shows the water-cured Portland ferro-cement specimen with ungalvanized mesh (1PWU) to be significantly stronger in monotonic flexure than the expansive ferro-cement specimer with ungalvanized reinforcement (4EWU). Table V presents a tabulation of monotonic and cyclic flexural data. Table VI shows the relationship between fatigue and monotonic strengths for the 1PXX and 4EXX specimen groups.

4. Conclusions

Comparison of the monotonic and cyclic flexure data indicates several inconsistencies. Since the monotonic data were taken from single representative specimens, it was expected that some relative cyclic and monotonic strengths would not agree. The expansive mortar specimens generally appear to have a lower monotonic strength than the Portland type V ferro-cement specimens; yet the expansive mortar specimens exhibit a greater fatigue-resistance.

C. UNREINFORCED MORTAR COMPRESSION

1. Test Specimens

Plain mortar cylinders four inches in diameter and eight inches long were formed in wax-impregnated cardboard tubes. Mortar compositions were identical to the mortars described in Table I for the 1PXX and 4EXX specimen groups. Three cylinders of both mortar types were steam-cured and three of each were water-cured. Although the cylinders were not made at the same time as the fatigue specimens, special care was exercised to ensure that mixing and curing procedures were identical to those used in the fatigue specimen fabrication. After curing,

the cylinders were capped with a commercial sulphur-based capping compound. The capping form and a typical capped cylinder are shown in Fig. 41. The capping was to provide a smooth parallel end surface on the cylinders upon which the compressive load was applied.

2. Experimental Procedure

a. Testing System

Compressive loads were applied with a 350,000 pound capacity Riehle Testing Machine. A spherically-seated loading head was used to transmit the load to the cylinder caps. Strain rate was maintained at 0.050 inches per minute for all compression tests. Cylinder strain was measured with the device shown in Figure 42. A Bentley-Nevada Model 304 proximity head connected to a Brush Mark 280 recorder provided a continuous record of mortar strain. The gage length was set at four inches. Pre-determined load points were manually marked on the strain record traces. The barrel micrometer installed as shown in Fig. 42 was used as the proximity head sensing surface and for calibration of the strain measurement system prior to each compression test.

b. Compressive Modulus of Elasticity (E_c)

The average unreinforced mortar compressive moduli of elasticity were calculated from the linear portion of the recorded load-strain data.

c. Ultimate Mortar Compressive Strength (S_c)

The applied load at cylinder failure was divided by the cylinder cross-sectional area to provide the ultimate compressive strength for plain mortar. Cylinder failure was sudden and violent in each test. Multiple shear planes were observed in failed cylinders of each mortar variation. A typical cylinder failure is shown in Fig. 43.

3. Results

The mortar compressive moduli of elasticity (E_c) and ultimate compressive strengths (S_c) are presented in Table V. All data were taken on the first compression cycle. Both E_c and S_c changed if the cylinder were cycled prior to taking data. This procedure allowed two cylinders for each mortar variation to be used in determining E_c and one with which to determine S_c for each variation.

The 0.45 water-to-cement ratio steam-cured Portland type V mortar demonstrated a lower E_c and S_c than did the water-cured Portland cement mortar. The water-cured expansive cement mortar showed a higher E_c but a lower S_c than did the steam-cured expansive mortar.

The relationship between the expansive mortar compressive and flexural strengths is not actually an inconsistency. The expansive cement is designed to develop its strength through a pre-stressing mechanism that is dependent upon the restraint provided by the reinforcing mesh. The mortar compression test specimens in the study had no reinforcement; therefore, the expansive mortar compression test results were not indicative of the true mortar strength.

D. REINFORCING MESH TENSILE STRENGTH

1. Test Specimens

Test specimens were fabricated as shown by specimen "A" in Fig. 44. Each test portion consisted of three welded mesh joints and the six adjacent wire sections parallel to the direction of the applied tensile force. The gripping tabs consisted of sulphur-based cylinder capping compound formed in a small mold in which the wire mesh test pieces had been positioned. Four reinforcing mesh variations were

tested. Three specimens each of the galvanized and ungalvanized welded mesh were prepared with the tensile force direction parallel to the long axis of the mesh as unrolled from the shipping roll. This was the mesh axis which was aligned parallel to the long specimen axes in both the cyclic and monotonic beam flexure test specimens. A similar set of tensile specimens were prepared with the transverse mesh wires placed in the direction of the tensile force.

2. Experimental Procedure

a. Testing System

The specimens were tested to failure in tension using an Instron Model 1102 testing machine. The tests were conducted at a constant strain rate of 0.20 inches per minute. A continuous record of load versus strain was maintained by the Instron recorder.

b. Average Failure Stress

The recorded load versus strain data provided the failure load for each of the three wires in each specimen. The failure loads were averaged and divided by the original wire cross-sectional area to provide the average engineering failure stress for each type of wire mesh.

3. Results

The reinforcement wire tensile test results are shown in Table VII. All failures occurred in a manner similar to that shown by specimen "B" in Fig. 44. The weakest regions in the reinforcing mesh appeared to be at or immediately adjacent to the mesh welds. The average failure stress data presented in Table VII indicates a definite strength advantage for the mesh oriented with the long axis of the mesh as unrolled from the shipping roll placed parallel to the direction of

tensile load. For that orientation, the ungalvanized mesh is stronger than the galvanized mesh.

4. Conclusions

For tensile loads applied to mesh aligned parallel to the fatigue specimen long axes, the ungalvanized mesh was stronger than the galvanized mesh. This is generally consistent with both the cyclic and monotonic flexure test results. The major inconsistency occurs in the monotonic flexure tests on the specimens from groups 4EWG and 4EWU. Cyclic failure data for these groups show the specimens made with ungalvanized mesh to be stronger than the specimens with galvanized mesh.

VI. FRACTURE INVESTIGATION

A. EXPERIMENTAL PROCEDURE

The investigation of the ferro-cement fatigue fracture region was conducted with a Cambridge Stereoscan scanning electron microscope (SEM) and a binocular visual microscope. The magnification range of the SEM was from 20X to 100,000X. The visual microscope could be adjusted up to 30X.

Specimen size for the SEM was restricted to about five millimeters thick and ten millimeters square. SEM specimens were required to be clean and free from loose particles since the observations were made in a mechanically-maintained vacuum. A freon aerosol was the most effective cleaning agent used, leaving almost no residue on the specimen. No specimen preparation was required for the visual microscope since an entire fatigue specimen could be mounted for viewing.

B. MORTAR/REINFORCEMENT INTERFACE

Figures 46 through 59 show the mortar-to-reinforcement interfaces of each of the Portland type V and expansive cement mortars. The rounded, deep-appearing voids in the interfaces were caused by gas or air bubbles in the mortar. The shallow, rough-edged voids were due to mortar adhering to the reinforcement wire. Cement products usually appeared slightly darker than did the aggregate particles, indicating that the cement products were somewhat more electrically conductive than the aggregate particles. In Figs. 46, 51, and 54, a few particles of cement products appear lighter than the rest of the specimen. This is due to these particles having retained a higher charge from the electron beam. These particles were poorly connected to the specimen and electrical grounding effects were therefore poor.

A comparison of the figures indicates that a better mortar-to-wire bond is achieved by the ungalvanized wire than by the galvanized. There appears to have been a chemical reaction at the mortar/galvanized wire interface, especially in the steam-cured specimens. This was apparent in all cases except the 1PWG and 1PWU groups. It was believed that the bubble voids shown in Fig. 51 were due to insufficient vibration during fabrication of the original ferro-cement panel. The panels were all mortared in a horizontal position and the placement of the mortar trapped air within the ferro-cement. The proper degree of mechanical vibration applied during mortar placement released the entrapped air while it also enabled full mortar penetration of the reinforcement mesh matrix. Excessive vibration caused aggregate separation and mortar mix water to migrate to the panel surface. Accordingly, vibration time was held to the minimum believed necessary and vibration was thought to

have been inadequate for the IPWU panels. Air entrapment does not appear to be a significant problem in mortar placement on non-horizontal surfaces, such as boat hulls.

The water-cured mortars appear to make a more complete bond with the reinforcement than do the steam-cured mortars. Additionally, the expansive mortars generally seem to bond with the wire better than the Portland mortars.

C. REINFORCEMENT FAILURE

Figures 60 through 71 show ferro-cement reinforcement mesh wire failure surfaces. Figures 60 through 63 are SEM photos of wires that failed during the reinforcement mesh tensile tests described in Chapter V. Figures 64 through 67 show the fracture surfaces of wires removed from the fourth (middle) mesh layer of ferro-cement fatigue specimen fracture surfaces. Figures 68 through 71 show wires from the first (outer) layer of ferro-cement fatigue specimens. These wires were also removed from the ferro-cement fatigue specimen fracture surface.

Figures 60-63 show classic ductile failures. The failures from the inner mesh layers were all similar in appearance to Figs. 64-67 and were also simple ductile failures. In Fig. 67, the ductile failure dimples can be seen in the central portion of the picture. The rest of the picture shows the effects of the broken wire ends rubbing together during the cyclic bending of the ferro-cement specimen. The wire fracture surfaces shown in Figs. 68-71 show some strain-hardening of the wire as evidenced by the lesser "necking down" prior to failure. Close examination of Figs. 69 and 71 reveals ductile dimples almost obliterated by the wear induced by the cyclic motion of the ferro-cement

fatigue specimen. The small striation marks at position "a" in Fig. 69 resemble fatigue striations; however, the marks are on a piece of beaten-over material and are due to cyclic wearing action.

In summary, no evidence was found to indicate any reinforcement fatigue failures. During cyclic flexure of the ferro-cement specimens, some cyclic hardening of the outer mesh layers was observed. Wire failure in all cases appeared to have been due to a fairly sudden increase in load applied to the wire, rather than to fatigue of the reinforcement. Further arguments to sustain this conclusion are presented in the next section.

D. MORTAR FAILURE

Ferro-cement beam specimens were observed through the binocular microscope while being manually flexed. Additionally, one-eighth inch thick slices were cut from fatigued and uncycled ferro-cement specimens. These were observed with the binocular microscope at rest and while being flexed. Unaided visual observations were made during the fatigue and monotonic flexure tests.

Flexural strain appeared to be distributed initially throughout the mortar by microcracks similar to that shown in Fig. 49. As the microcracks propagated, the mortar-to-reinforcement bond surface became fragmented as shown in Fig. 59 and the wire assumed more of the load. At some point the mortar in the outer reinforcement layers reached a crack size threshold and cracks such as those shown in Figs. 50, 54, and 56 appeared. This was believed to be the point corresponding to the start of a new elastic "plateau" region in the dynamic modulus of elasticity curves shown in Fig. 30. During cyclic flexure,

the crack size at some specific region in the fatigue specimen started to grow at a higher rate than that for the rest of the specimen. This served to relieve the surrounding mortar volume which in turn accelerated the growth rate of the relieving crack. It was felt that at this time the mortar rapidly ceased to sustain any tensile load and the reinforcement wire in the region of the rapidly growing mortar crack was subjected to a much greater tensile load in a fairly sudden manner. This resulted in the simple ductile wire failures observed in Figs. 64-71. The fatigue specimen would then fail rapidly as the mortar and wires in the inner layers received progressively greater stresses.

The relieving action of the final failure crack is illustrated by a comparison of Figs. 72 and 73. Figure 72 shows the surface crack pattern of an uncycled fatigue specimen which failed in a monotonic bending test. The strain was obviously well-distributed along the beam length. At some crack size threshold, the mortar ceased to sustain additional tensile loading and the specimen would support no higher load, thereby reaching the previously defined ultimate stress (S_u).

Figure 73 shows a bending fatigue failure. The surface cracks do not appear to have developed into a well-defined pattern prior to the start of the final failure crack. Additionally, they could not be seen without wetting the specimen since they are much smaller cracks than those shown in Fig. 72. Damage due to fatigue failure appears to be highly localized, leaving the rest of the specimen with significant strength and elasticity.

Examination of slices and whole ferro-cement specimens during flexure did not reveal a preferred crack initiation site. Much of the aggregate was of the same size as the reinforcement wire and cracks appeared to start at any discontinuity, whether at mortar-to-wire interfaces, cementious product-to-aggregate interfaces, or even voids. Propagating cracks were either stopped or turned at wire or aggregate interfaces. No splitting of aggregate particles was observed.

E. CONCLUSIONS

Failure of ferro-cement in either fatigue or monotonic flexure appears to be primarily a function of the mortar strength and elasticity. The reinforcement serves to distribute the loading throughout the mortar as long as the load-carrying capability of the wire is sufficiently high. Under fatigue loading, the wire was observed to be unable to carry the load after the mortar cracks had sufficiently developed.

VII. CONCLUSIONS AND RECOMMENDATIONS

A. CONCLUSIONS

The data developed by this study indicates that of the specimens tested, the best overall ferro-cement variation was the ungalvanized mesh with a water-cured mortar. The water-cured expansive cement mortar appeared to be slightly more fatigue-resistant, but the water-cured Portland type V mortar showed greater short-term strength. It should be noted that although the ungalvanized-mesh-reinforced ferro-cement was stronger than the galvanized-mesh configuration in this

study, the effects of seawater penetration and subsequent deterioration upon painted and plain ferro-cement fatigue strengths have yet to be evaluated. Until load-control cyclic flexure tests are conducted on both the galvanized and ungalvanized reinforcement ferro-cement configurations exposed to seawater, it would be unsafe to assert that one type of reinforcement is better than the other.

Table VI suggests a rough rule-of-thumb for estimating the flexural strength at 10^7 cycles for the ferro-cement configurations tested. The average strength at 10^7 cycles of the Portland type V cement ferro-cement specimens was 15% of their ultimate monotonic stress; for the expansive cement specimens, the average endurance limit to monotonic strength ratio was 20%. It should be noted from Table V that the monotonic strengths for the expansive mortar ferro-cement were less than those for the Portland specimens.

B. RECOMMENDATIONS

In addition to the load-control fatigue tests in seawater previously discussed, the effects of cycle frequency and specimen size upon ferro-cement fatigue response require investigation. Applied stresses for this study were primarily uniaxial. Biaxial fatigue stress effects on ferro-cement fatigue-life should be examined. The behavior of ferro-cement subjected to high stress, low cycle fatigue is an additional topic of interest to ferro-cement designers.

This study has raised more questions than it has answered. The future development of ferro-cement technology depends heavily on the experimental and analytical research applied to increasing the available data on ferro-cement. The opportunities for original research in ferro-cement have only been touched upon.

APPENDIX A CALCULATIONS

1. Fatigue Stress*

Using simple beam theory:

$$S = \frac{Mh}{2I} = \frac{6M}{bh^2} \text{ (psi)}$$

However,

$$M = \frac{RP}{2} = 3P \text{ (lbf-in)}$$

Therefore,

$$S = \frac{18P}{bh^2} \text{ (psi)}$$

where

S = applied fatigue bending stress (psi)

M = applied bending moment amplitude (lbf-in)

P = amplitude of cyclic force produced by test machine (lbf)

R = fatigue bending fixture moment arm (6 in)

h = specimen thickness (in)

b = specimen width (in)

I = specimen cross-section moment of inertia

---

*Refer to Figs. 9 and 74 for illustrations of variables.

The general error equation from Kline and McClintock [23] is:

$$\text{error} = \pm\sqrt{\left(\frac{\partial S}{\partial P}\omega_1\right)^2 + \left(\frac{\partial S}{\partial b}\omega_2\right)^2 + \left(\frac{\partial S}{\partial h}\omega_3\right)^2}$$

and $\omega_1 = 1.0$ lbf
$\omega_2 = 0.01$ in
$\omega_3 = 0.01$ in

} estimates of maximum parameter error

Thus the fatigue stress error equation becomes:

$$\text{error} = \pm\sqrt{\left(\frac{1}{bh^2}\right)^2 \left[324 + \left(\frac{0.18P}{b}\right)^2 + \left(\frac{0.36P}{h}\right)^2\right]}$$

2. Dynamic Modulus of Elasticity in Cyclic Bending*

The dynamic modulus is defined as:

$$E_d = \frac{SRL}{hy} = \frac{18PRL}{bh^3y} = \frac{864P}{bh^3y} \text{ (psi)}$$

where E_d = dynamic modulus of elasticity (psi)

S = applied fatigue bending stress (psi)

P = amplitude of cyclic force produced by the test machine (lbf)

R = fatigue bending fixture moment arm (6 in)

L = specimen free beam length (8 in)

h = specimen thickness (in)

b = specimen width (in)

y = one-half peak-to-peak specimen deflection (in)

---

*Refer to Figures 9 and 74 for illustrations of variables.

The general error equation from Kline and McClintock [23] is:

$$\text{error} = \pm\sqrt{\left(\frac{\partial E_d}{\partial P}\,\omega_1\right)^2 + \left(\frac{\partial E_d}{\partial b}\,\omega_2\right)^2 + \left(\frac{\partial E_d}{\partial h}\,\omega_3\right)^2 + \left(\frac{\partial E_d}{\partial y}\,\omega_4\right)^2}$$

$$\left.\begin{aligned} \text{and } \omega_1 &= 1.0 \text{ lbf} \\ \omega_2 &= 0.01 \text{ in} \\ \omega_3 &= 0.01 \text{ in} \\ \omega_4 &= 0.01 \text{ in} \end{aligned}\right\} \quad \text{estimates of maximum parameter error}$$

Thus the dynamic modulus of elasticity error equation becomes:

$$\text{error} = \pm\sqrt{\left(\frac{864}{bh^3y}\right)^2 \left[1 + \left(\frac{0.01P}{b}\right)^2 + \left(\frac{0.03P}{h}\right)^2 \left(\frac{0.01P}{y}\right)^2\right]}$$

3. Standard Deviation

Standard deviation is defined as:

$$\text{std. dev.} = \sqrt{\frac{\Sigma(X-\bar{X})^2}{N}}$$

where X = data point value

$\bar{X}$ = average of set of data point values

N = number of data points in set

4. Monotonic Flexural Strength

Using simple beam theory:

$$S = \frac{Mh}{2I} = \frac{6M}{bh^2} \text{ (psi)}$$

For the monotonic bending fixture:

$$M = \frac{RP}{2} = \frac{3P}{2} \text{ (lbf-in)}$$

Therefore:

$$S = \frac{9P}{bh^2} \text{ (psi)}$$

where S = applied flexural stress (psi)

M = applied bending moment (lbf-in)

R = monotonic bending fixture moment arm (3 in)

P = total load applied by test machine (lbf)

h = specimen thickness (in)

b = specimen width (in)

I = specimen cross-section moment of inertia

5. Monotonic Flexural Modulus of Elasticity

From simple beam theory:

$$v = \frac{PR}{48E_m I}\left[3L^2 - 4R^2\right] \quad \text{(in)}$$

where

v = deflection of specimen measured at beam midpoint (in)

E_m = monotonic flexural modulus of elasticity (psi)

L = length of beam between load points (14 in)

and the remaining parameters are the same as described for the monotonic flexural strength.

Accordingly,

$$E_m = \frac{414P}{vbh^3} \text{ (psi)}$$

But flexural stress $(S) = \frac{9P}{bh^2}$ from the preceding section.

Thus,

$$E_m = \frac{46S}{hv} \text{ (psi)}$$

Using the linear portion of the stress-deflection curve:

$$E_m = \frac{46\ (S_2 - S_1)}{h\ (v_2 - v_1)} \text{ (psi)}$$

APPENDIX B TABLES

Numerical values presented in these tables have been rounded to reflect measurement accuracy. In Table I, an "X" in a specimen group column signifies that the fabrication element in that row was used in making that specimen group. The "beach" and "quarry" in Table II refer to the source of the particular aggregate. The "Fatigue Stress Error" in Table III was obtained by averaging the stress calculation errors for all the data in each group. The term "as unrolled" in Table VII refers to the reinforcement wire mesh shipping rolls. The mesh was supplied in one hundred feet long, three feet wide strips and rolled into a tight cylinder for shipping.

Table I. Composition of Ferro-Cement Specimens

Fabrication Elements	Specimen Groups										
	1PSG	1PSU	1PWG	1PWU	2PWG	2PWU	3PWG	4ESG	4ESU	4EWG	4EWU
Portland Type V Cement	X	X	X	X	X	X	X				
Expansive Cement (Kaiser CHEMCOMP)								X	X	X	X
Beach Sand (washed, dried, graded)	X	X	X	X	X	X	X				
Quarry Sand (dried)								X	X	X	X
Galvanized Mesh, Parallel Layers	X		X		X			X		X	
Ungalvanized Mesh, Parallel Layers		X		X		X			X		X
Galvanized Mesh 45^{o} Alternate Layers							X				
.025 Pozzolan/Sand Ratio (by wt.)	X	X	X	X	X	X	X				
.5 Cement/Sand Ratio (by wt.)	X	X	X	X	X	X	X	X	X	X	X
.45 Water/Cement Ratio (by wt.)	X	X	X	X			X	X	X	X	X
.40 Water/Cement Ratio (by wt.)					X	X					
160 ppm CRO_3 Water Additive	X	X	X	X	X	X	X	X	X	X	X

TABLE II. Aggregate Sieve Analysis

Tyler Standard Sieve Size	Percent Passing	
	Beach	Quarry
8	100	100
10	99	84
14	93	78
20	64	65
28	39	52
35	25	No data
48	13	No data
80	0.5	3
150	Trace	2
200	0	1

Table III. Specific Reinforcement Surface (K) and Fatigue Stress Error

Specimen Group	K (average) (in^2/in^3)	Std. Deviation of K (in^2/in^3)	Fatigue Stress Error ($\pm$%)
1PSG	5.712	0.65	2.4
1PSU	5.818	0.19	3.9
1PWG	5.512	0.22	3.7
1PWU	6.318	0.47	3.5
2PWG	6.381	0.20	3.7
2PWU	6.284	0.12	3.7
3PWG	5.815	0.36	3.8
4ESG	5.403	0.29	3.7
4ESU	5.409	0.26	3.8
4EWG	6.019	0.25	3.7
4EWU	6.096	0.18	3.5

Table IV. Yield Point Criteria Comparison

Specimen Group	S_v/S_u	S_p/S_u	S_y/S_u
1PSG	0.87	0.55	0.76
1PSU	0.98	0.52	0.79
1PWG	0.90	0.60	0.73
1PWU	0.70	0.48	0.73
2PWG	0.46	0.62	0.87
2PWU	0.47	0.59	0.76
3PWG	0.67	0.61	0.78
4ESG	0.97	0.63	0.76
4ESU	0.67	0.63	0.76
4EWG	0.71	0.51	0.79
4EWU	0.66	0.68	0.79
Std. Deviation	0.17	0.06	0.04

Table V. Cyclic and Monotonic Test Results

Specimen Group	Cyclic Loading		Monotonic Beam Flexure				Mortar Compression	
	S_n*	S_f	S_v	S_y	S_u	E_m	S_c	E_c
1PSG	680		4800	4200	5500	1,350.000	4,400	2,410,000
1PSU		1040	5300	4300	5450	960,000	4,400	2,410,000
1PWG	710		3950	3200	4400	1,230,000	7,050	3,880,000
1PWU	950		5350	5600	7650	1,100,000	7,050	3,880,000
2PWG	900		2050	3800	4400	1,050,000		
2PWU	750		2800	4500	5950	1,100,000		
3PWG	600		3600	4200	5350	1,230,000	4,400	2,410,000
4ESG	750		3550	2800	3650	820,000	6,600	1,100,000
4ESU		860	3200	3600	4750	730,000	6,600	1,100,000
4EWG	950		3950	4400	5550	1,200,000	5,100	1,580,000
4EWU		1100	3150	3800	4800	850,000	5,100	1,580,000

* All table entries in (psi)

Table VI. Fatigue/Monotonic Strength Ratios

Specimen Group	S_n/S_u	S_n/S_y	Specimen Group	S_n/S_u	S_n/S_y
1PSG	.12	.16	4ESG	.21	.27
1PSU	.19	.24	4ESU	.18	.24
1PWG	.16	.22	4EWG	.17	.22
1PWU	.12	.17	4EWU	.23	.29
Average	.15	.20	Average	.20	.25
Std. Deviation	.03	.04	Std. Deviation	.03	.03

Table VII. Reinforcement Wire Tensile Test Results

Specimen Group	Wire Type	Tensile Force Direction	Average Failure Stress (psi)
GA	Galvanized	Long mesh axis as unrolled	125,000
UA	Ungalvanized	Long mesh axis as unrolled	150,000
GB	Galvanized	Short mesh axis as unrolled	118,000
UB	Ungalvanized	Short mesh axis as unrolled	114,000

APPENDIX C - FIGURES

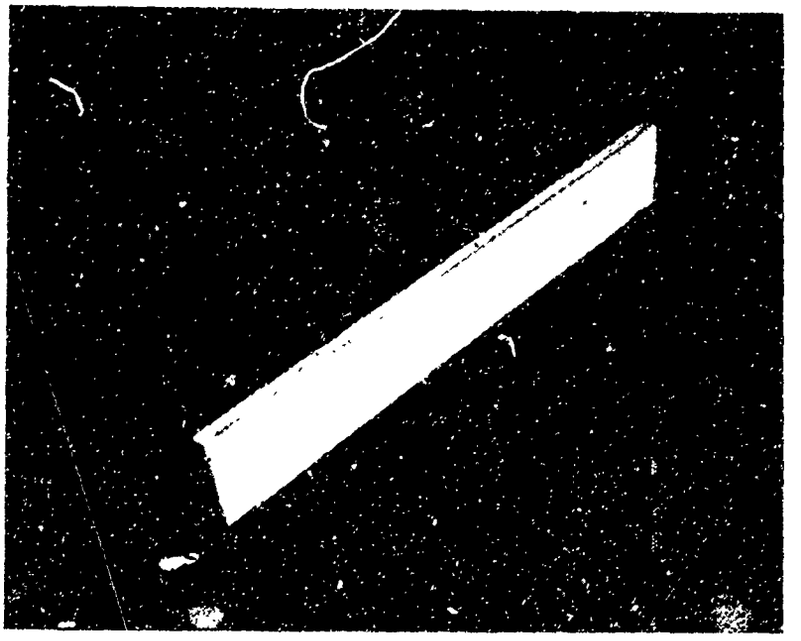

FIGURE 1 TYPICAL FERRO-CEMENT FATIGUE SPECIMEN

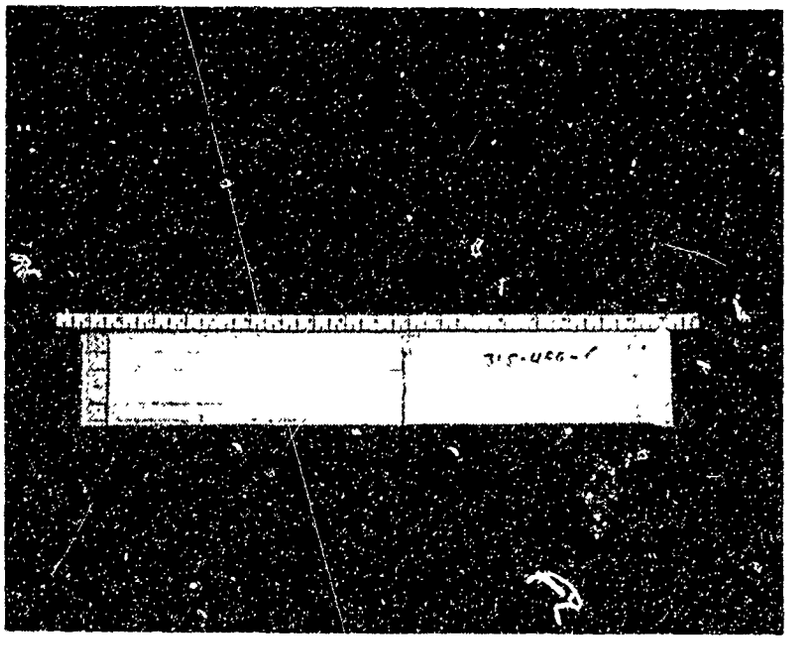

FIGURE 2 TOP VIEW OF FATIGUE SPECIMEN

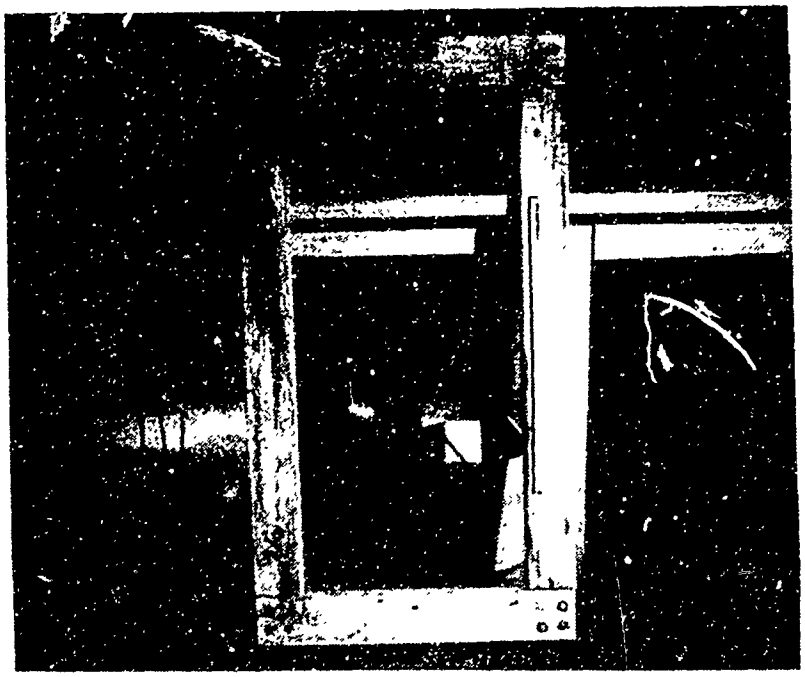

FIGURE 3 FRAME FOR CONSTRUCTION OF FERRO-CEMENT PANELS

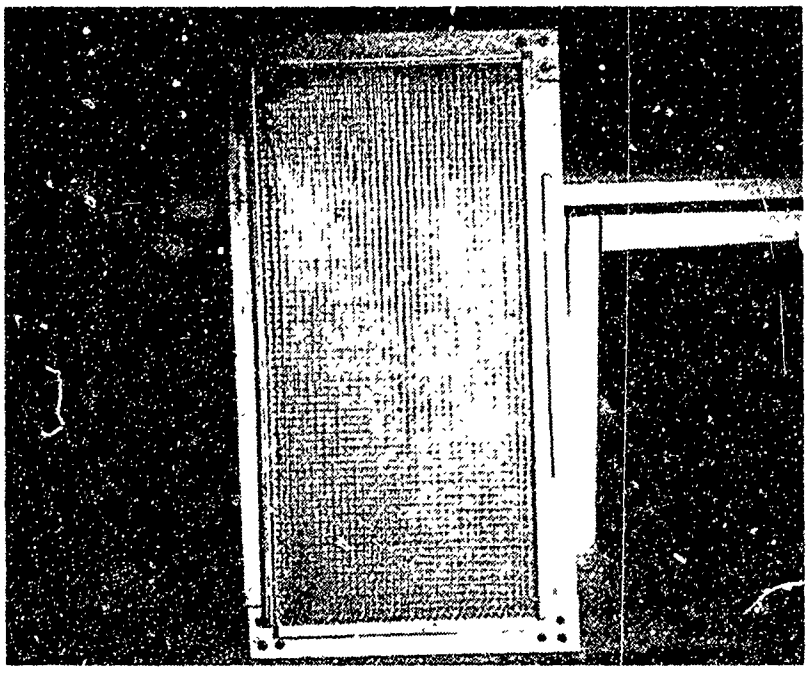

FIGURE 4 COMPLETE FERRO-CEMENT PANEL FORM

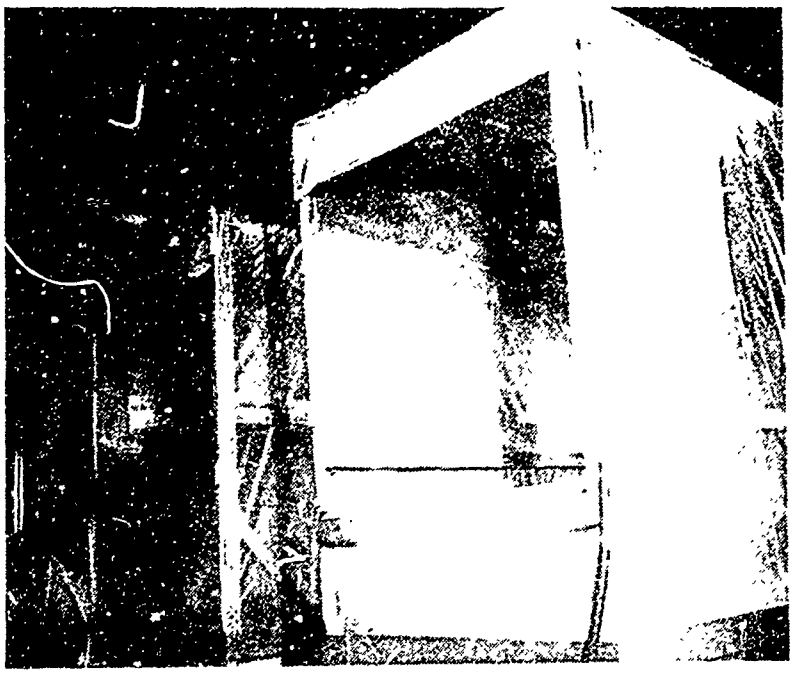

FIGURE 5 WATER AND STEAM CURING CHAMBERS

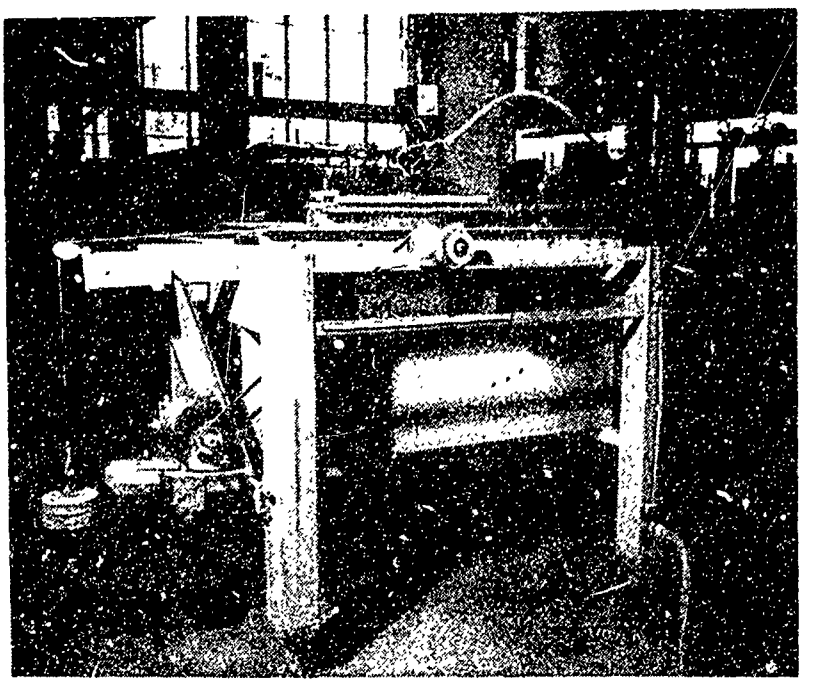

FIGURE 6 SAW ASSEMBLY FOR CUTTING FERRO-CEMENT PANEL

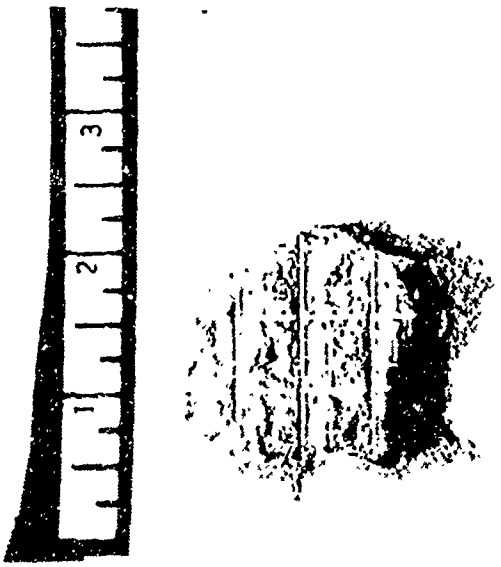

FIGURE 7 LARGE GAS BUBBLE IN FERRO-CEMENT PANEL WITH CRACKED SURFACE MORTAR REMOVED

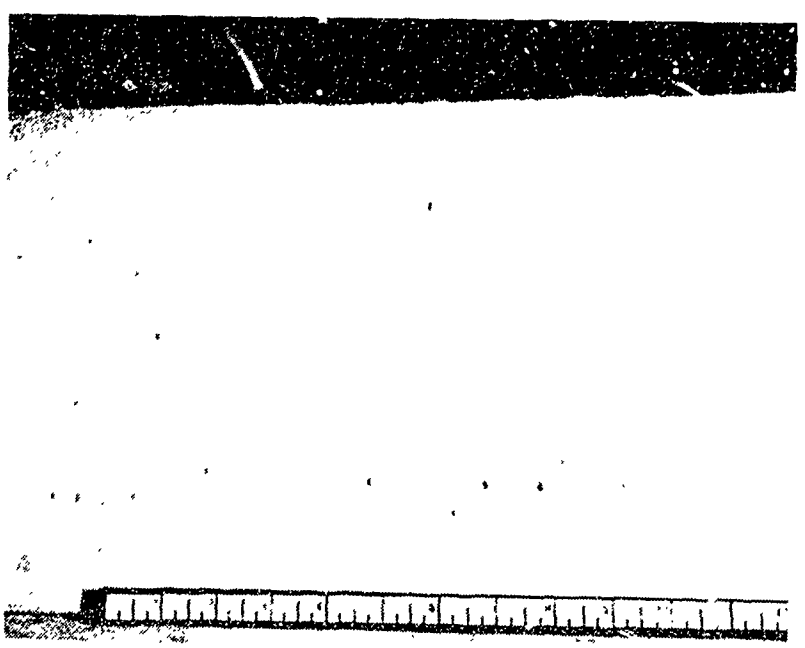

FIGURE 8 FERRO-CEMENT PANEL WITH SMALL GAS BUBBLES

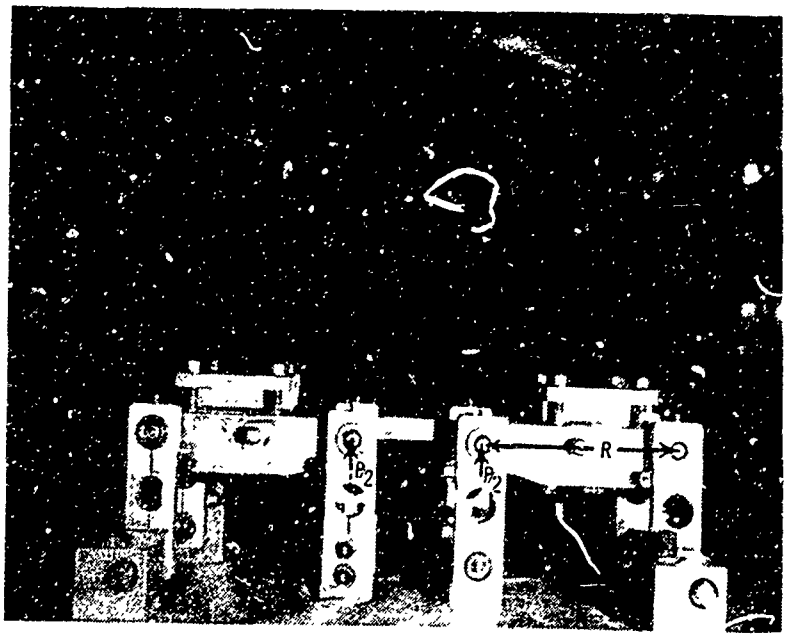

FIGURE 9 CYCLIC BENDING FIXTURE WITH TEST SPECIMEN IN PLACE

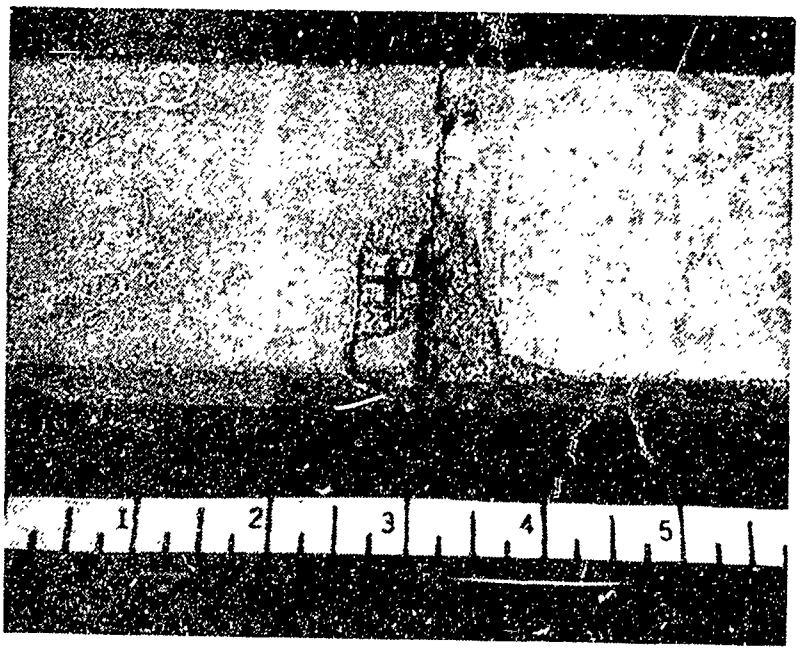

FIGURE 10 TYPICAL FATIGUE FAILURE

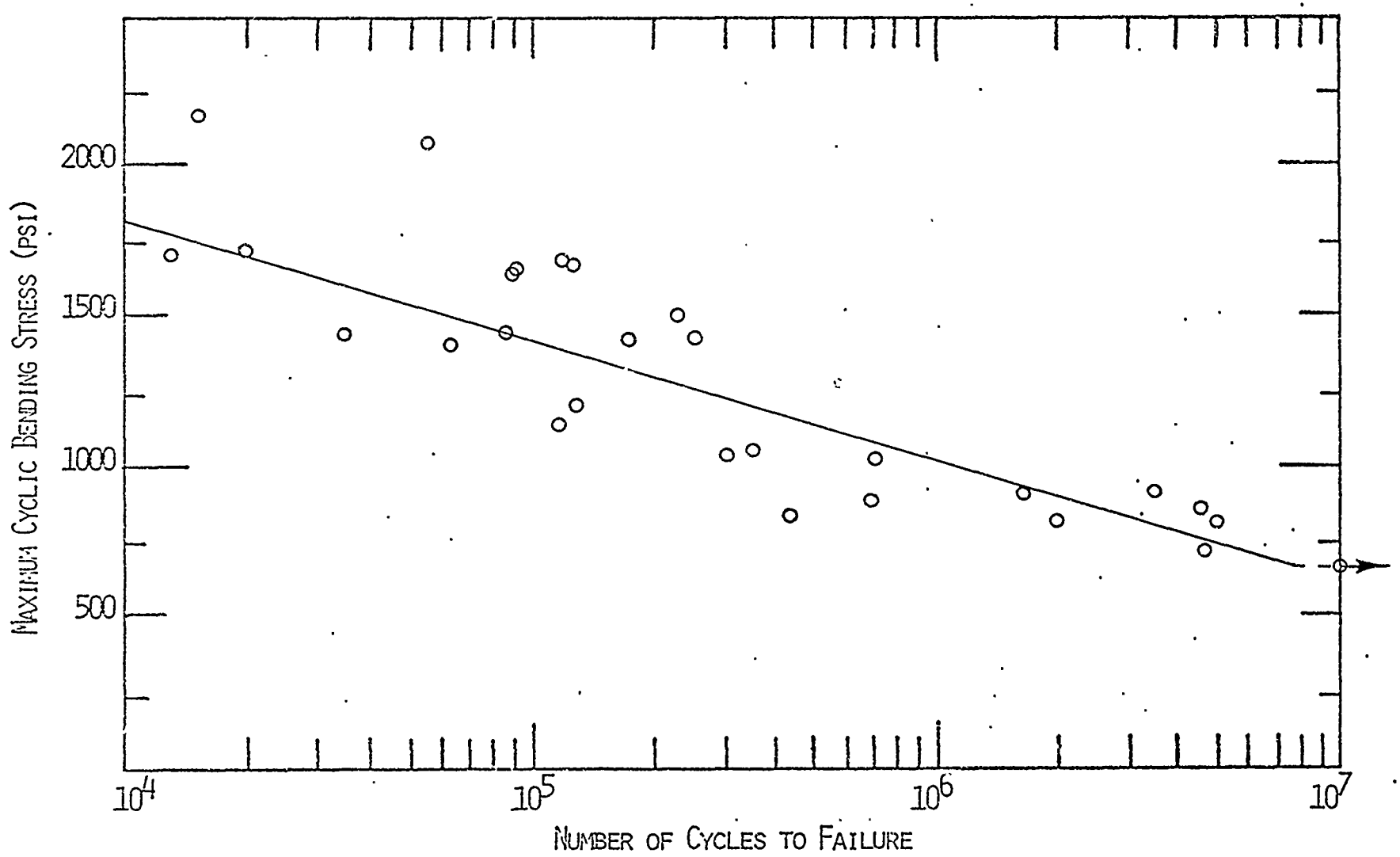

FIGURE 11. S-N PLOT FOR STEAM-CURED FERRO-CEMENT WITH GALVANIZED REINFORCEMENT, PORTLAND TYPE V CEMENT, AND 0.45 WATER-TO-CEMENT RATIO (1PSG)

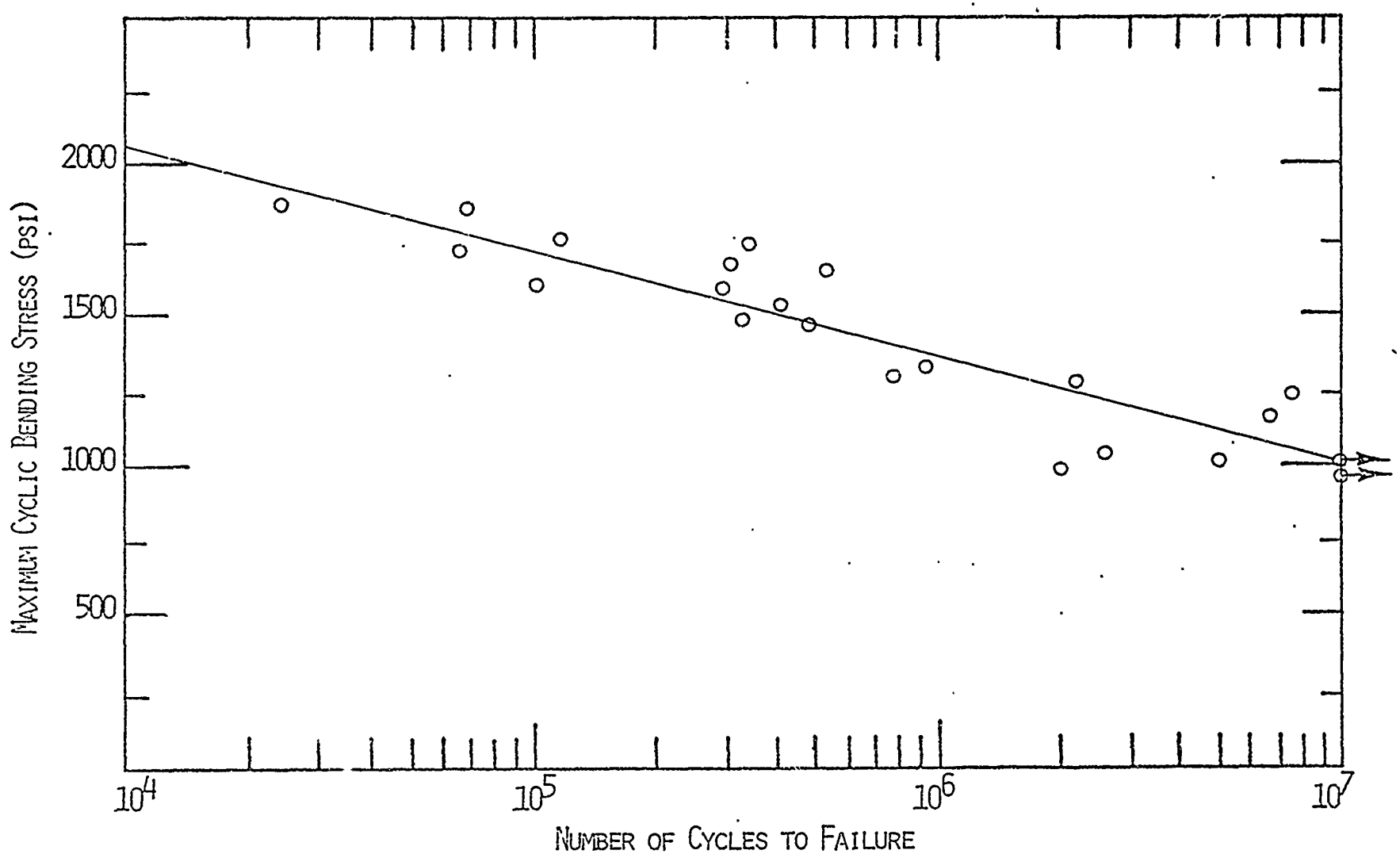

FIGURE 12. S-N Plot for Steam-Cured Ferro-Cement with Ungalvanized Reinforcement, Portland Type V Cement, and 0.45 Water-to-Cement Ratio (1PSU)

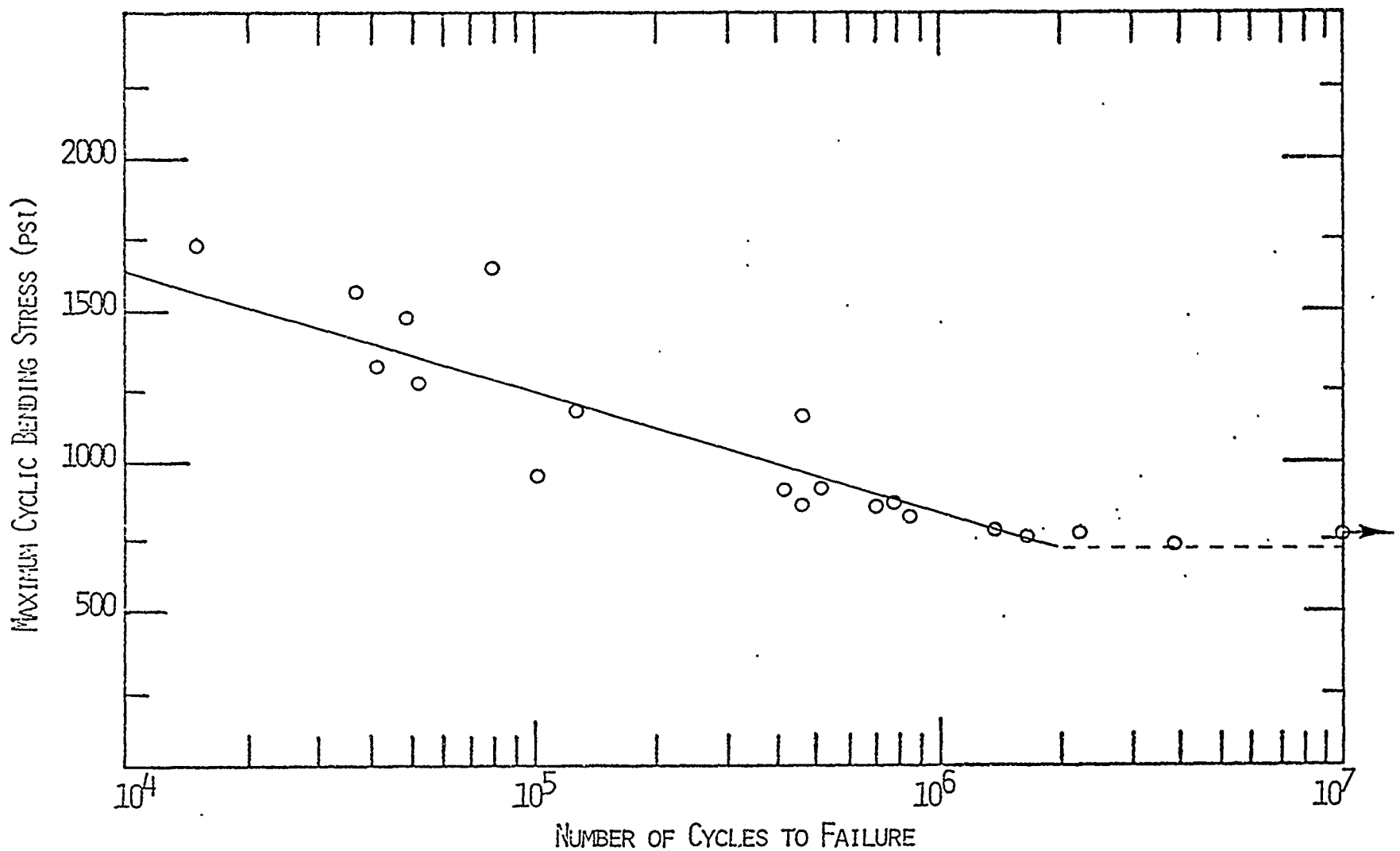

FIGURE 13. S-N Plot for Water-Cured Ferro-Cement with Galvanized Reinforcement, Portland Type V Cement, and 0.45 Water-to-Cement Ratio (1PWG)

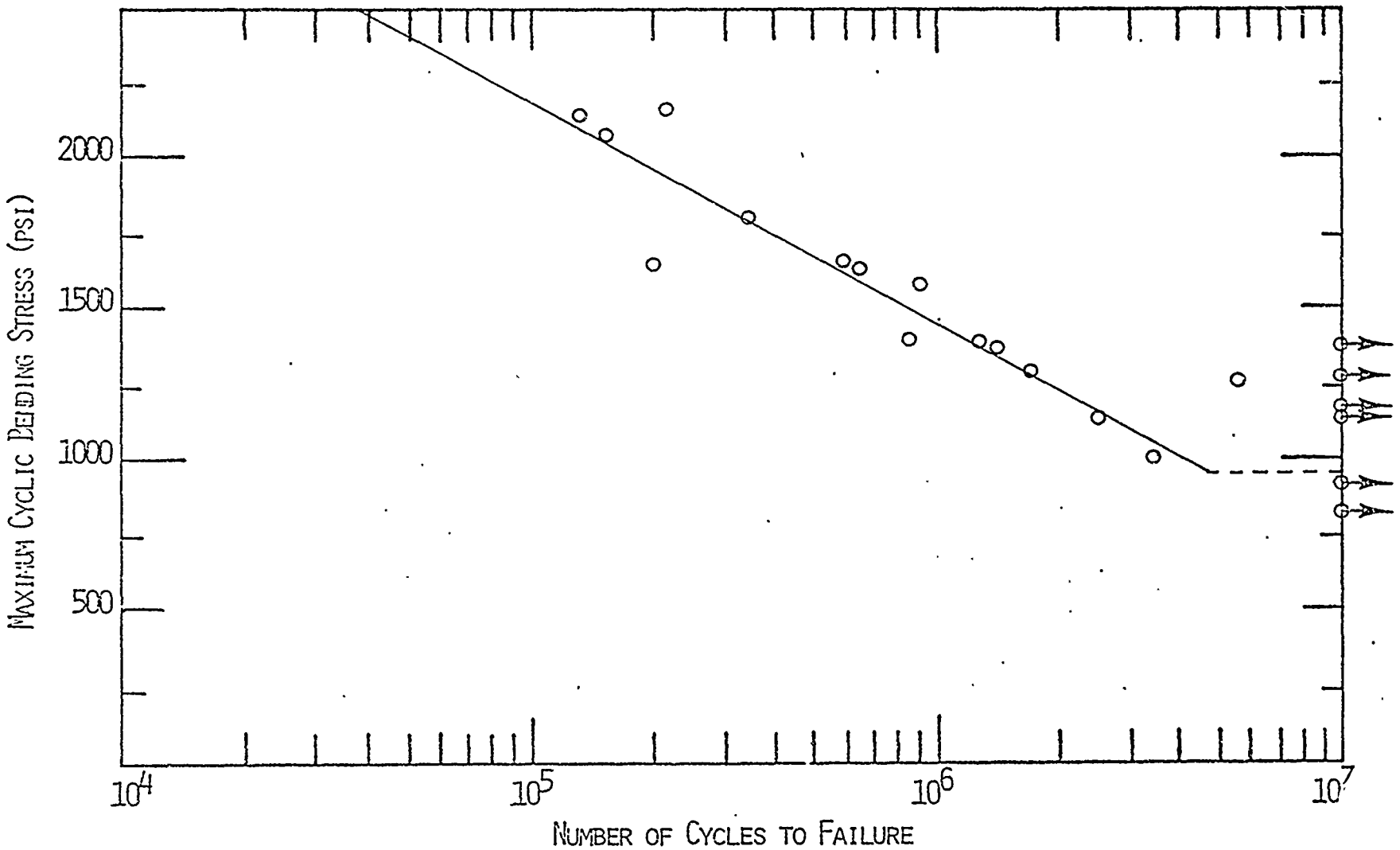

FIGURE 14. S-N Plot for Water-Cured Ferro-Cement with Ungalvanized Reinforcement, Portland Type V Cement, and 0.45 Water-to-Cement Ratio (1PWU)

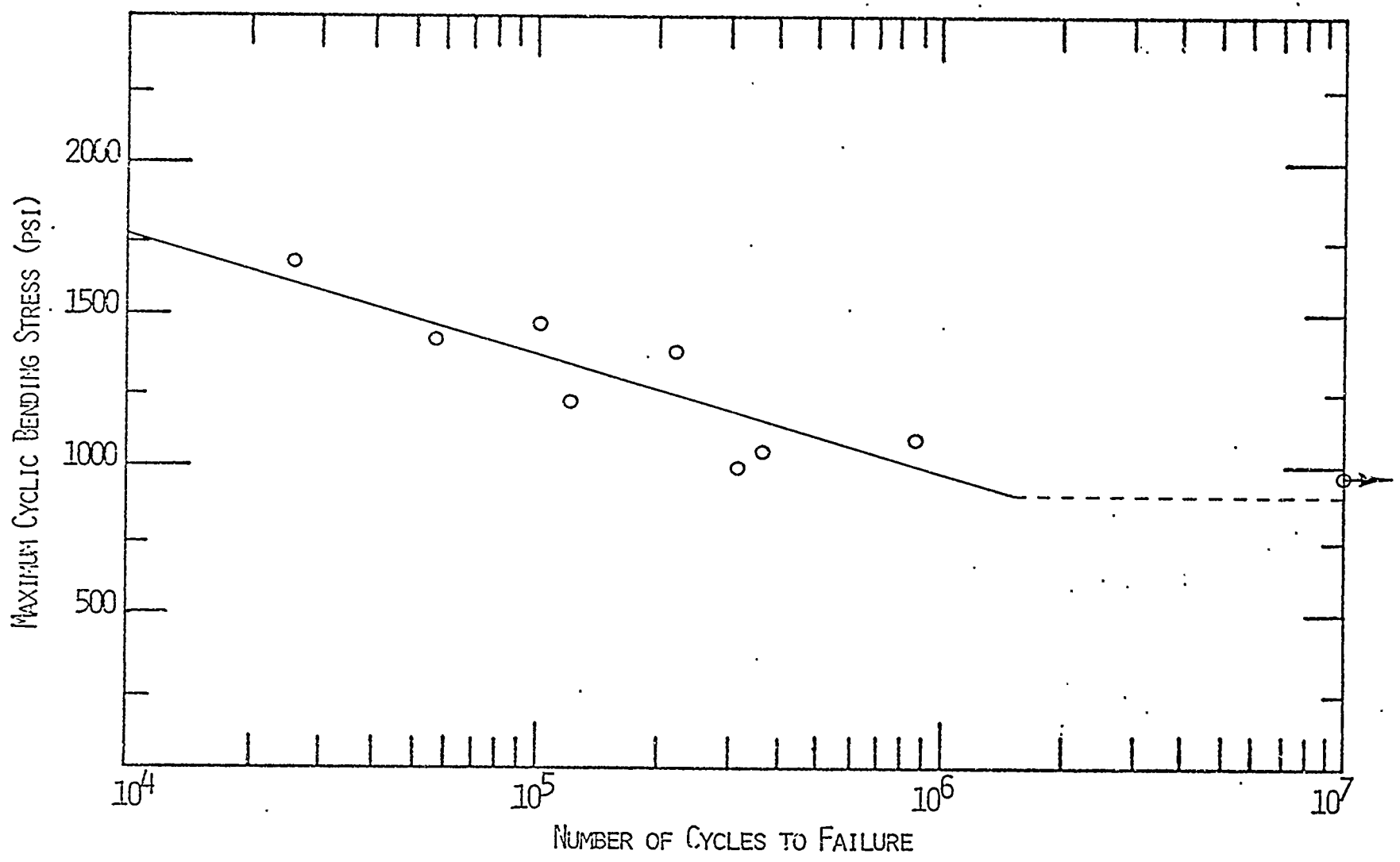

FIGURE 15. S-N PLOT FOR WATER-CURED FERRO-CEMENT WITH GALVANIZED REINFORCEMENT, PORTLAND TYPE V CEMENT, AND 0.40 WATER-TO-CEMENT RATIO (2PWG)

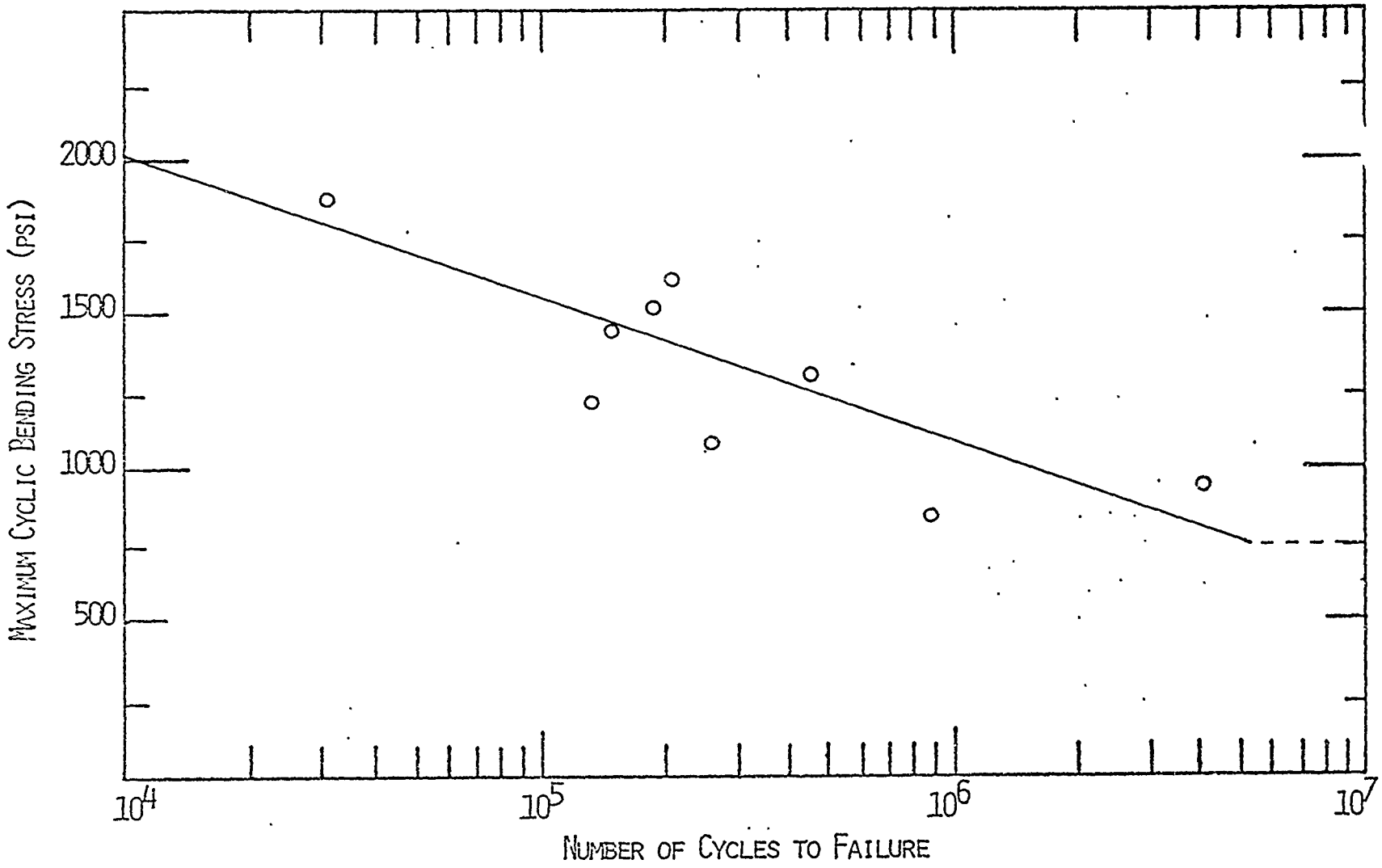

FIGURE 16. S-N Plot for Water-Cured Ferro-Cement with Ungalvanized Reinforcement, Portland Type V Cement, and 0.40 Water-to-Cement Ratio (2PNU)

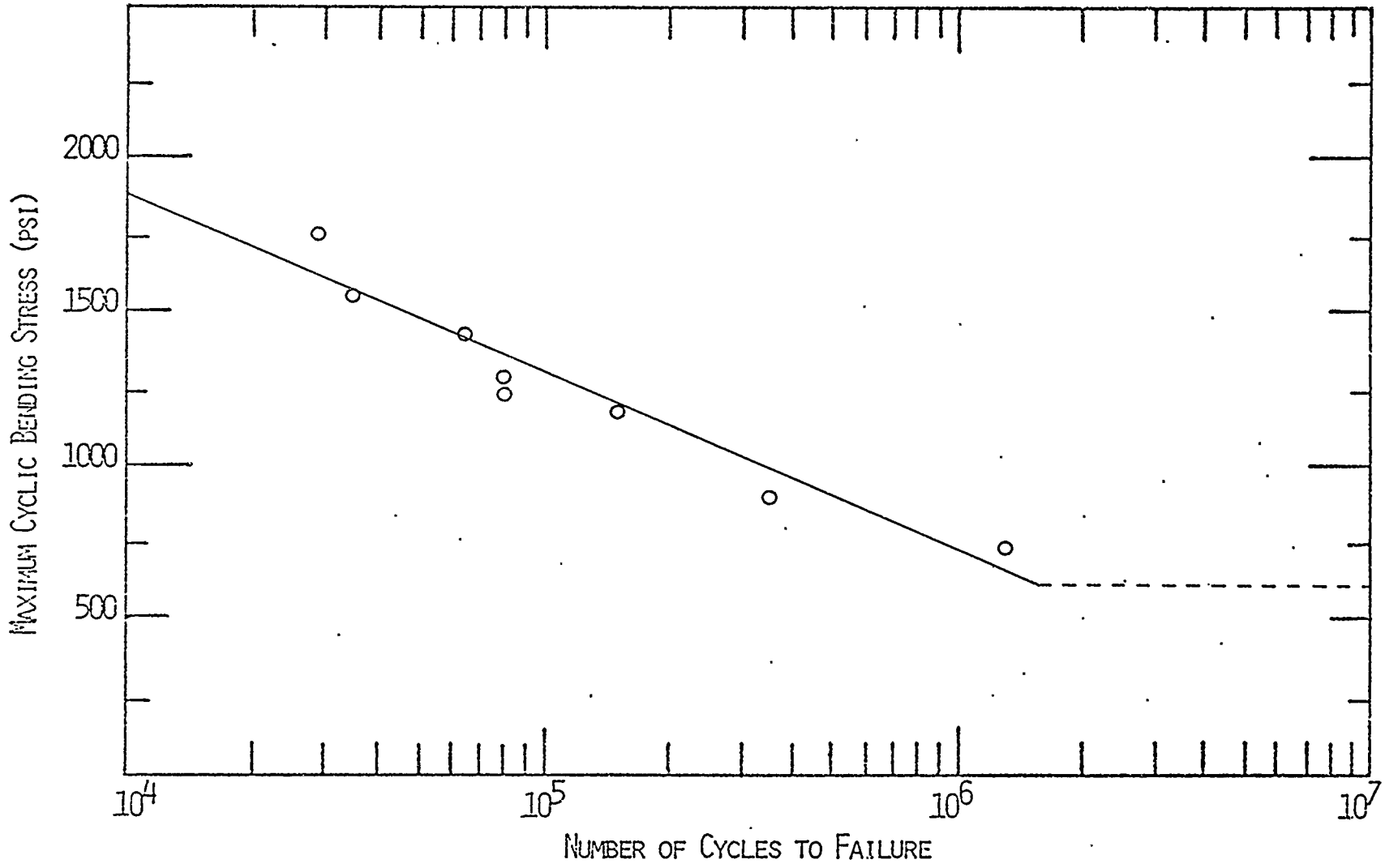

FIGURE 17. S-N PLOT FOR WATER-CURED FERRO-CEMENT WITH PORTLAND TYPE V CEMENT, 0.45 WATER-TO-CEMENT RATIO, AND GALVANIZED REINFORCEMENT, ALTERNATE LAYERS 45° TO SPECIMEN AXIS (3PWG)

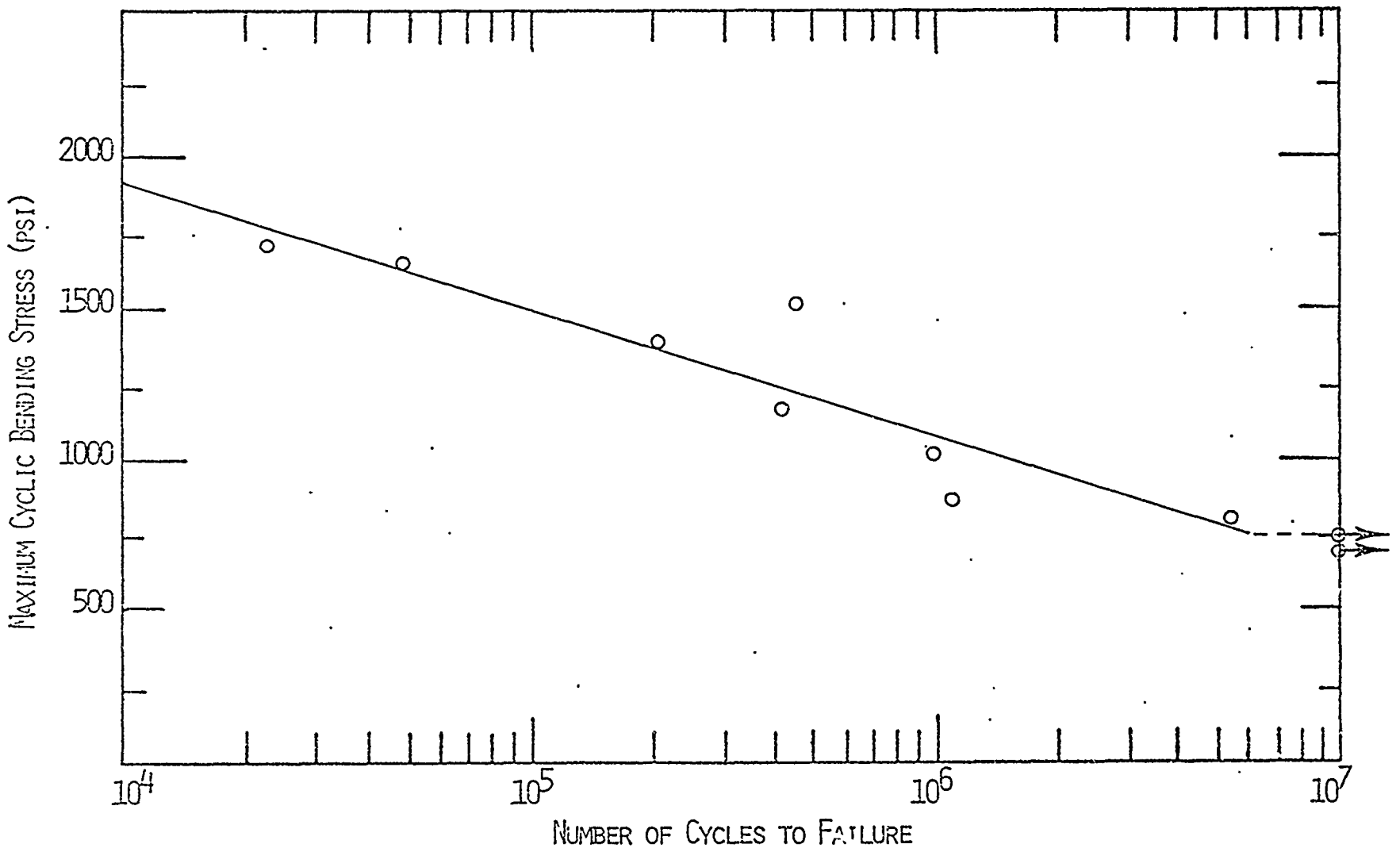

FIGURE 18. S-N PLOT FOR STEAM-CURED FERRO-CEMENT WITH GALVANIZED REINFORCEMENT, EXPANSIVE CEMENT, AND 0.45 WATER-TO-CEMENT RATIO (4ESG)

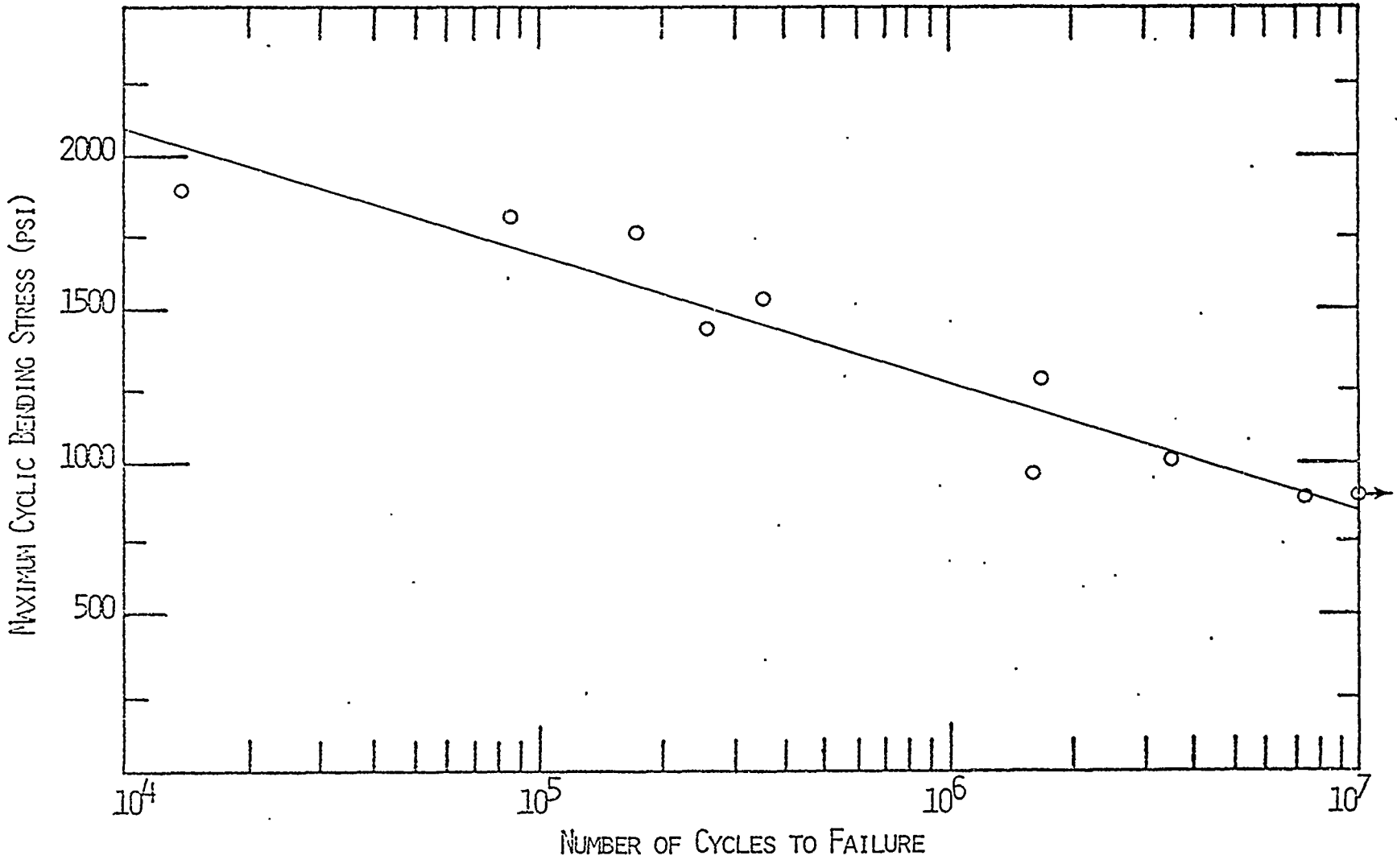

FIGURE 19. S-N Plot for Steam-Cured Ferro-Cement with Ungalvanized Reinforcement, Expansive Cement, and 0.45 Water-to-Cement Ratio (4ESU)

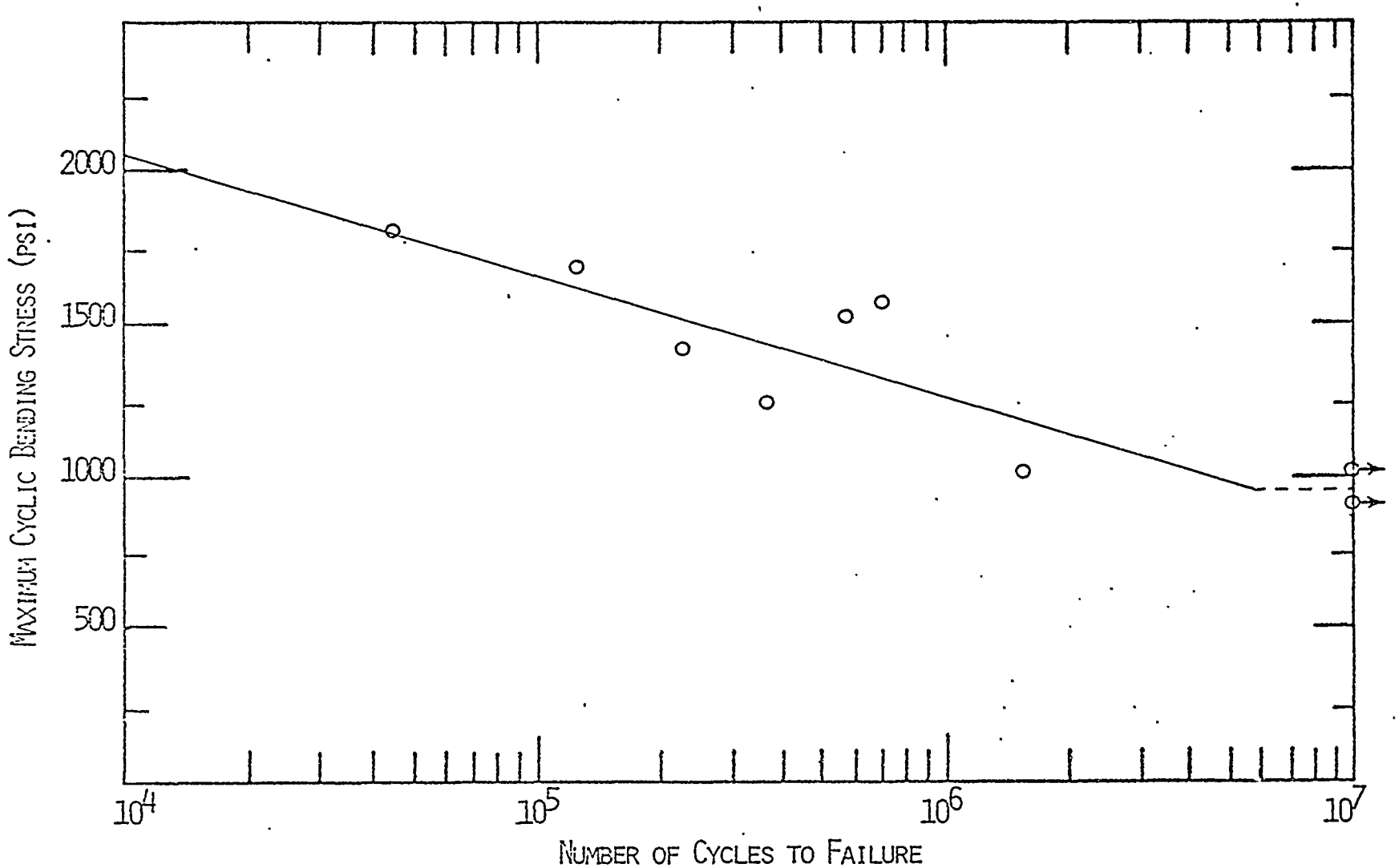

FIGURE 20. S-N Plot for Water-Cured Ferro-Cement with Galvanized Reinforcement, Expansive Cement, and 0.45 Water-to-Cement Ratio (4EWG)

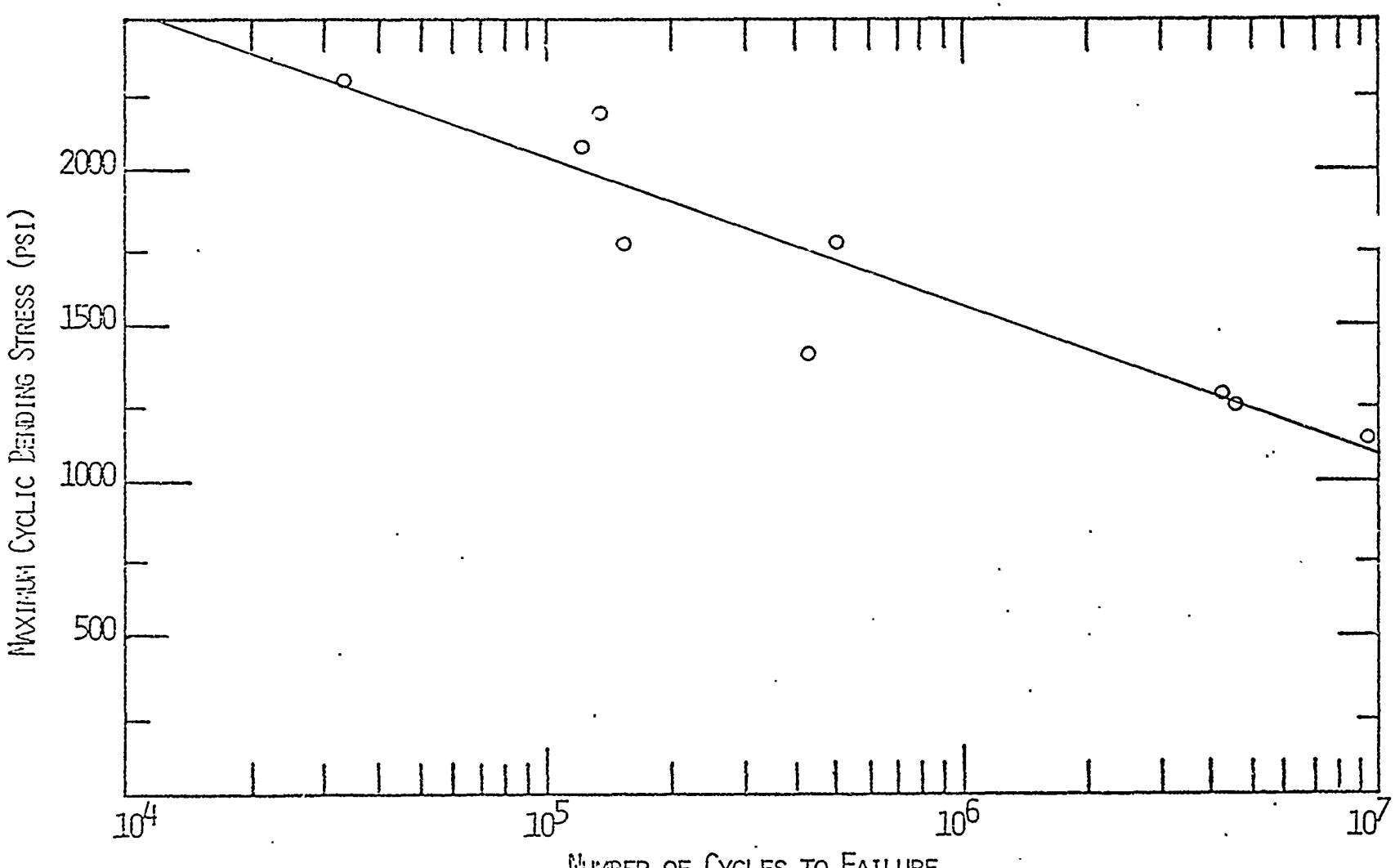

FIGURE 21. S-N Plot for Water-Cured Ferro-Cement with Ungalvanized Reinforcement, Expansive Cement, and 0.45 Water-to-Cement Ratio (4EWU)

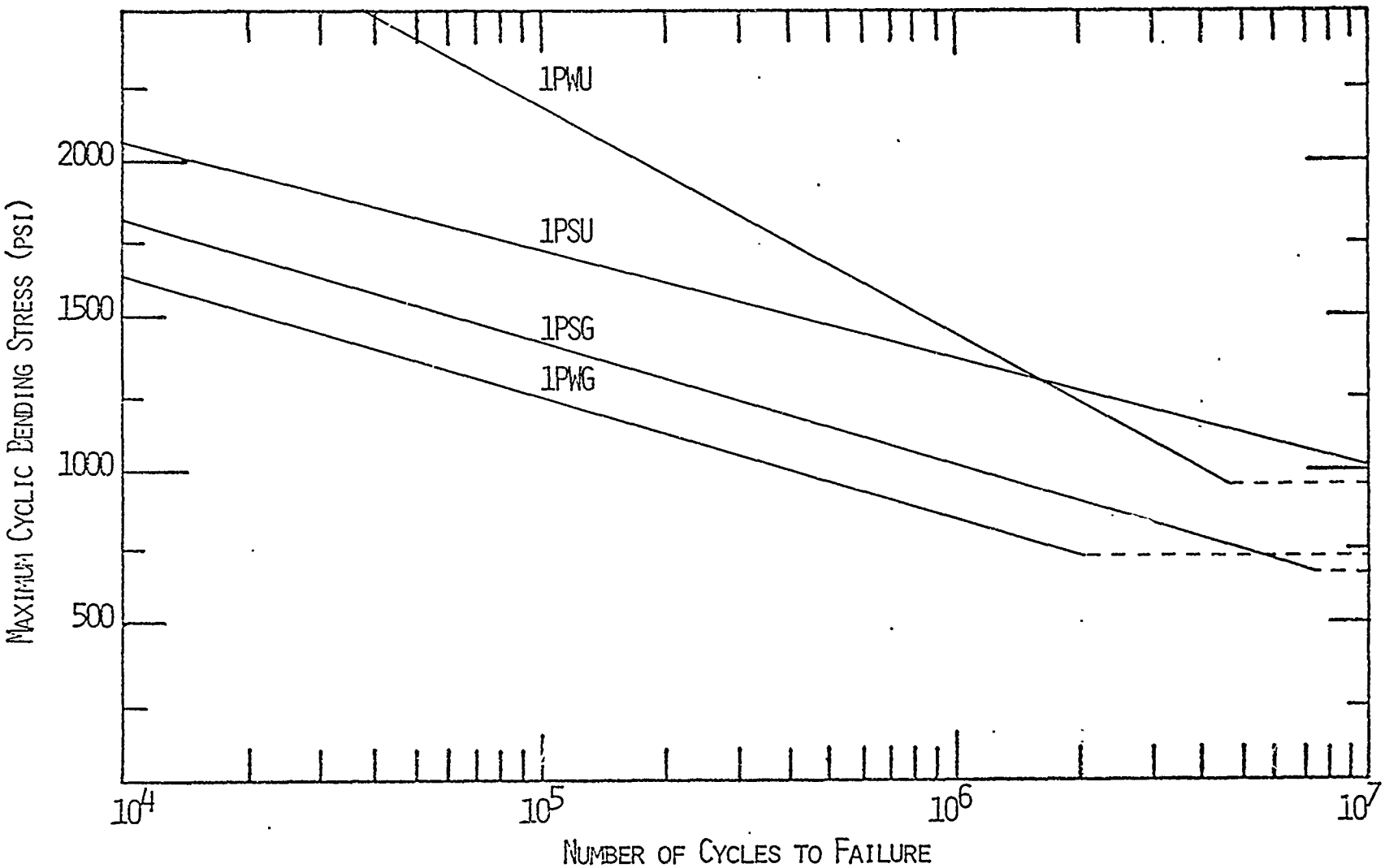

FIGURE 22. S-N Plots Comparing the Effects of Wire Type and Curing Method for Portland Type V Mortar Specimens

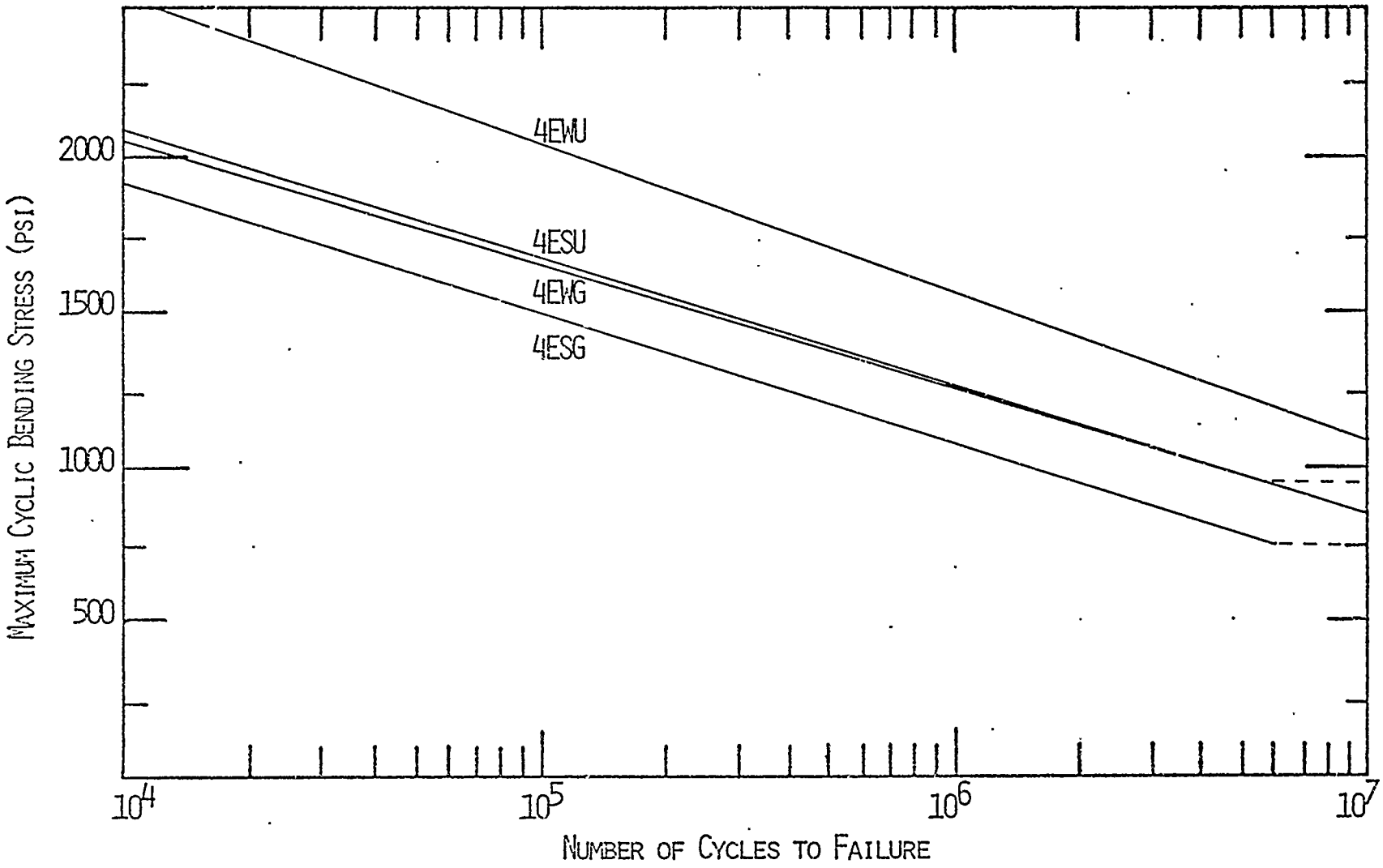

FIGURE 23. S-N Plots Comparing the Effects of Wire Type and Curing Method for Expansive Mortar Specimens

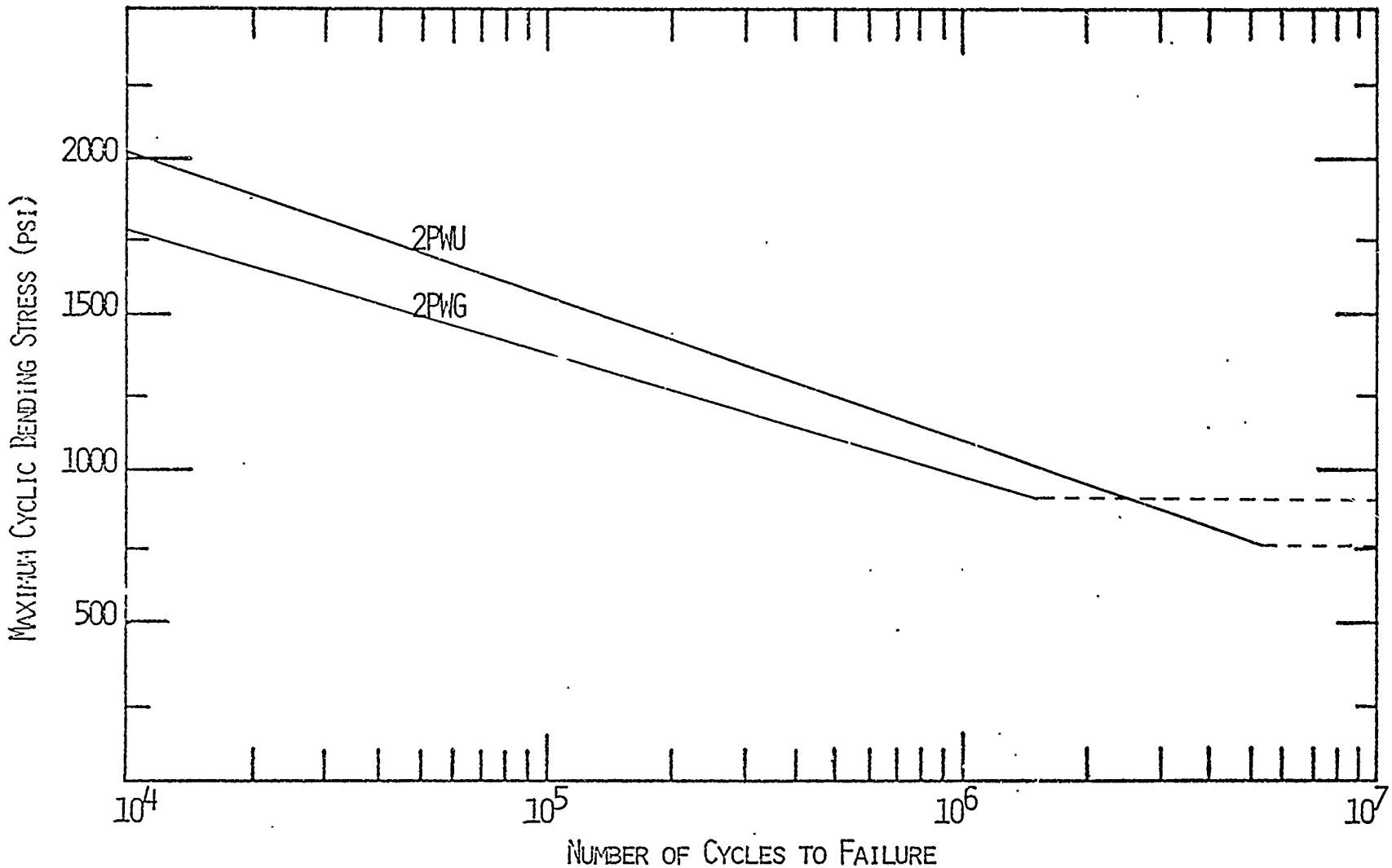

FIGURE 24. S-N PLOTS COMPARING WIRE TYPES IN 0.40 WATER-TO-CEMENT RATIO, PORTLAND TYPE V MORTAR SPECIMENS

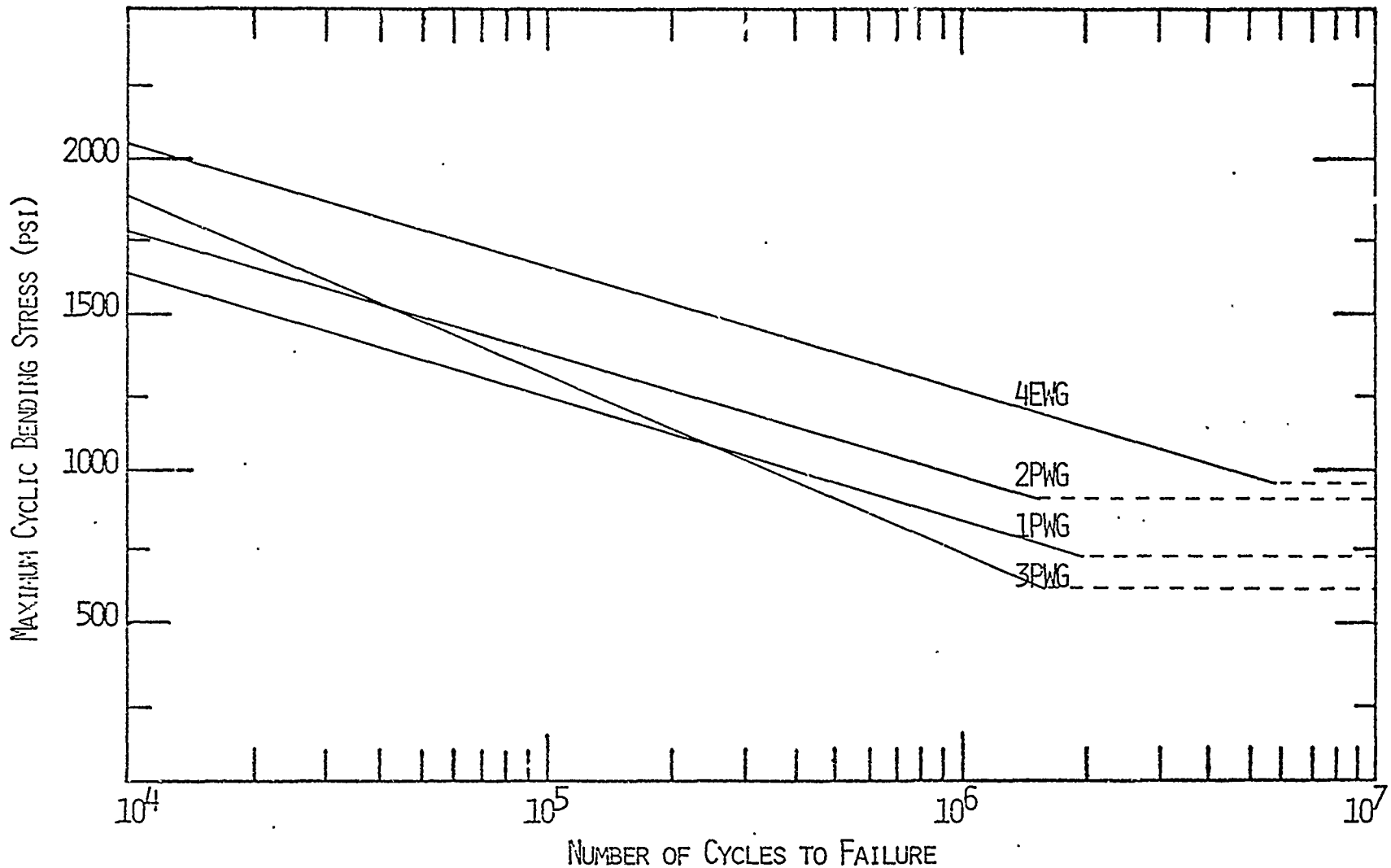

FIGURE 25. S-N PLOTS COMPARING REINFORCEMENT ORIENTATION AND WATER-CURED MORTAR VARIATIONS

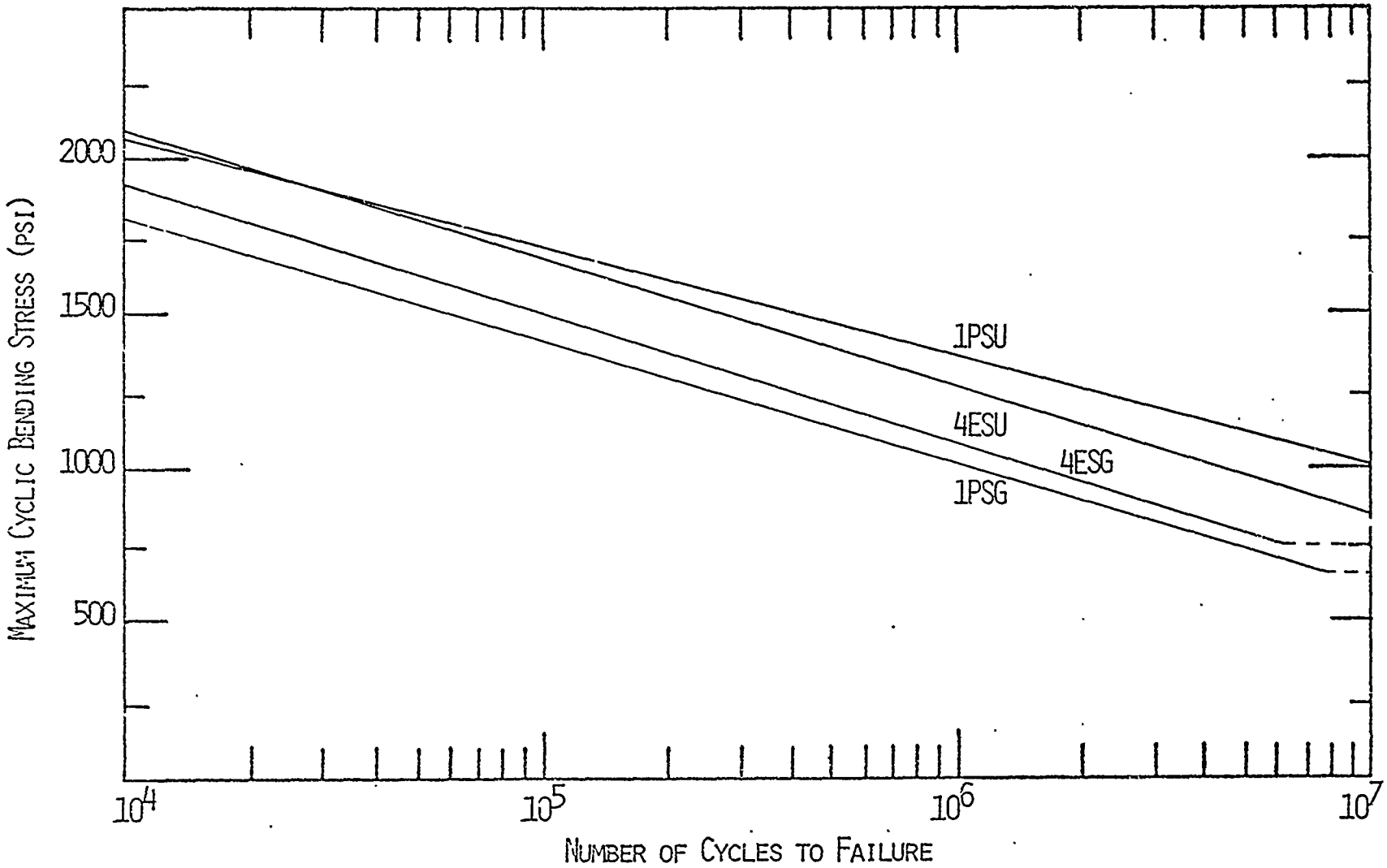

FIGURE 26. S-N PLOTS COMPARING STEAM-CURED MORTAR VARIATIONS

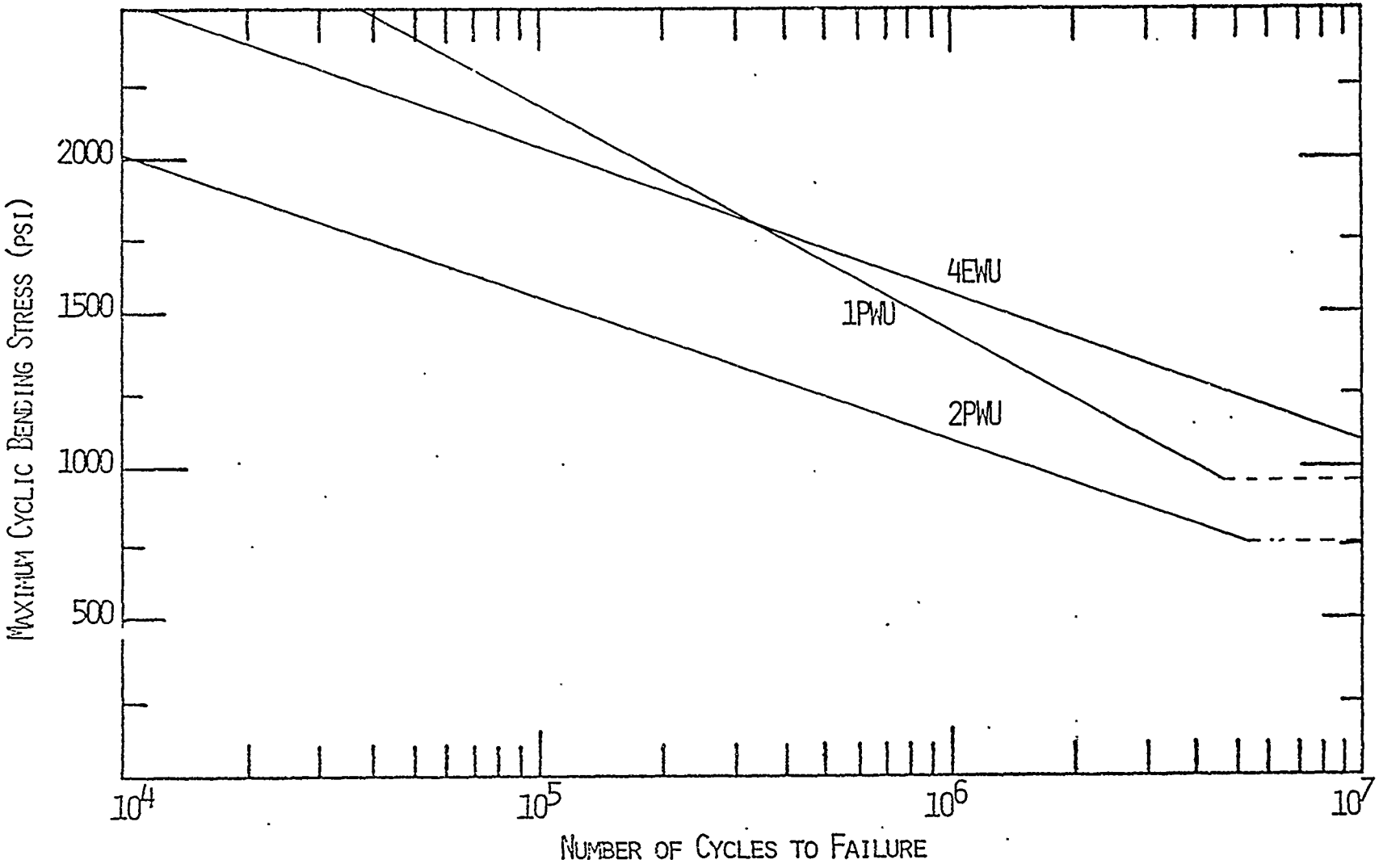

FIGURE 27. S-N PLOTS COMPARING WATER-CURED MORTAR VARIATIONS WITH UNGALVANIZED MESH

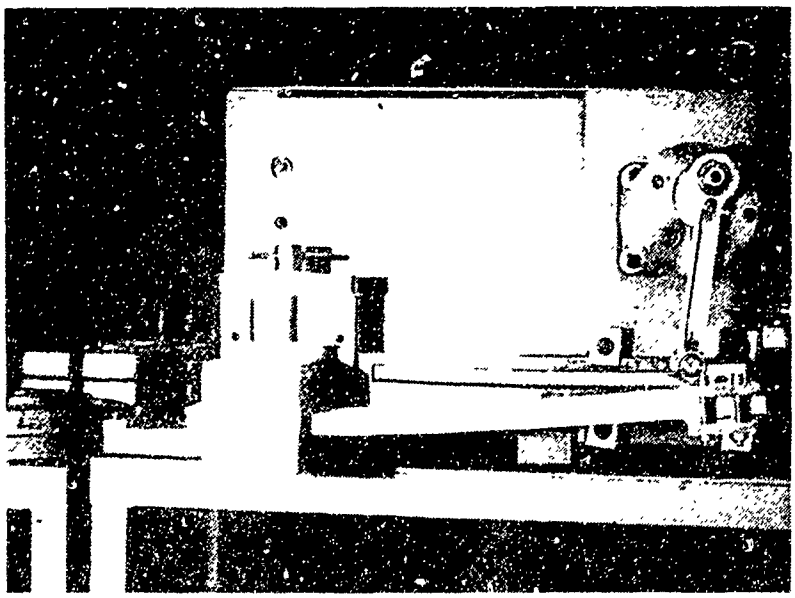

FIGURE 28 STRAIN-CONTROL BENDING FATIGUE MACHINE WITH FERRO-CEMENT SPECIMEN IN PLACE

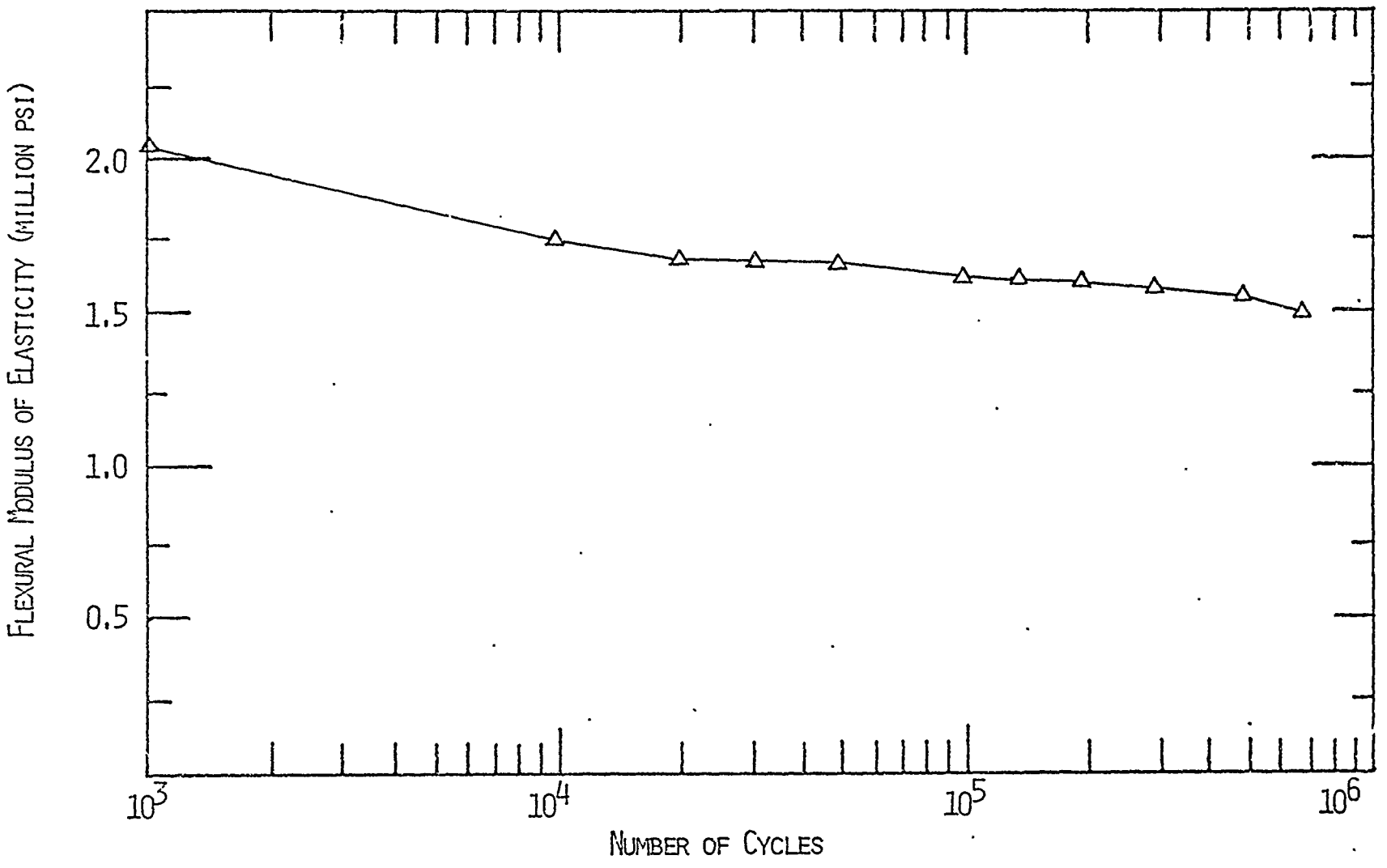

FIGURE 29. FLEXURAL MODULUS OF ELASTICITY VS. CYCLES IN STRAIN-CONTROL BENDING

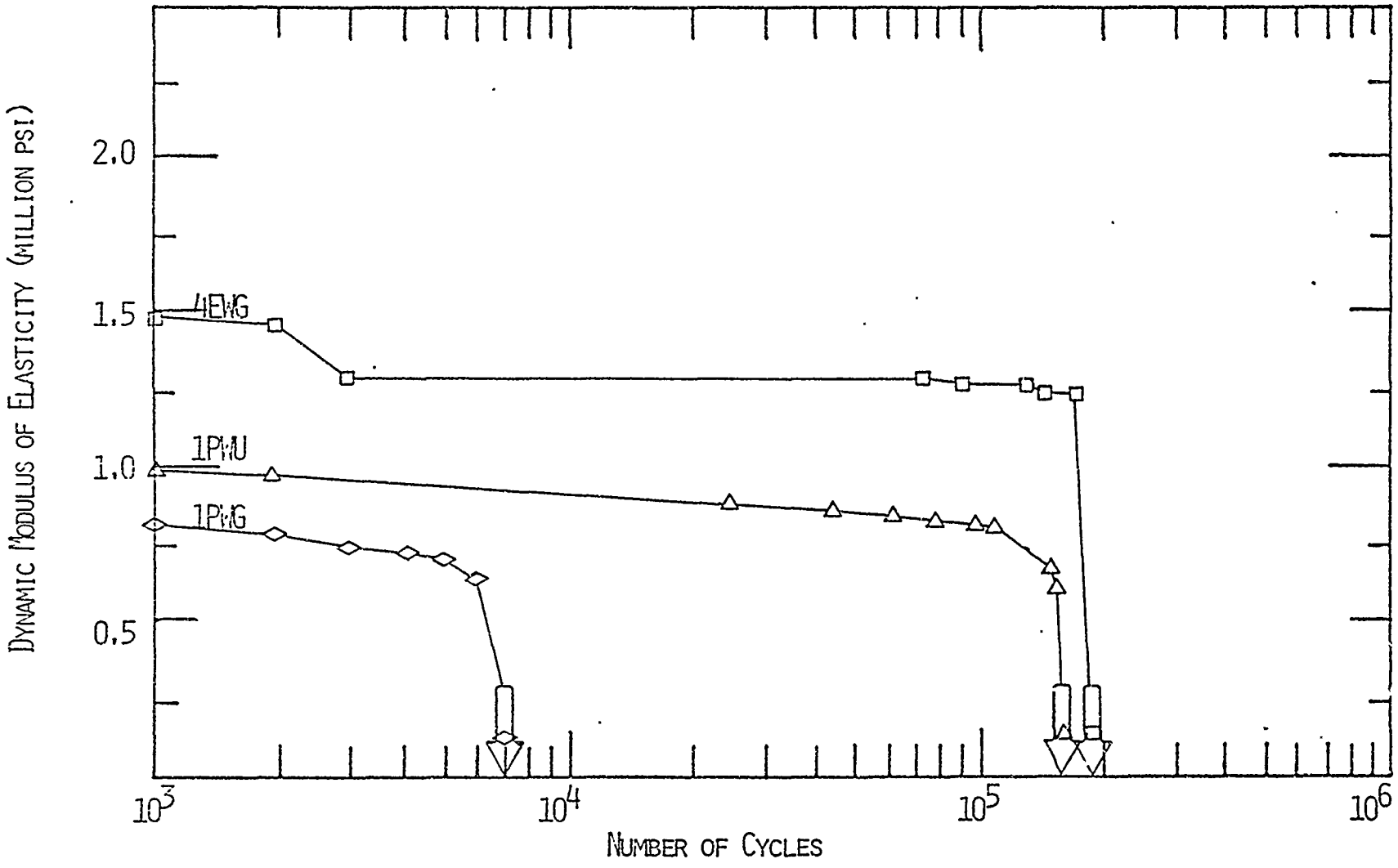

FIGURE 30. EFFECT OF CYCLIC LOADING ON THE DYNAMIC MODULUS OF ELASTICITY AT 1750 PSI STRESS

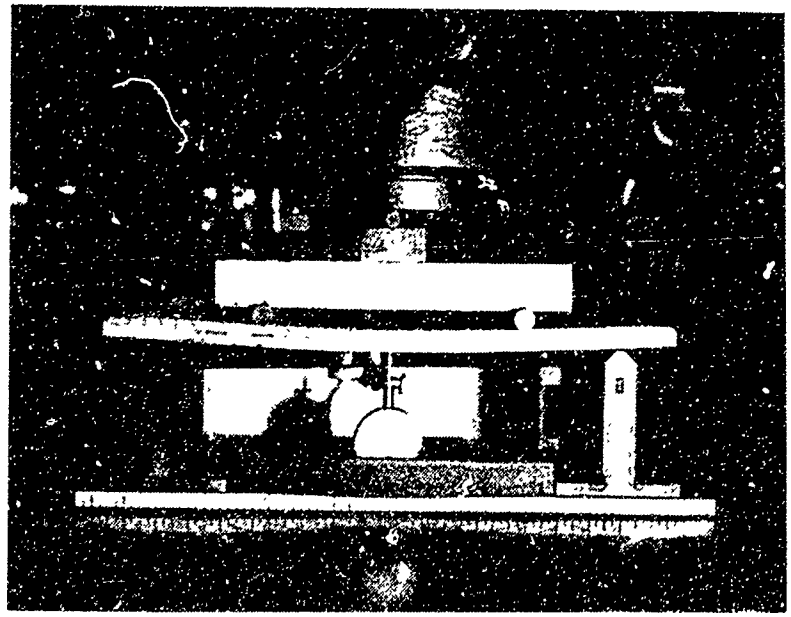

FIGURE 31 MONOTONIC BEAM FLEXURE TEST ARRANGEMENT

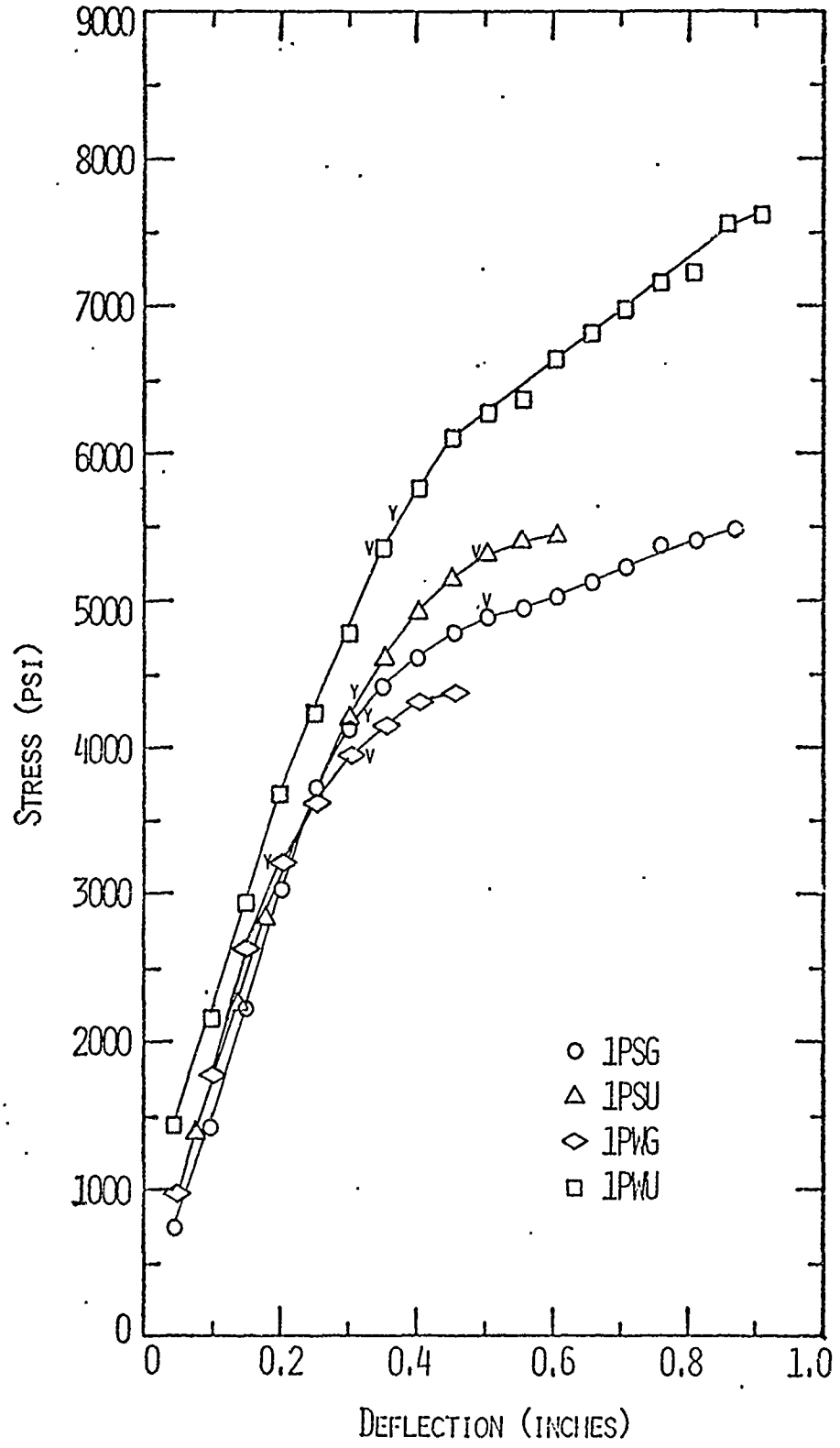

FIGURE 32. MONOTONIC BEAM FLEXURE STRESS VS. DEFLECTION (1PXX SERIES)

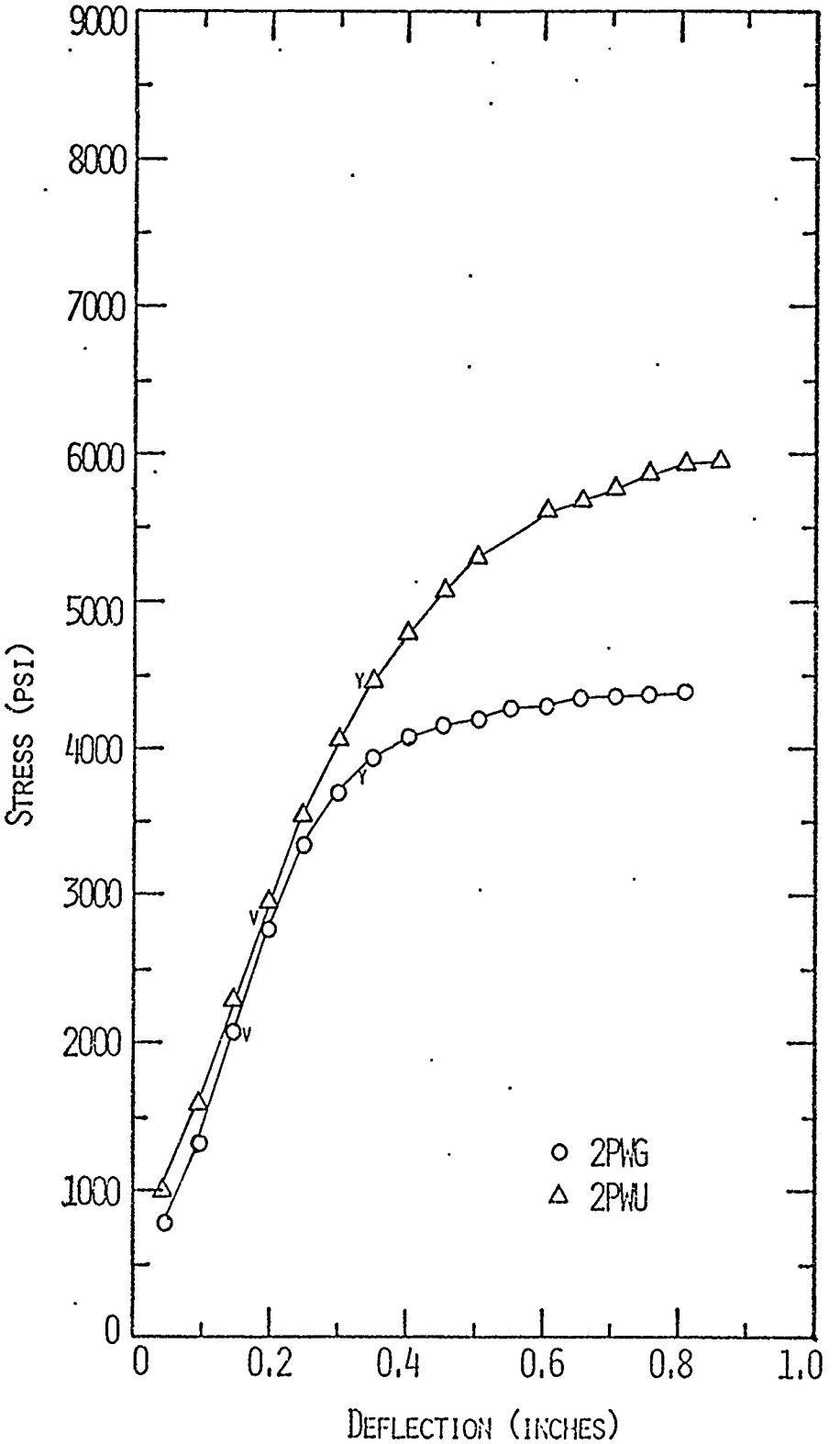

FIGURE 33. MONOTONIC BEAM FLEXURE STRESS VS. DEFLECTION (2PWX SERIES)

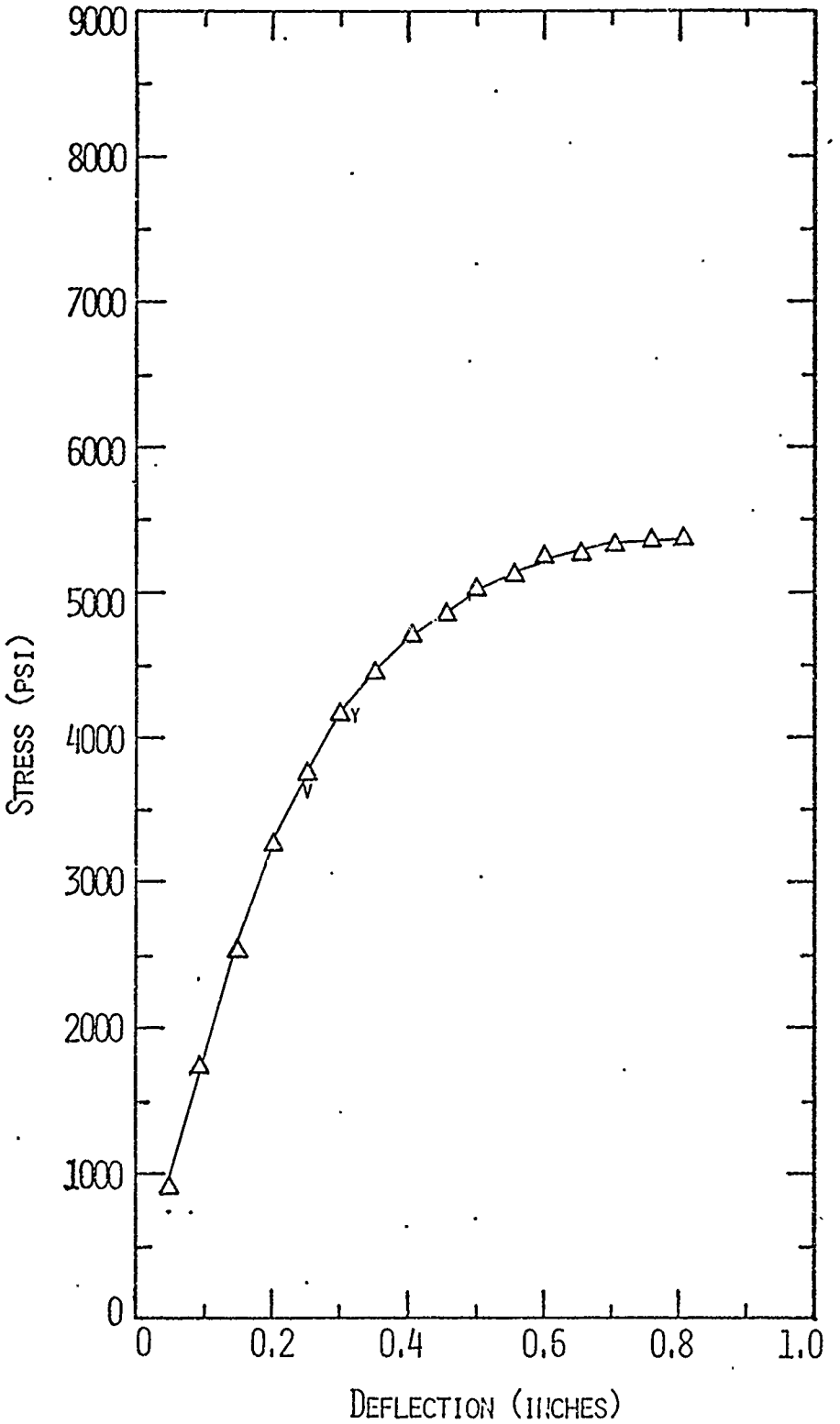

FIGURE 34. MONOTONIC BEAM FLEXURE STRESS VS. DEFLECTION (3PWG GROUP)

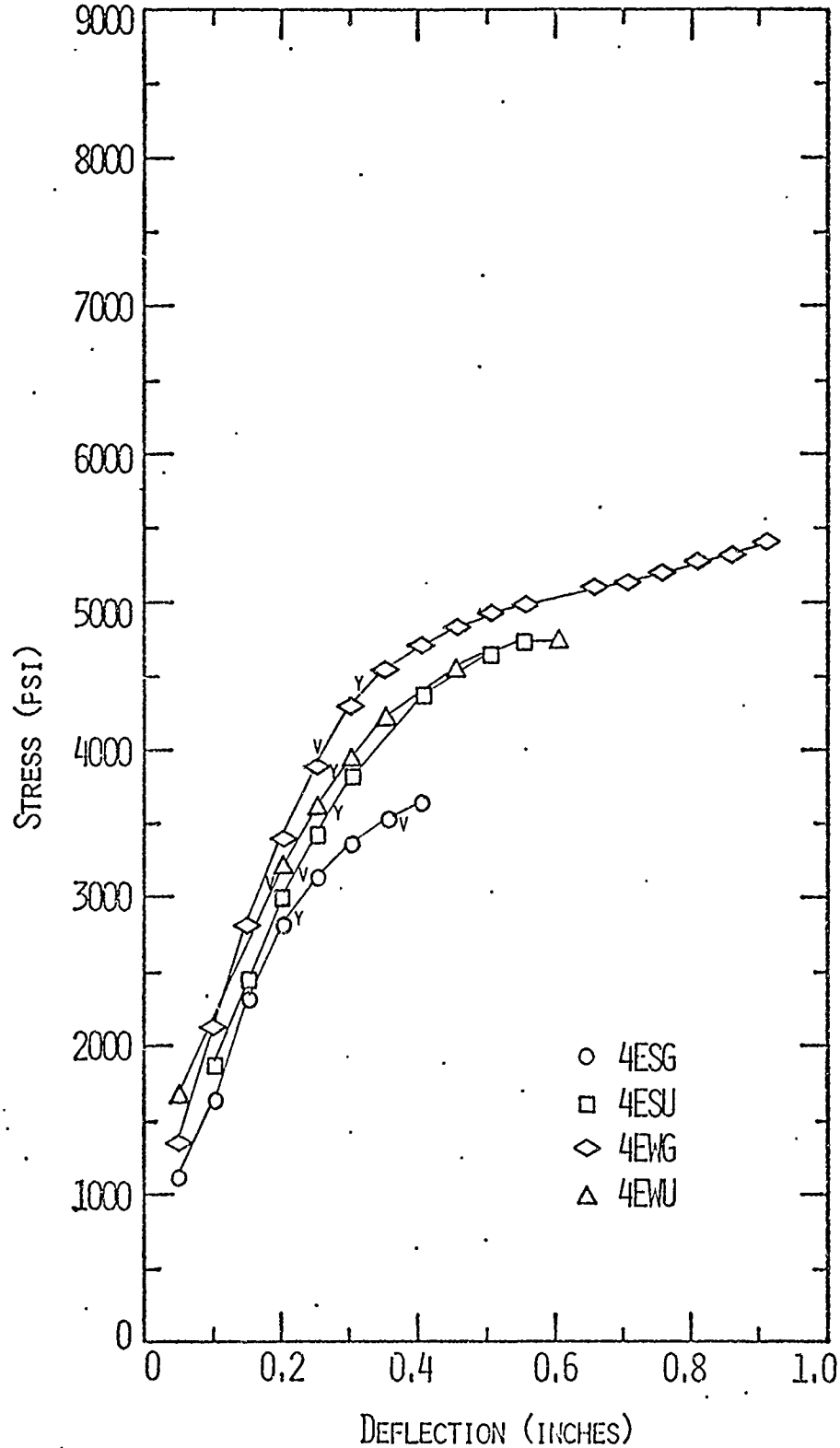

FIGURE 35. MONOTONIC BEAM FLEXURE STRESS VS. DEFLECTION (4EXX SERIES)

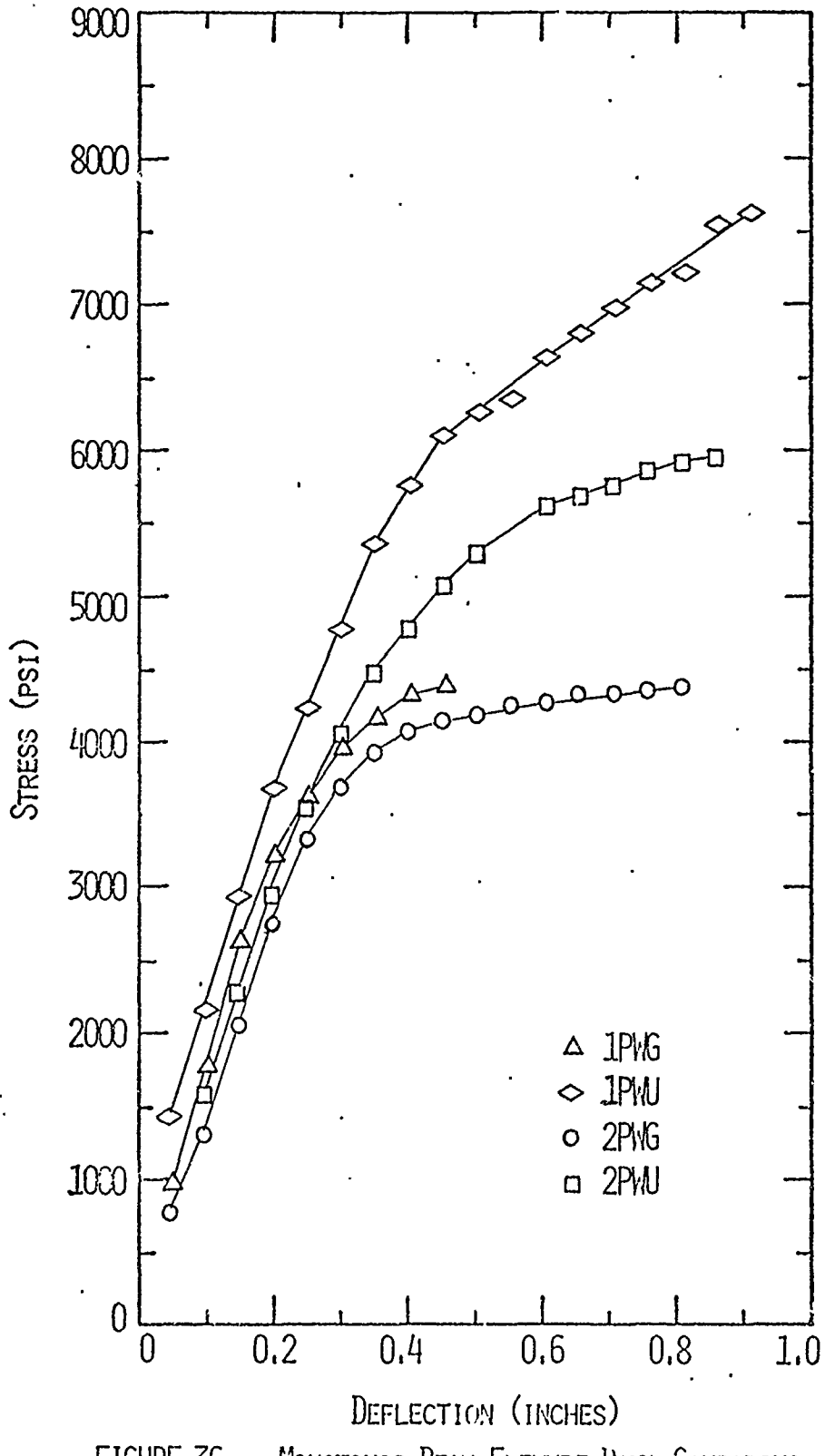

FIGURE 36. MONOTONIC BEAM FLEXURE DATA COMPARING MESH TYPES AND WATER-TO-CEMENT RATIOS

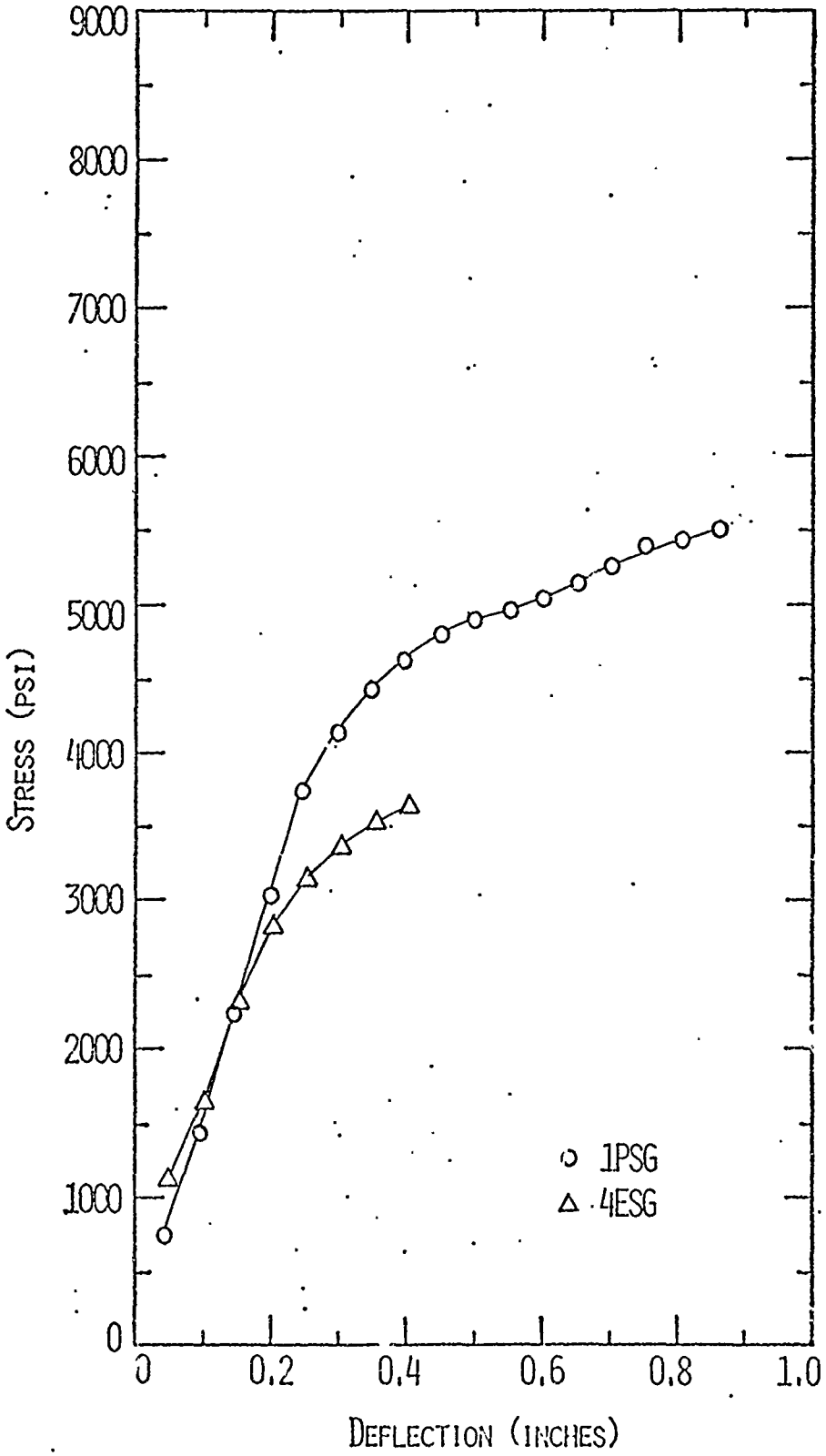

FIGURE 37. MONOTONIC BEAM FLEXURE DATA COMPARING CEMENT TYPES (GALVANIZED MESH, STEAM-CURED)

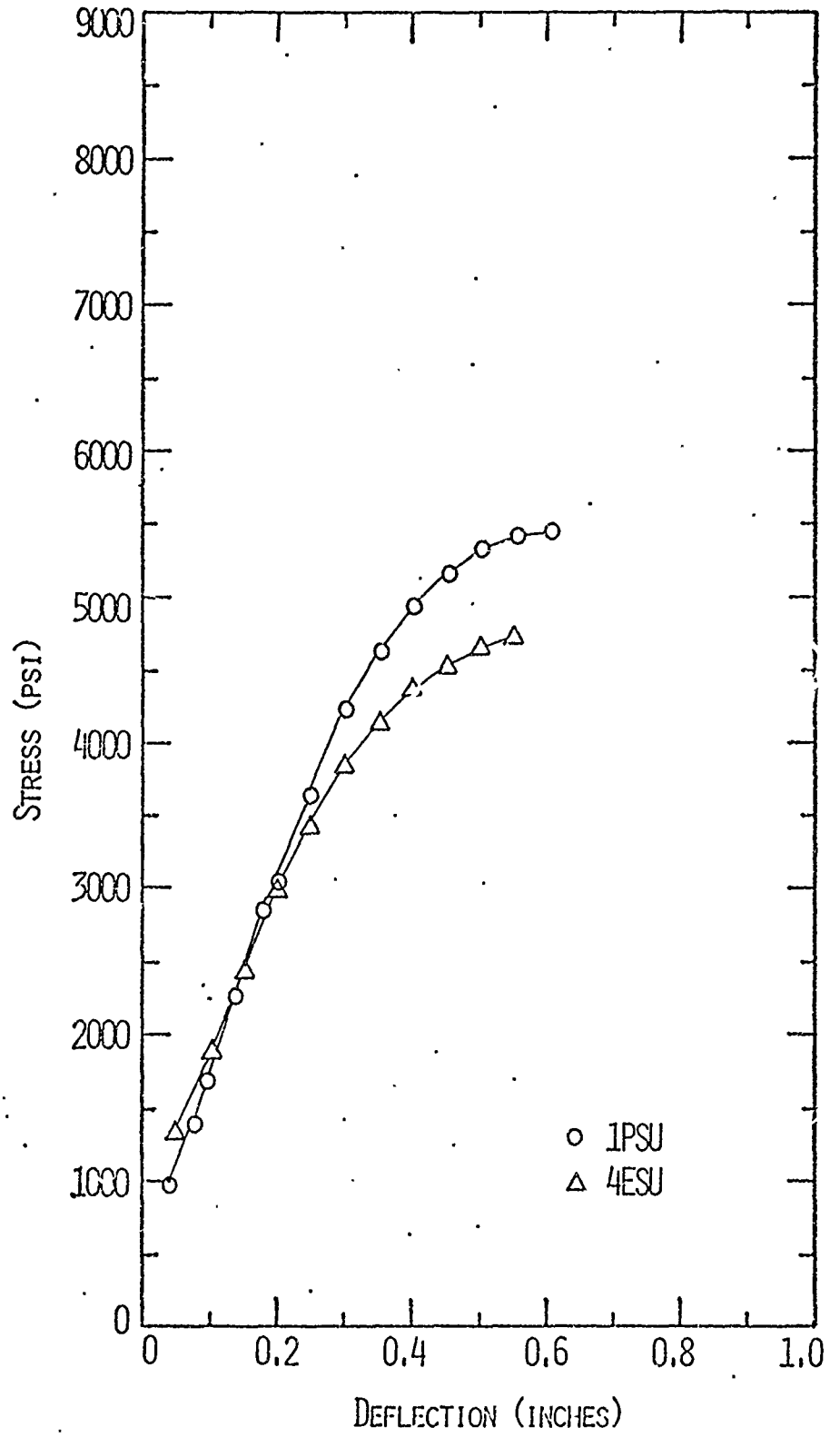

FIGURE 38. MONOTONIC BEAM FLEXURE DATA COMPARING CEMENT TYPES (UNGALVANIZED MESH, STEAM-CURED)

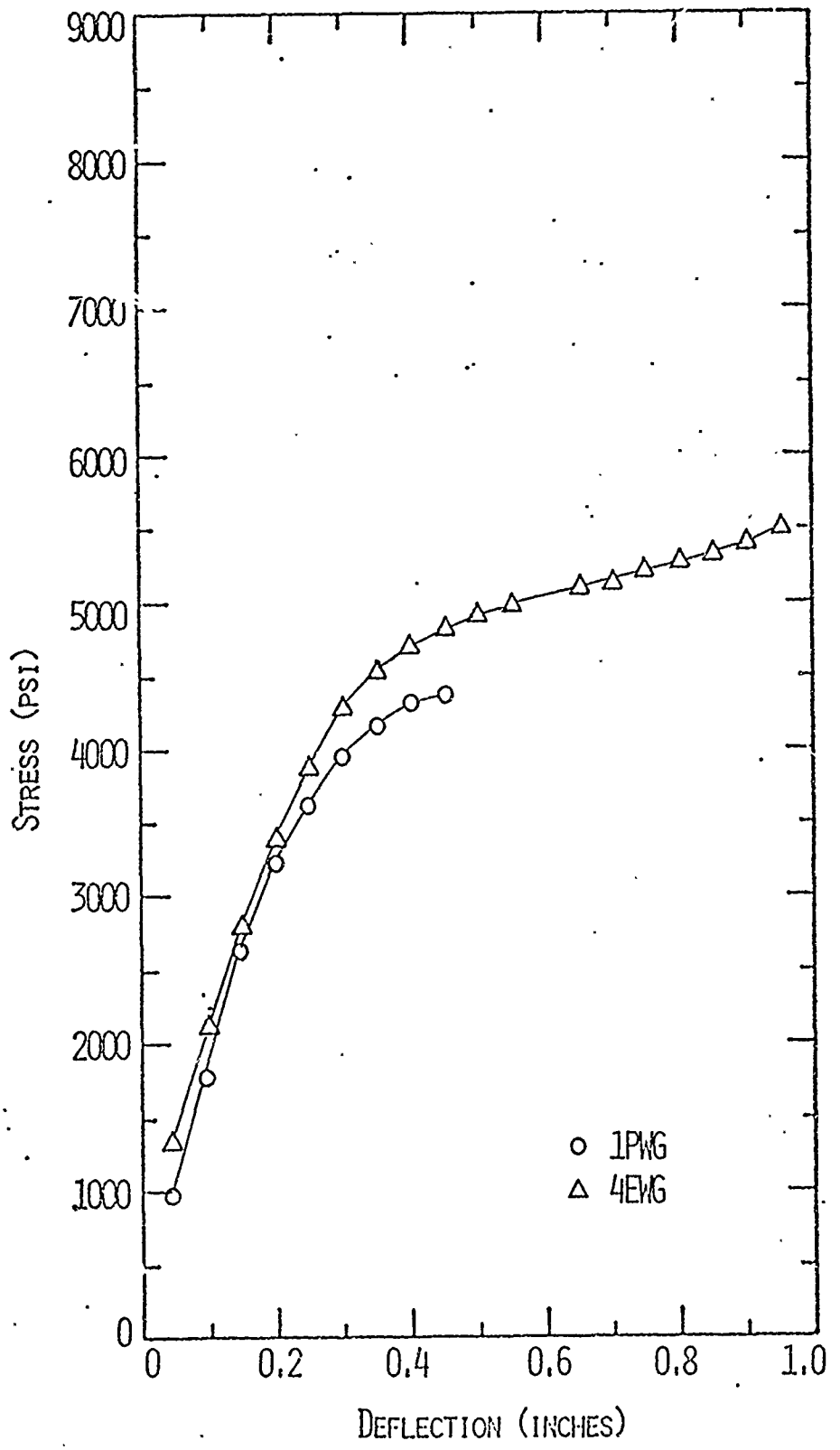

FIGURE 39. MONOTONIC BEAM FLEXURE DATA COMPARING CEMENT TYPES (GALVANIZED MESH, WATER-CURED)

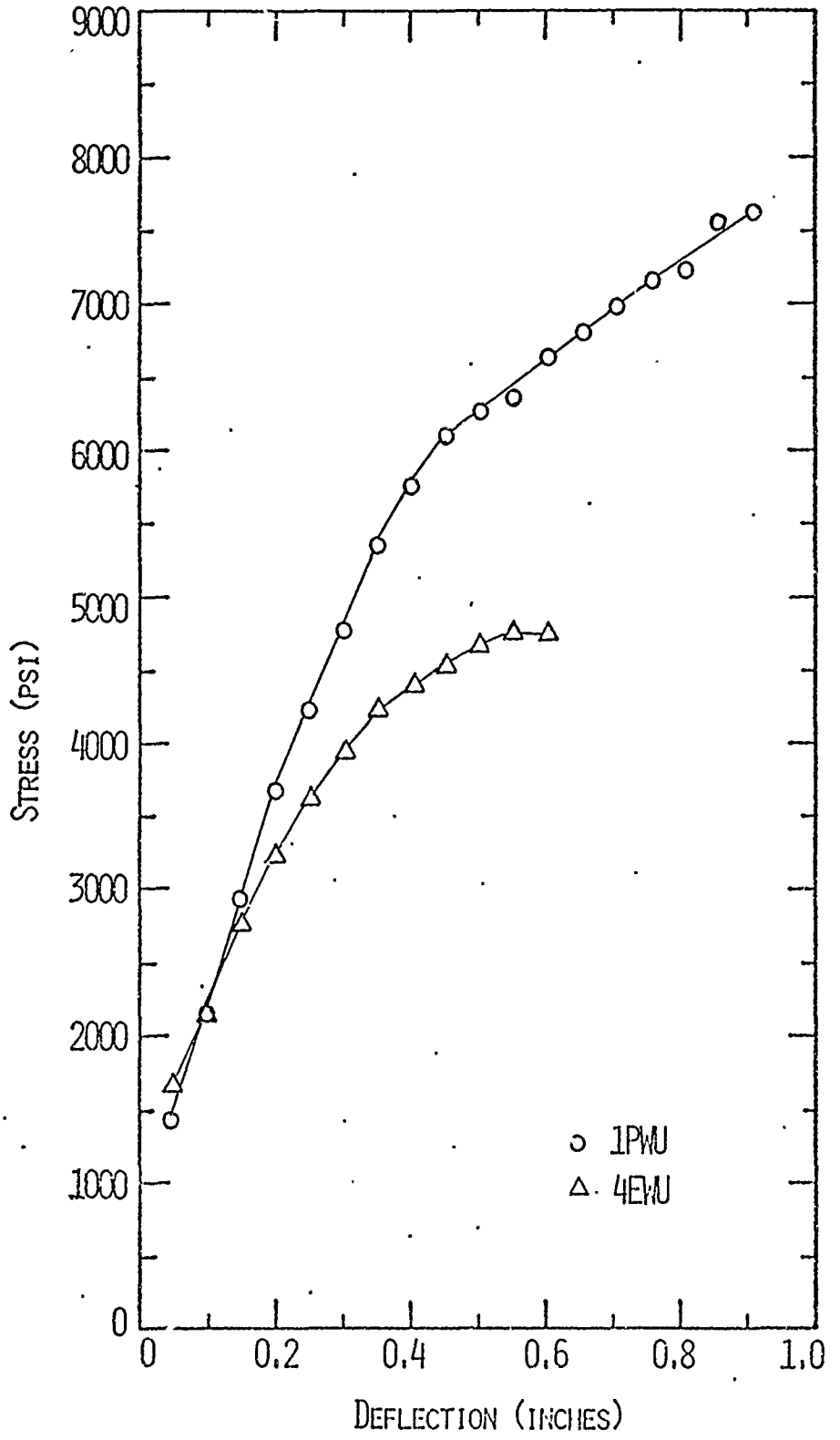

FIGURE 40. MONOTONIC BEAM FLEXURE DATA COMPARING CEMENT TYPES (UNGALVANIZED MESH, WATER-CURED)

FIGURE 41 MORTAR COMPRESSION TEST SPECIMEN WITH CAPPING FORM

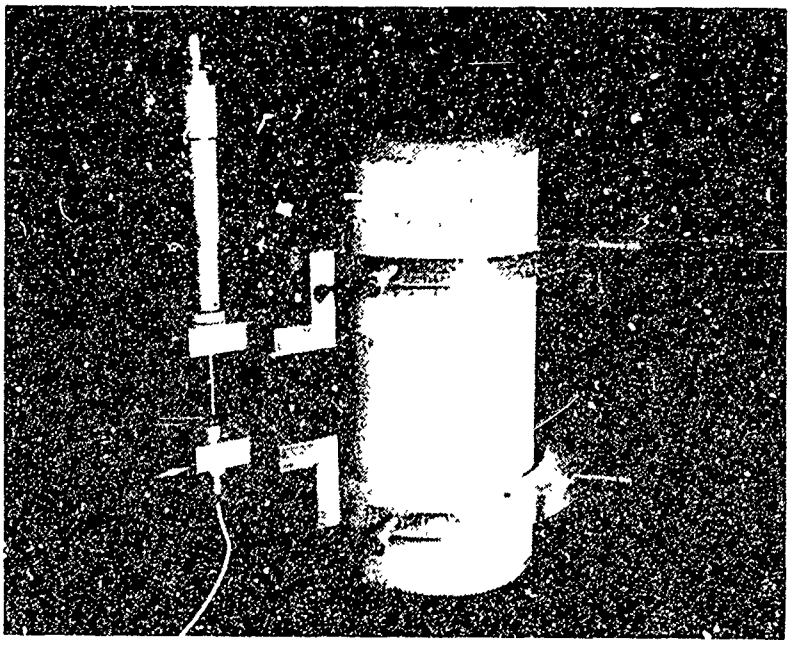

FIGURE 42 MORTAR COMPRESSION TEST STRAIN MEASUREMENT APPARATUS

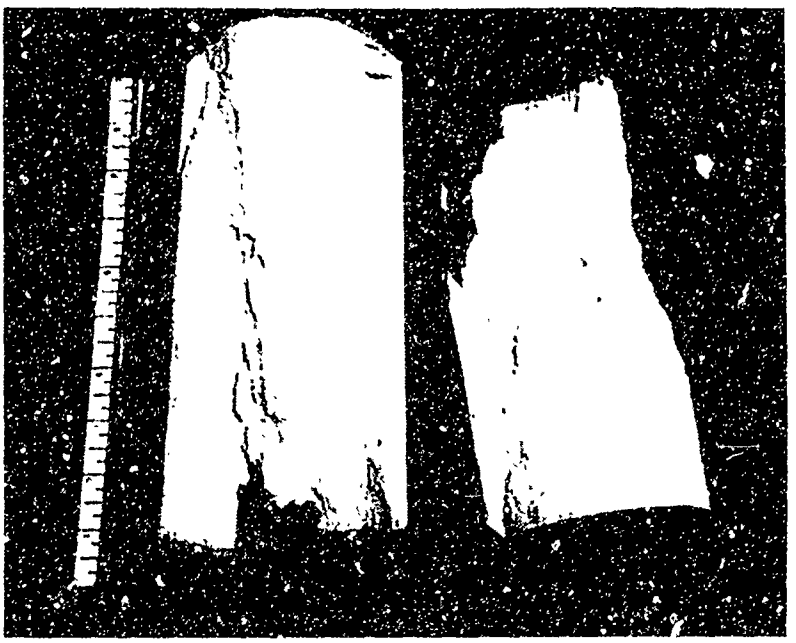

FIGURE 43 MORTAR COMPRESSION SPECIMEN AFTER FAILURE

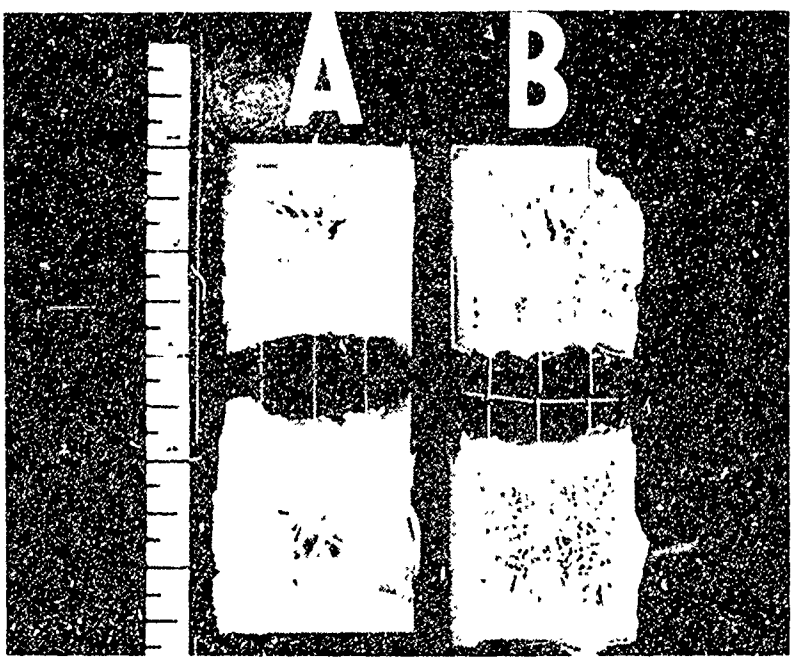

FIGURE 44 REINFORCING MESH TENSILE STRENGTH TEST SPECIMENS

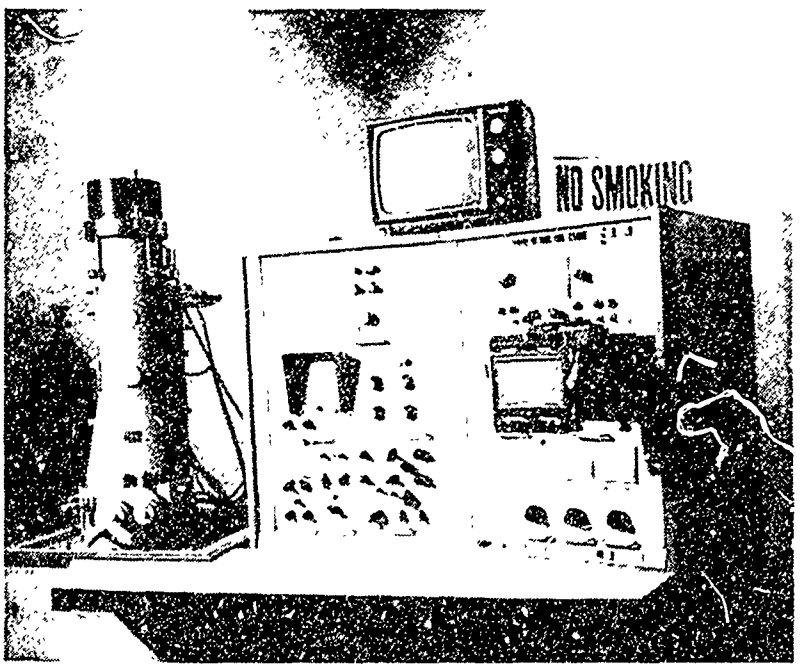

FIGURE 45. CAMBRIDGE STEREOSCAN SCANNING ELECTRON MICROSCOPE (SEM)

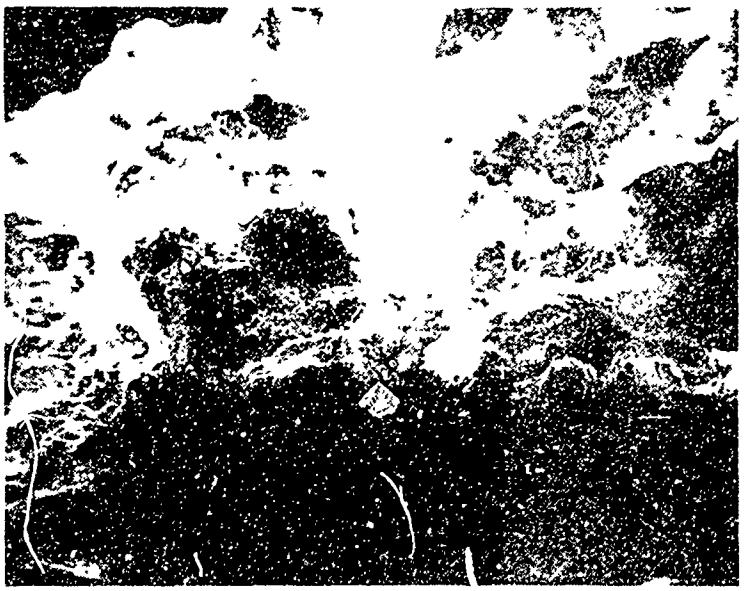

FIGURE 46 MORTAR-TO-WIRE INTERFACE, 1PSG GROUP (24X)

FIGURE 47 CLOSE-UP VIEW OF INTERFACE SHOWN IN FIGURE 46 (120X)

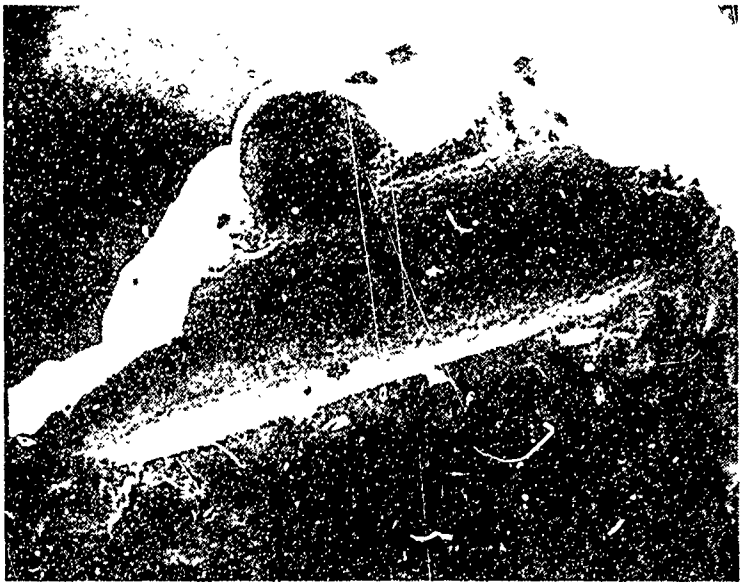

FIGURE 48 MORTAR-TO-WIRE INTERFACE, 1PSU GROUP (24X)

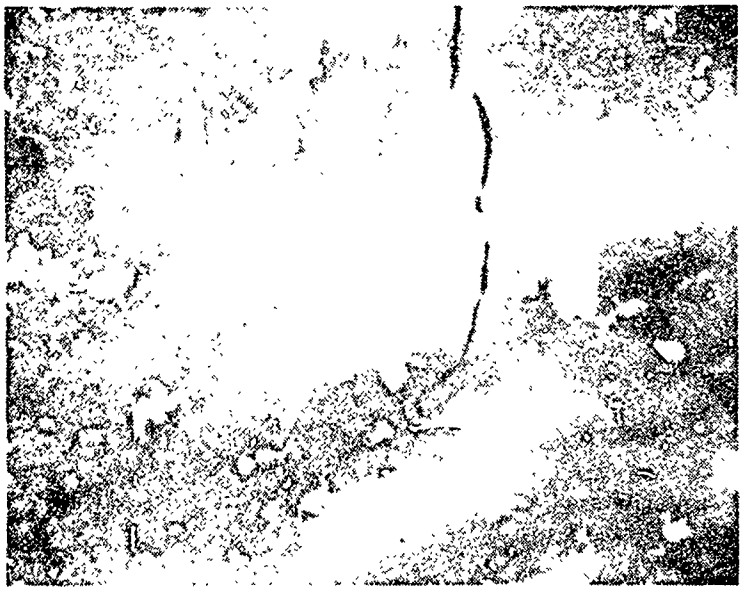

FIGURE 49 CLOSE-UP VIEW OF INTERFACE SHOWN IN FIGURE 48 (6000X)

FIGURE 50 MORTAR-TO-WIRE INTERFACE, 1PWG GROUP (67X)

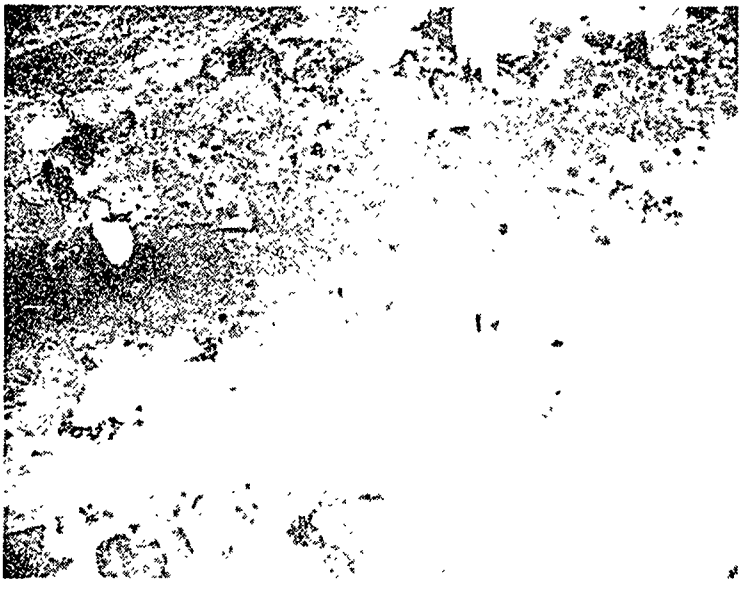

FIGURE 51 MORTAR-TO-WIRE INTERFACE, 2PWU GROUP (60X)

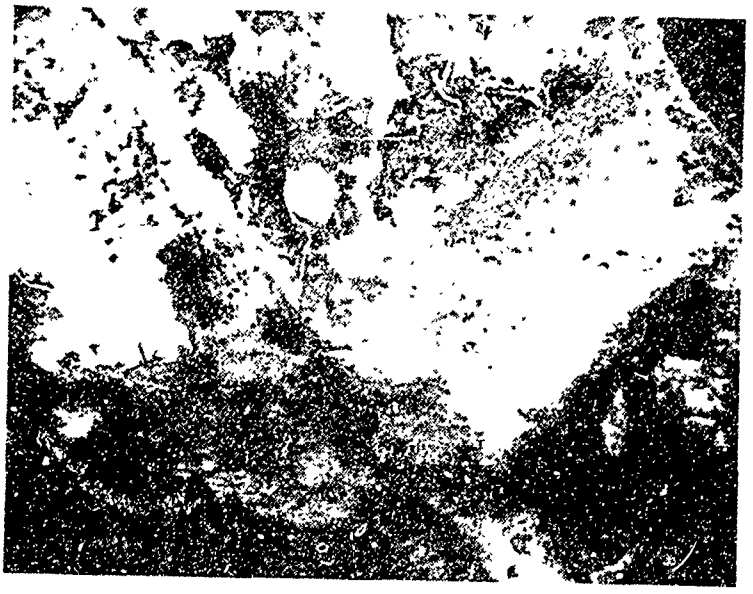

FIGURE 52 MOR ..?-TC-WIRE INTERFACE, 4ESG GROUP (26X)

FIGURE 53 CLOSE-UP VIEW OF INTERFACE SHOWN IN FIGURE 52 (65X)

FIGURE 54 MORTAR-TO-WIRE INTERFACE, 4ESU GROUP (26X)

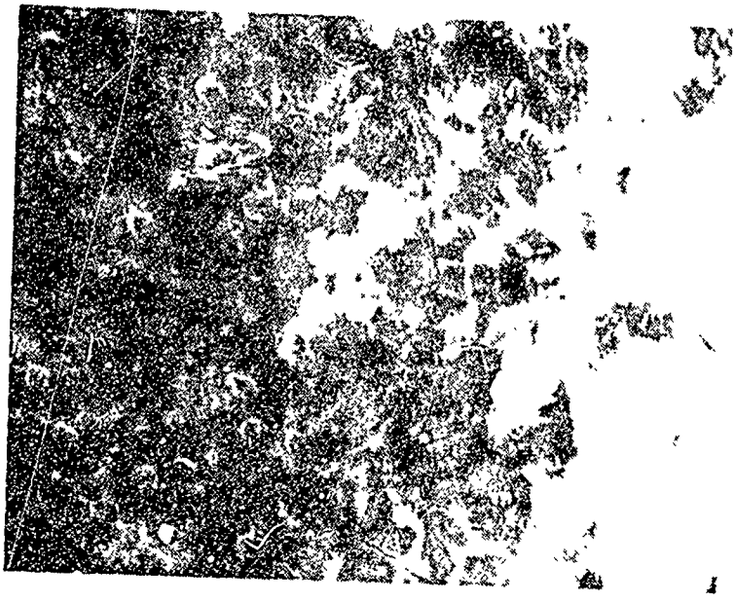

FIGURE 55 CLOSE-UP VIEW OF INTERFACE SHOWN IN FIGURE 54 (260X)

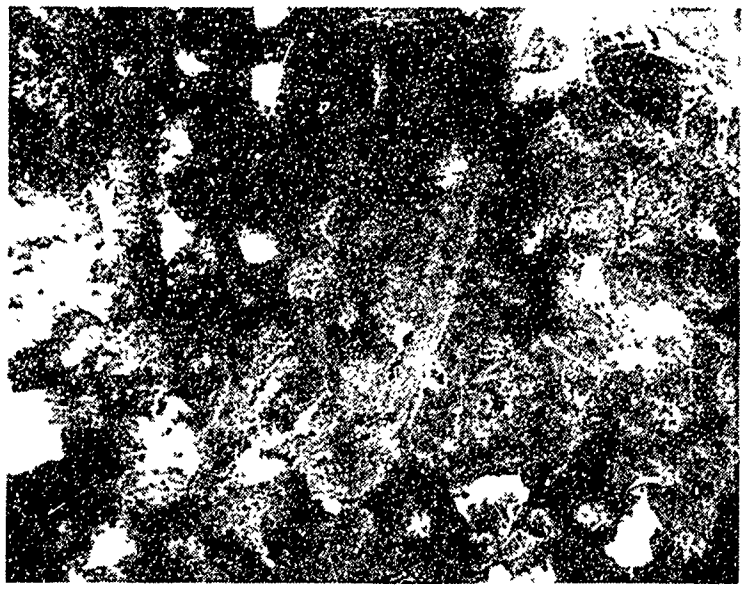

FIGURE 56 MORTAR-TO-WIRE INTERFACE, 4EWG GROUP (24X)

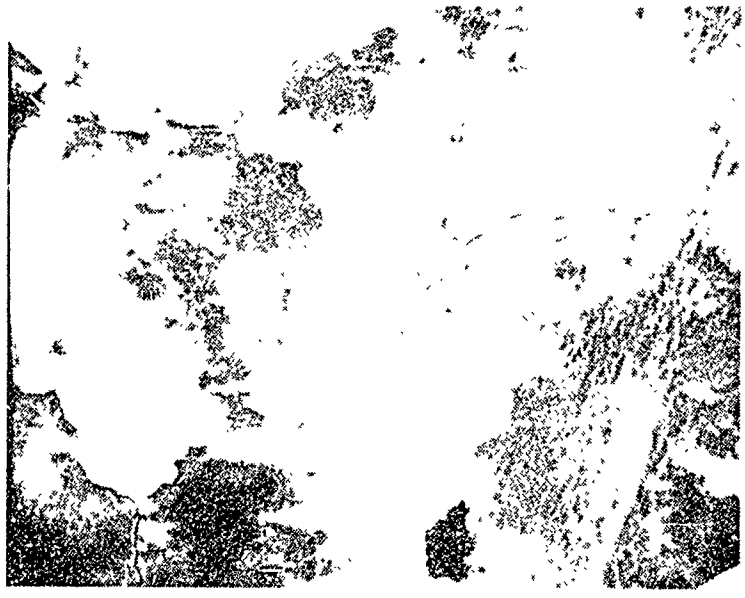

FIGURE 57 CLOSE-UP VIEW OF INTERFACE SHOWN IN FIGURE 56 (120X)

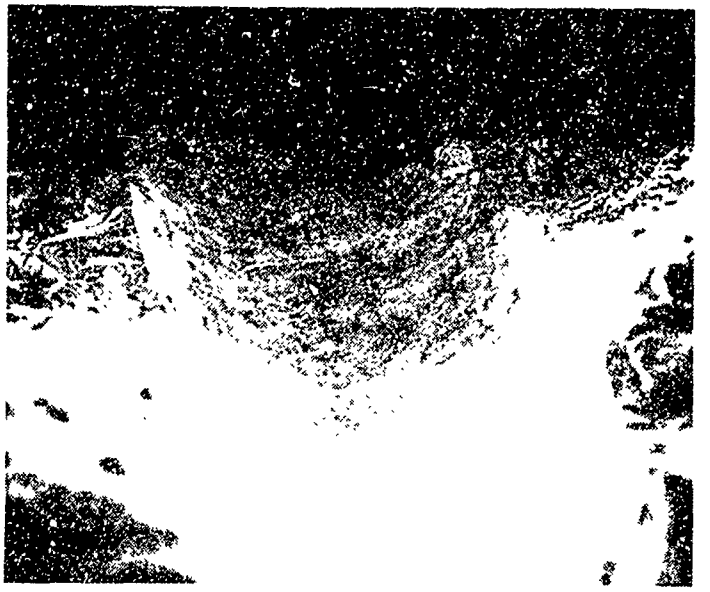

FIGURE 58 MORTAR-TO-WIRE INTERFACE, 4EWU GROUP (54X)

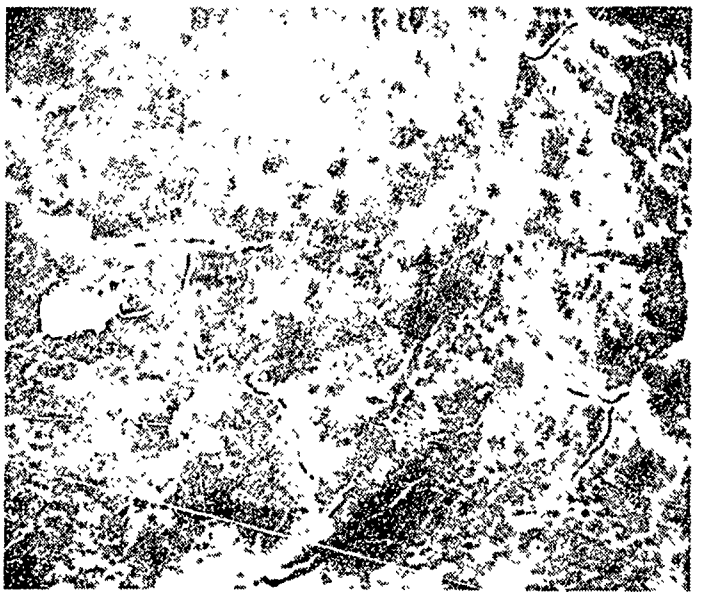

FIGURE 59 CLOSE-UP VIEW OF INTERFACE SHOWN IN FIGURE 58 (220X)

FIGURE 60 GALVANIZED REINFORCEMENT WIRE FRACTURE (56X), TENSILE TEST

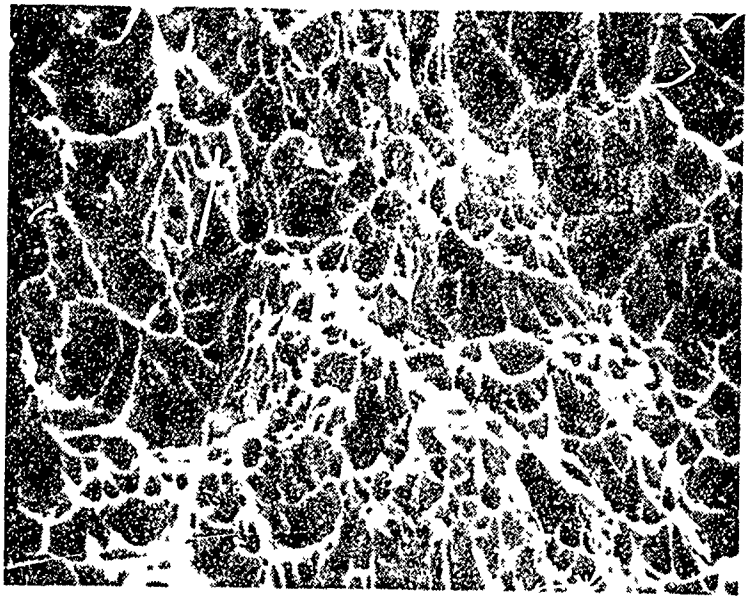

FIGURE 61 CLOSE-UP VIEW OF FRACTURE SURFACE SHOWN IN FIGURE 60 (2200X)

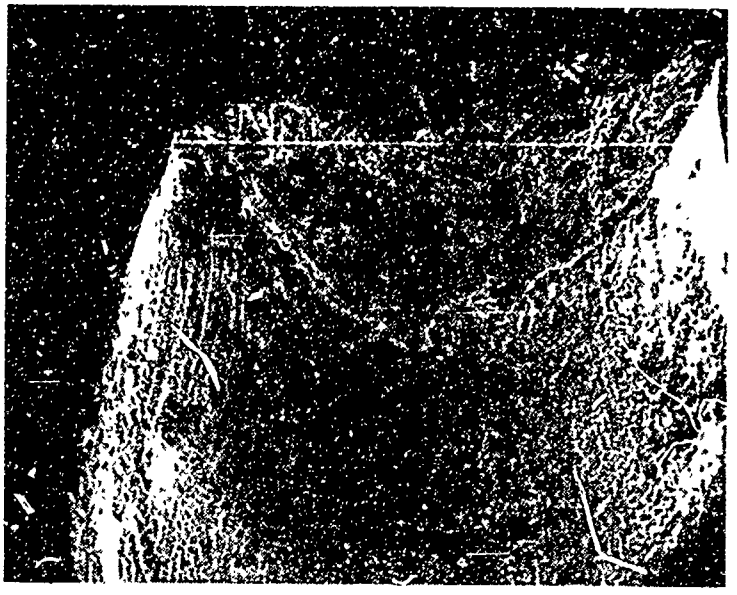

FIGURE 62 UNGALVANIZED REINFORCEMENT WIRE FRACTURE (100X), TENSILE TEST

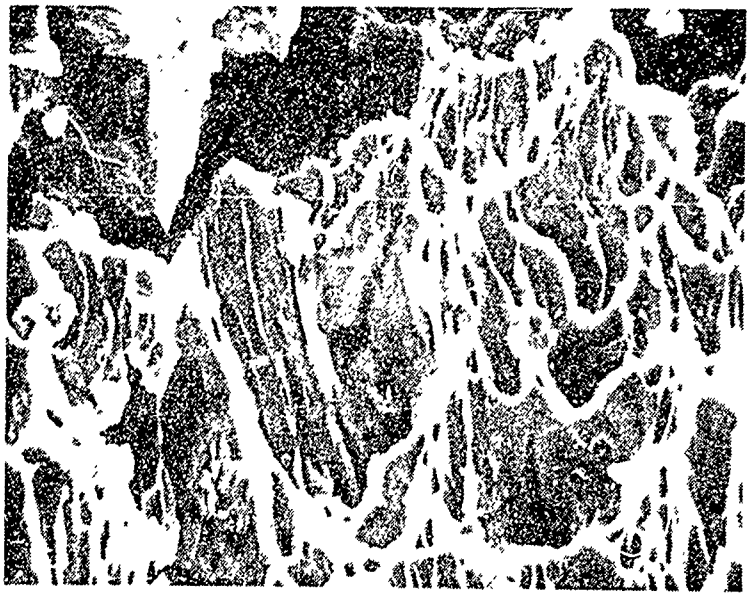

FIGURE 63 CLOSE-UP VIEW OF FRACTURE SURFACE SHOWN IN FIGURE 62 (2000X)

FIGURE 64 GALVANIZED REINFORCEMENT WIRE FRACTURE (125X), MIDDLE LAYER OF FERRO-CEMENT FATIGUE SPECIMEN, 2PWG GROUP

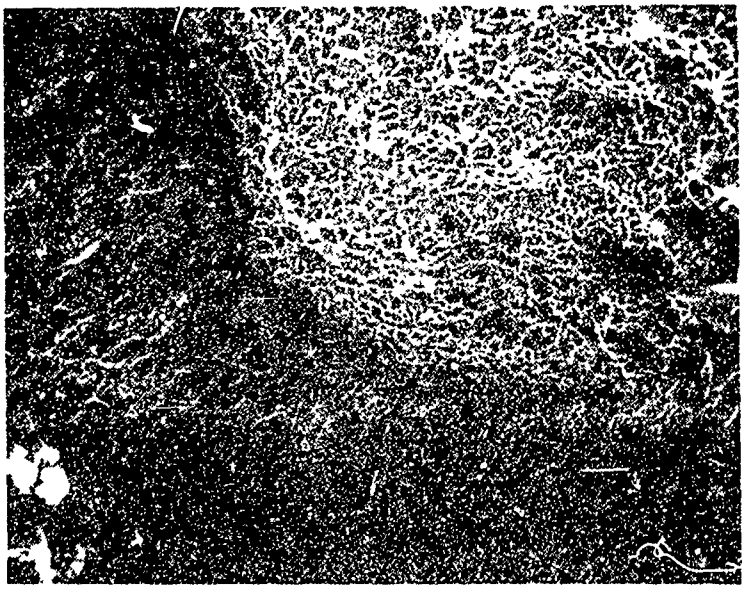

FIGURE 65 CLOSE-UP VIEW OF FRACTURE SURFACE SHOWN IN FIGURE 62 (630X)

FIGURE 66 GALVANIZED REINFORCEMENT WIRE FRACTURE (60X), MIDDLE LAYER OF FERRO-CEMENT FATIGUE SPECIMEN, 4EWG GROUP

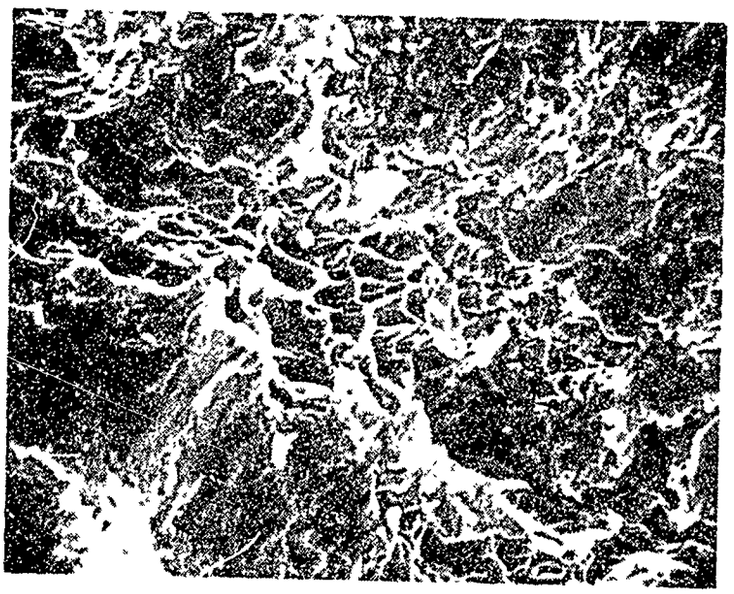

FIGURE 67 CLOSE-UP VIEW OF FRACTURE SURFACE SHOWN IN FIGURE 66 (1200X)

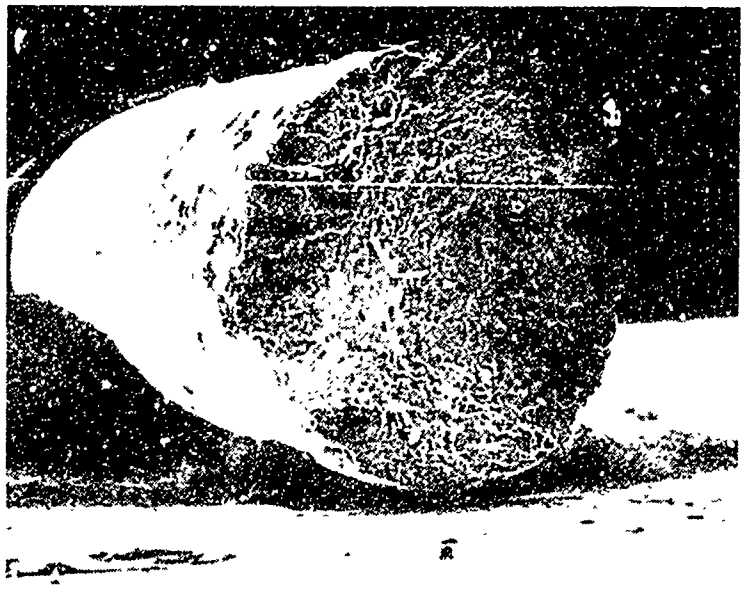

FIGURE 68 GALVANIZED REINFORCEMENT WIRE FRACTURE (57X), OUTER LAYER OF FERRO-CEMENT FATIGUE SPECIMEN, 1PWG GROUP

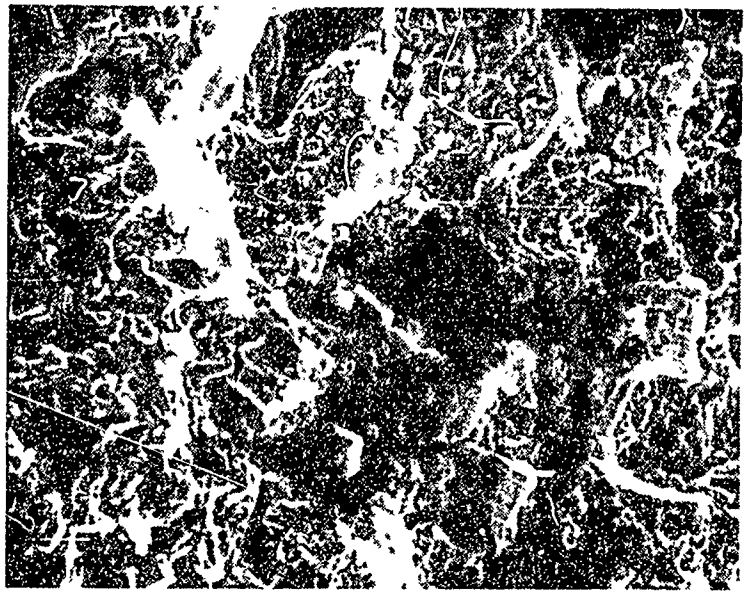

FIGURE 69 CLOSE-UP VIEW OF FRACTURE SURFACE SHOWN IN FIGURE 68 (1120X)

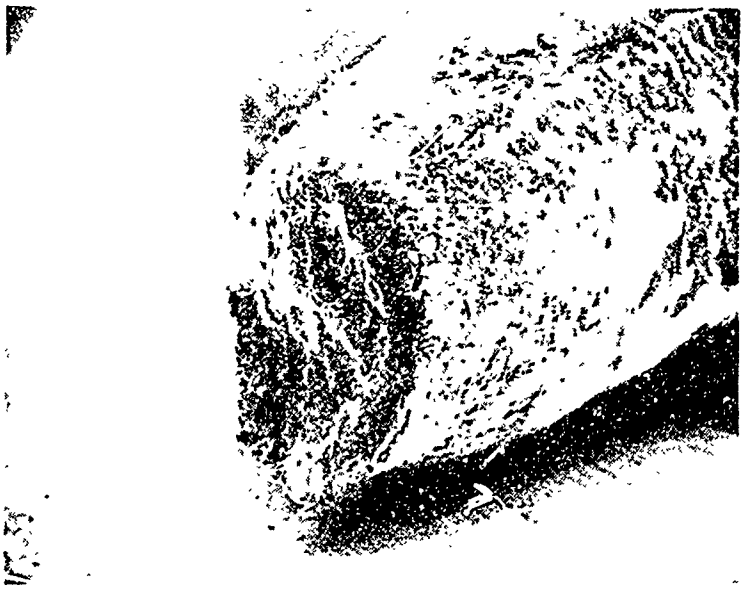

FIGURE 70 GALVANIZED REINFORCEMENT WIRE FRACTURE (58X), OUTER LAYER OF FERRO-CEMENT FATIGUE SPECIMEN, 4EWG GROUP

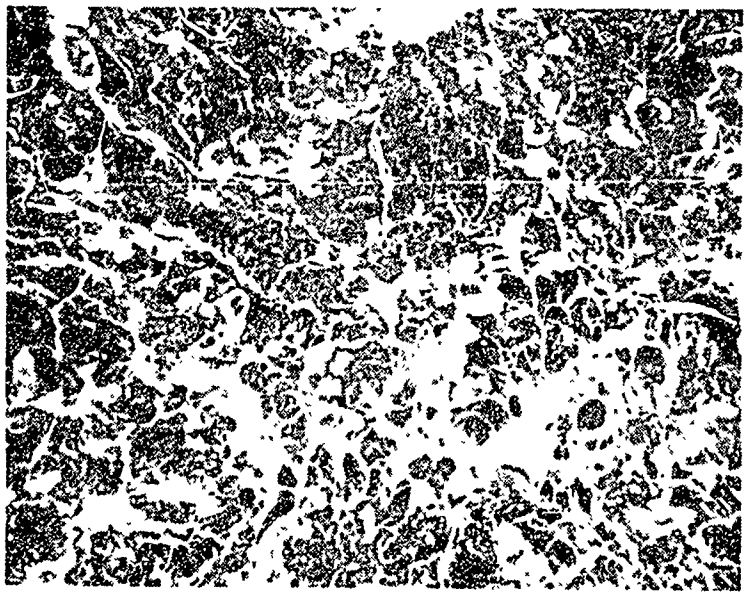

FIGURE 71 CLOSE-UP VIEW OF FRACTURE SURFACE SHOWN IN FIGURE 70 (640X)

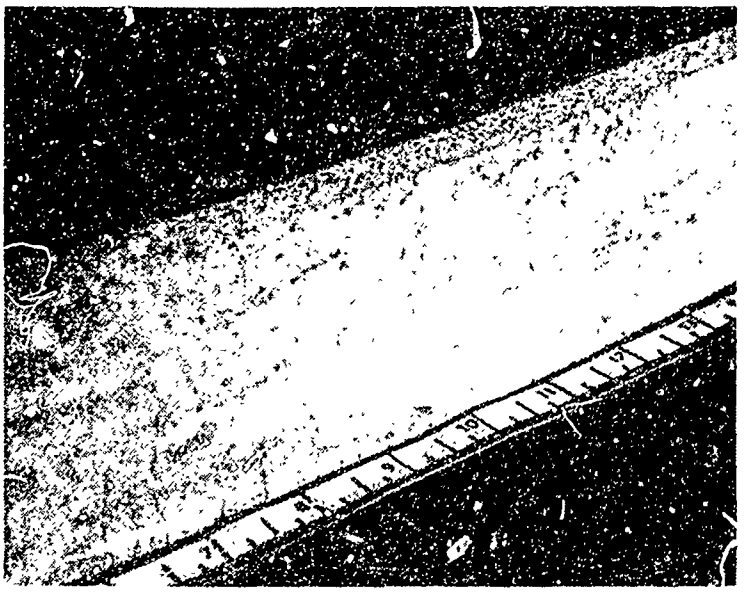

FIGURE 72 SURFACE OF FERRO-CEMENT SPECIMEN FAILED IN MONOTONIC BEAM FLEXURE

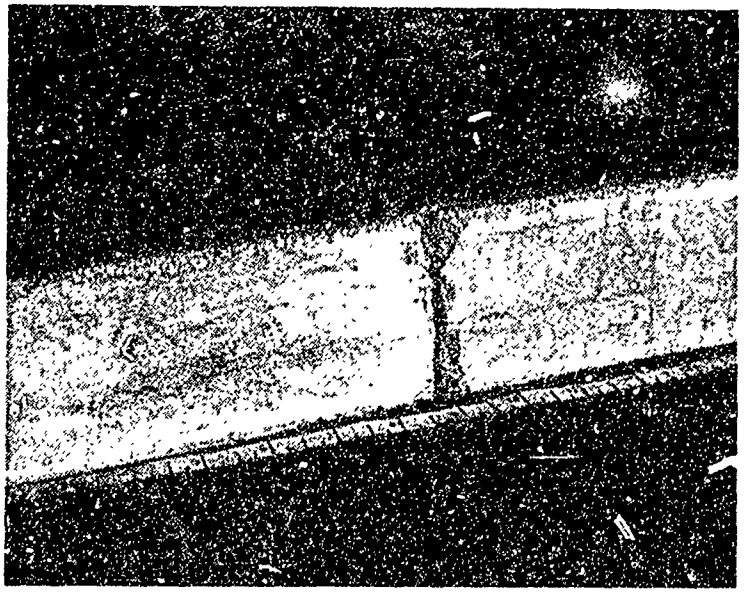

FIGURE 73 SURFACE OF FERRO-CEMENT SPECIMEN FAILED IN BENDING FATIGUE

FIGURE 74. FREE BODY DIAGRAM OF FATIGUE BENDING SPECIMEN

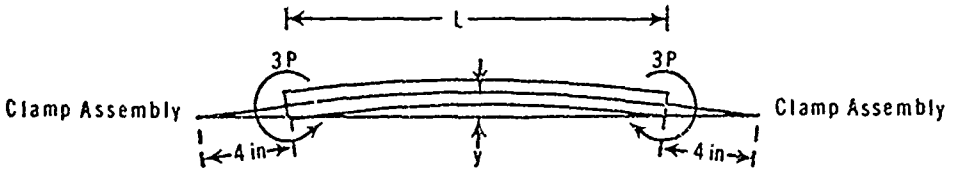

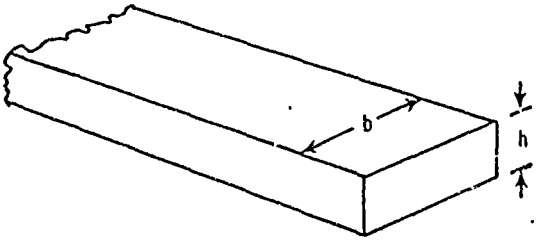

LIST OF REFERENCES

1. Hurd, M. K., "Ferro-Cement Boats," ACI Journal, p. 202-204, March, 1969.

2. Nervi, P. L., "Ferro-Cement: Its Characteristics and Potentialities," L'Ingegnere, V. 1, 1951.

3. Bezukladov, V. F., and others, Ship Hulls Made of Reinforced Concrete, 1968, Navships Translation No. 1148.

4. Whitener, J. R., Ferro-Cement Boat Construction, Cornell Maritime Press, 1971.

5. Samson, J. and Wellens, G., How to Build a Ferro-Cement Boat, Samson Marine Design Enterprises Ltd., 1968.

6. Department of the Environment (Canada), Industrial Development Branch Report No. 42, Ferro-Cement for Canadian Fishing Vessels, compiled and edited by W. G. Scott, August 1971.

7. Department of the Environment (Canada), Industrial Development Branch Report No. 48, Ferro-Cement for Canadian Fishing Vessels, V. 2, by A. W. Greenius and John D. Smith, January 1972.

8. Department of the Environment (Canada), Industrial Development Branch Report No. 48, Ferro-Cement for Canadian Fishing Vessels, V. 3, prepared by The British Columbia Research Council, August 1972.

9. Naval Ship Research and Development Center, Annapolis, Chronological Photographic Record Depicting Construction of the Cement Riverine Assault Boat, CRAB, prepared by NSRDC, Code 287, 1 June 1972.

10. Brauer, F. E., "Ferrocement for Boats and Craft," Naval Engineers Journal, V. 85, p. 93-105, October 1973.

11. Naval Ship Engineering Center, Ferro-Cement: Its Potential for Naval Craft (A State of the Art Study), by D. A. Perry and J. E. Pinto, 15 July 1969.

12. Naval Ship Research and Development Center Report 3979, Comparison Study of Aluminum, Ferro-Cement, and Fiber-Reinforced Plastic for Small Craft in Korea, by B. Whang, December 1972.

13. U. S. Army Limited War Laboratory Technical Memo No. 69-04, Investigation of Ferro-Cement for Potential Military and Para-Military Uses in South East Asia, by J. T. Gurganious, September 1969.

14. Naval Civil Engineering Laboratory Technical Report R753, Polymer-Impregnated Concrete Spherical Hulls Under Hydrostatic Loading, by H. H. Haynes and N. D. Albertsen, December 1971.

15. Monfort, P., A Revolution in Ferro Construction, Aladdin Products, Inc., 1973.

16. Naval Ship Research and Development Center Report 3588, The Mechanical Properties of Ferrocement, by F. E. Brauer, August 1972.

17. Bailey, L. E., Fatigue Strength of Steel Fiber Reinforced Concrete, Master of Science (Civil Engineering) Thesis, Clarkson College of Technology, October 1966.

18. McKenney, J. L., Tensile Strength of Steel Fiber Reinforced Concrete, Master of Science (Civil Engineering) Thesis, Clarkson College of Technology, May 1964.

19. Naval Civil Engineering Laboratory Technical Report R772 Flexural Strength of Ferro-Cement Panels, by H. H. Haynes and J. E. Tancreto, August 1972.

20. Simpson, M. G. and Tucker, R. S., Fatigue Testing Ferro-Cement, unpublished term paper, U. S. Naval Postgraduate School, March 1973.

21. University of California (Berkeley) Report No. UC SESM 71-14, Solving the Galvanic Cell Problem in Ferro-Cement, by K. A. Christiansen and R. B. Williamson, July 1971.

22. Department of the Environment (Canada), Industrial Development Branch Report No. 52, An Introduction to Design for Ferrocement Vessels, by G. W. Bigg, January 1972.

23. Kline, S. J. and McClintock, F. A., "Describing Uncertainties in Single Sample Experiments," Mechanical Engineering, p. 3-8, January 1953.